Ca' Foscari
University
of Venice

Master's Degree programme

In SUSTAINABLE
CHEMISTRY AND
TECHNOLOGIES

Department of
Molecular Sciences and
Nanosystems

Experimental thesis

Supported Palladium Nanoparticles on *N*-doped carbons as catalysts for green process

Supervisor
Ch. Prof. Alvise Perosa

Assistant supervisor
Dr. Daily Rodríguez-Padrón

Graduand
Oscar Trentin
876032

Academic Year
2022 / 2023
Ca' Foscari University of Venice

CONTENTS

ABSTRACT

This thesis work aims at the design of metal-based heterogeneous catalysts for the formation of new C-C bonds, through Heck and Suzuki-Miyaura cross-coupling reactions. In this regard, nitrogen-doped carbonaceous materials were synthesized starting from chitin as both carbon and nitrogen precursors. The synthesis of supported Pd nanoparticles on *N*-doped carbons was performed through two different approaches, namely impregnation and solution methods. Following both strategies, three catalytic materials were prepared, respectively, using different Pd loadings (1%, 2.5%, 5%). The physico-chemical, structural and morphological features of the resulting catalytic samples were explored using a multi-technique approach, involving XPS, XRD, SEM, TEM, ICP-MS and N_2-physisorption. The catalytic behaviour of the samples was investigated in the cross-coupling reactions under batch conditions. All catalysts were tested in both reactions and a complete parametric analysis was carried out to optimize the experimental conditions, considering reaction time, temperature, solvent, base and catalyst amount. Moreover, several substrates were tested, in both reactions, with the aim to demonstrate the versatility of the catalytic systems. Importantly, the stability and reusability of the designed catalysts was addressed by performing a recyclability study together with a post-characterization analysis. The reactions outcome, in terms of conversion and selectivity, was monitored by ^{1}H-NMR and GC-FID in order to verify reproducibility. On the other hand, GC-MS and NMR spectroscopy (^{1}H NMR, ^{13}C NMR and bi-dimensional NMR) were employed for products identification. In the final stage of this thesis work, the synthesis and the applications of the aforementioned catalytic materials were also addressed through a mechanochemical approach, by using a twin-screw extruder. Significantly, with this technique both the synthesis of the catalytic materials and their application were performed under solvent free and continuous-flow conditions, improving not only the sustainability of the whole process but also the reaction productivity.

INTRODUCTION

After 1950, the advent of the industrial revolution has triggered an economic and demographic explosion, closely aligned with the development of the chemical industry. This industry has played a fundamental role in supplying fuels, fertilizers, detergents, pharmaceuticals, additives, polymers, and fabrics, which have enabled the world to evolve into what we know today.[1] The significant societal development observed over the past century has been heavily reliant on the intensive utilization of non-renewable resources such as coal, oil, and natural gas, primarily due to their perceived cost-effectiveness. However, this dependence has also resulted in ecological imbalances and the occurrence of natural disasters. It is imperative to reconsider a more sustainable society model, particularly in light of the anticipated global population growth (it has been estimated around 9.7 billion of people by the 2050[2]) and consequently the increased energy demands. In this sense, in 2015 the United Nations adopted the "2030 Agenda for Sustainable Development" with 17 Goals and 169 targets aimed at achieving a shared global vision towards sustainable development[3]. The chemical industry has a fundamental role in enabling this ecological transition which can be articulated through the development of four key areas[4,5]:

- Low-carbon economy: reducing CO_2 emissions and other greenhouse gases (GHG) by promoting the development of innovative technologies based on the use of renewable raw materials;
- Resource efficiency: designing processes that require fewer resources and with lower energy consumption during the entire life cycle and maximizing the recovery and reuse of materials;
- Circular economy: includes recovering, reusing, remanufacturing and recycling waste materials (the 4R rule);
- Care for people and the planet: using and producing chemicals with minimal impact on both public health and environmental pollution.

In this context, with the aim of directing the chemical industry towards more sustainable scenarios, ensuring the production of chemicals and materials that can improve our daily lives while minimizing their environmental footprint, Paul Anastas and John C. Warner defined the 12 principles of Green Chemistry in 1998. These principles serve as a set of actionable criteria, guidelines, and priorities that underpin the foundation of this "green" paradigm shift.[6,7]
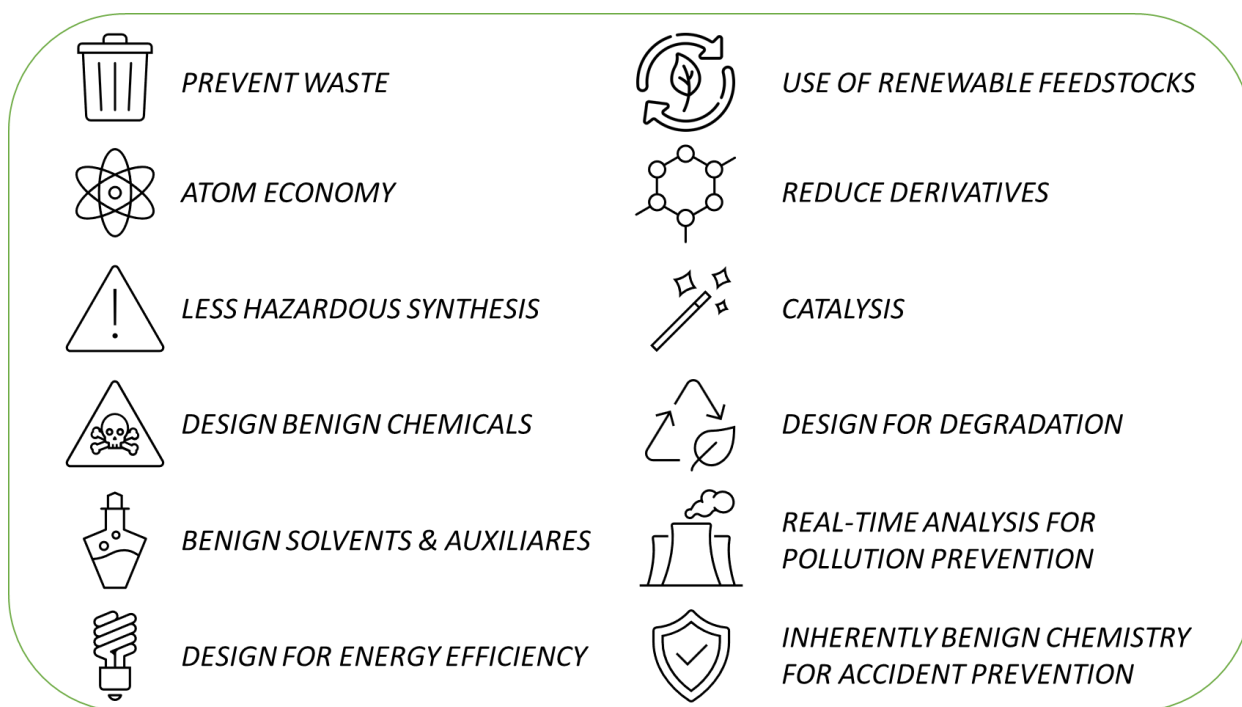
Figure 1: 12 principles of green chemistry.

Among the 12 principles of green chemistry, the seventh principle pertains to the utilization of renewable resources. Presently, the majority of chemicals are still derived from non-renewable sources and are manufactured within a linear economic model: starting with a raw material, undergoing transformation (resulting in processing waste), and subsequently distributing and employing the desired product, often multiple times, until it eventually becomes waste at the end of its lifecycle.[8]
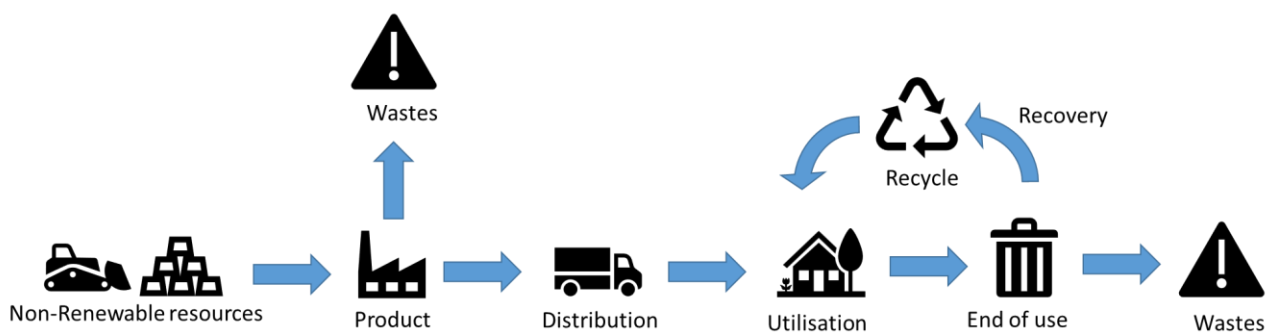
Figure 2: Linear economy model

The unsustainable economic model that has been adopted until now is no longer viable, given the environmental issues it has caused and the scarcity of resources it has led to. Consequently, one of

the current goals is to implement the circular economy model within the industry. This approach begins with renewable resources and strives to follow the 4R rule: recover, reuse, remanufacture, and recycle waste. Under this model, the waste generated by one production chain becomes the raw material for another industry, allowing to produce chemicals in a more sustainable manner.[9]
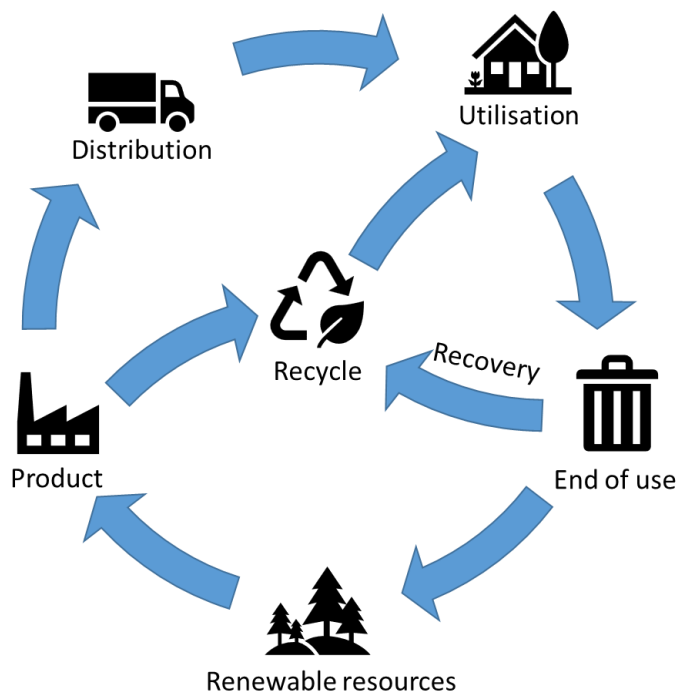
Figure 3: Circular economy model

In this context, besides carbon dioxide, biomass stands out as the primary renewable source of carbon (essential to produce chemicals, materials and biofuels) becoming a crucial component of the transition to more sustainable practices. Biomass is defined as any material formed through biological processes, encompassing waste products such as forest residues, agricultural leftovers, industrial byproducts, non-food chain competing crops, and other similar materials. Biomass is considered a renewable and sustainable source because its current utilization does not deplete the potential for future generations to use it. As a resource, biomass can be harnessed for various purposes, including the production of:

- Biomass derived-chemicals, which are platform molecules, enabling the production of a wide array of other products;
- Biomass derived-materials, such as bio-plastics or catalysts;
- Bio-energy, in the form of heat, which can be converted into electrical energy.

- Bio-fuels, like biodiesel or bioethanol.[10]

Chemical research typically focuses on working with two main categories of biomass wastes:

- Lignocellulosic Biomass: This includes materials like wood, crop residues, and dedicated energy crops, primarily composed of lignin, cellulose, and hemicellulose.
- Waste from Agro-Food Industry: This category covers agricultural and food processing residues, such as fruit peels, straw, spent grains, seafood waste. [11]

In the field of food waste, the seafood sector is of particular interest. Seafood accounts for nearly 20% of current animal-food global production[12] and in 2020, the seafood production reached 178 million tons (MTs).[13] Among the various fish species (such as tuna, mackerel, salmon, etc.) and crustaceans (like shrimp, crabs, mussels, etc.) produced by this sector, the latter generates a larger amount of waste. Indeed, the yield of meat from tuna can reach approximately 75% of the total weight, whereas for crustaceans, this percentage drops significantly to around 40%.[14] Every year, the crustacean industry produces between 6 to 8 million tons of waste, which includes crab, shrimp, and lobster shells. Notably, a significant portion of this waste, approximately 1.5 million tons, originates solely from Southeast Asia.[14] This continent is particularly active in shrimp production, providing 80% of the global supply.[15] As observed in the graph below, the trend is clearly upward (excluding the contractions during pandemic years), with India and Ecuador experiencing significant growth in this sector.[16]
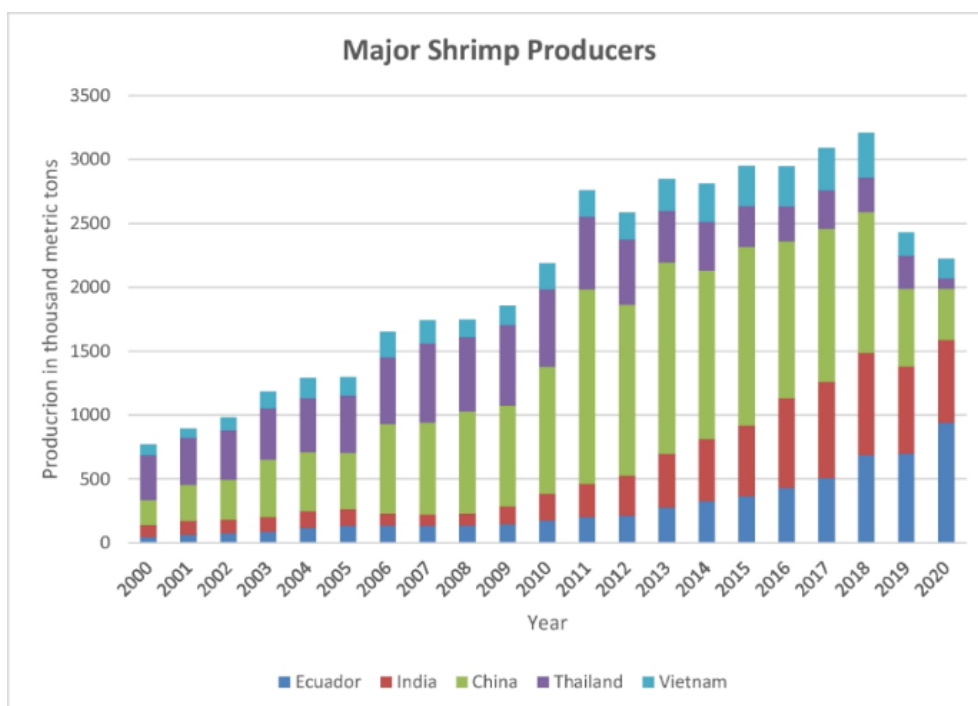

Figure 4: Major shrimp producers from 2000 to 2020.[16]

The processing of shrimp, however, generates enormous amounts of waste. In fact, between the head and shell, 48-56% of the weight (depending on the species) is discarded.[17] Disposing of such a significant biomass represents not only an economic loss but also an environmental detriment. To date, only a small portion of this biological waste, approximately 5%, is treated and mixed with other substances for use as animal feed.[15] Conventional treatment involves sun drying on beaches, which has drawbacks such as an unpleasant smell in coastal areas, surface pollution, and other environmental issues.[18] Additionally, dried shrimp shells are valued at only approximately $100 per ton.[16,19] The majority of shrimp waste remains underutilized and is typically disposed of in landfills, incinerated, or dumped into the oceans.

At these disposal sites, the rapid degradation of shrimp waste leads to the production of biogenic amines, emitting unpleasant odors that can attract rodents, mosquitoes, and flies, potentially serving as disease vectors.[16] Additionally, this contributes to heightened environmental pollution and poses a threat to endangered species.[20] For these reasons, it is crucial to valorise this waste so that it can become a raw material for other industrial sectors, leading to both environmental and economic benefits in a circular economy perspective. Indeed, through efficient treatment of shrimp waste, it is possible to obtain compounds of higher added value, ultimately enhancing the overall profitability of the sector. These compounds mainly include calcium carbonate (20–50%), protein (20–40%), and chitin (15–40%).[16] Some studies have also focused on extracting pigments such as carotenoids (astaxanthin).[17,21] In this thesis work, the primary focus was on chitin, as a renewable carbon and nitrogen source, for the preparation of new catalytic materials. These materials were subsequently characterized and evaluated for their performance and properties.

CHITIN FROM SHRIMP SHELLS: A RENWABLE RAW MATERIAL

Due to the significant amount of waste generated each year, one of the challenges in chemical research is to valorise shrimp waste by converting it into materials or substances with higher added value, following the principles of green chemistry and circular economy. Among the potential opportunities that this waste offers, one of the most compelling revolves around the extraction and production of chitin. With 100 billion tonnes produced every year, chitin is the second most abundant biopolymer on Earth after cellulose.[15] Unlike cellulose, chitin originates from animals and can be found in fungi or plankton.[22] However, its primary source is the exoskeleton of insects and

crustaceans, where chitin is the major component.[23] Additionally, it has been found in some species of invertebrates.[24]

Structurally, chitin is a poly-beta-1,4-*N*-acetylglucosamine. Its numerous intermolecular hydrogen bonds make it insoluble in water, unlike its deacetylated derivative, chitosan. Chitin exhibits variations in properties and structure depending on its source. In nature, there are three types of chitin:[25]

- α-Chitin, the most abundant and studied type, primarily sourced from crab and shrimp shells. Its antiparallel chain arrangement maximizes hydrogen bonds, providing strong structural stability.

- β-Chitin, less common, obtained from molluscs such as squid, has a parallel chain arrangement.

There is also a γ form of chitin, but it appears to be simply a variant of the α form,[25] since it can be converted into this form by treatment with lithium thiocyanate.[26] γ form contains two parallel and one anti-parallel strands of chitin.[23]
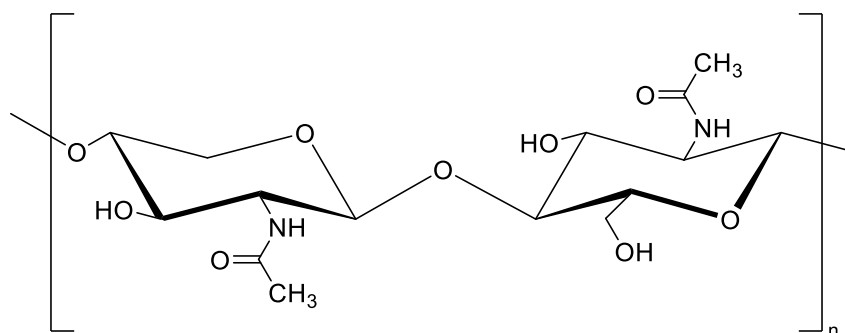
Figure 5: repetitive unit of chitin.

The demonstration of the presence of nitrogen within the chitin structure was carried out by the scientist Lassaigne in 1843. This material indeed contains 6-7% of nitrogen in its structure and can serve as a source of both carbon and nitrogen (C:N = 8:1).[23] Chitin is not only a biocompatible and biodegradable material but also possesses antibacterial and wound-healing properties.[15] These qualities have made it a subject of study for biomedical applications.[27–29] Furthermore, literature reveals a wide range of applications of this material in various fields, such as agriculture, wastewater treatment, bionanotechnology, and materials science.[23,30–34]

Shrimp waste contains 15-40% chitin, with the remaining part primarily consisting of calcium carbonate and proteins. Therefore, in conventional processes for chitin extraction, shrimp shells

undergo a deproteinization and demineralization process.[35] In the first phase, they are treated with a 4% sodium hydroxide (NaOH) solution at elevated temperatures (70–120°C), causing the decomposition of proteins, which are then brought into solution and separated by filtration.[15] In the subsequent step, the remaining solid fraction is treated with 4% hydrochloric acid (HCl), neutralizing the calcium carbonate and producing CO_2, H_2O, and soluble calcium chloride ($CaCl_2$), which is removed by filtration. The use of strong acids has negative effects on the chemical and physical properties of chitin, and it also requires the purification of wastewater, resulting in increased production costs.[36] Therefore, research has shifted towards non-conventional approaches for the demineralization phase, such as the use of weak organic acids (lactic acid and acetic acid), ionic liquids, enzymes, or microorganisms that directly extract chitin through a fermentation process. [37–40]

CHITIN IN HETEROGENEOUS CATALYSIS

Among the various fields of application for this biopolymer, the focus of this thesis work involves utilizing chitin derived from shrimp shells in the synthesis of novel catalytic materials based on *N*-doped carbons. Catalysis plays a fundamental role in designing environmentally friendly syntheses, as it can help reduce waste generation and energy consumption.[41]

For these reasons, one of the principles of green chemistry promotes the use of catalysis in the chemical industry.[6] According to the International Union of Pure and Applied Chemistry (IUPAC), catalysts are substances that increase the rate of a reaction without modifying the overall standard Gibbs energy change in the reaction.[42] Their role in the reaction is to alter the mechanism by lowering the activation energy of the rate-determining step. In this way, not only does it accelerate the reaction rate and enable the use of milder conditions, but it also remains unchanged at the end of the reaction and can therefore be added in sub-stoichiometric quantities. Catalytic systems can be classified into two major classes:

- Homogeneous Catalysts: These catalysts are present in the same phase as the reactants, maximizing the contact between the reactant and the catalyst. Since the entire catalyst is available, these systems are typically highly efficient. Furthermore, because the exact chemical structure of the catalyst is known, it is often possible not only to identify the reaction mechanism but also to exert greater control over the products by modifying the catalyst's structure. The main drawback of these systems lies in the difficulty of separating and recovering the catalyst for reuse once the reaction is completed.

- Heterogeneous Catalysts: These catalysts exist in a different phase from the reaction mixture. In this case, the reaction occurs at specific points (active sites) dispersed along the surface of the catalyst, which is typically a porous material. To form products, the reactants must diffuse into the pores to reach the active site. Since the reaction rate not only relies on reaction kinetics but also on the rate at which the reactants diffuse, leading to a transition from a kinetic to a diffusion-controlled regime, these systems are typically less active than homogeneous ones. The porosity of the catalyst is a crucial parameter because it not only increases the surface area (and hence the number of active sites) but also influences selectivity based on pore size (shape selectivity) and confines the reactants to a small volume, locally increasing reactant concentration and thus accelerating the reaction. The primary advantage of these catalytic systems lies not only in their suitability for use in continuous flow reactions but also, above all, in the easy separation of the catalyst from the reaction mixture, which reduces waste production and aligns with the first principle of green chemistry (preventing waste). This is why, in the realm of green chemistry, heterogeneous catalysis is generally favoured over homogeneous catalysis.

Over time, the performance of numerous heterogeneous catalytic systems has been tested and fine-tuned in various organic transformations. These systems generally consist of noble and non-noble metals dispersed on various supports made of stable inorganic oxides such as alumina (Al_2O_3), titania (TiO_2), zirconia (ZrO_2), ceria (CeO_2) and zeolites, among others. In addition to inorganic oxides, carbon-based materials have also shown to be promising supports for heterogeneous catalysts, being among the most commercialized in the industry, due to their favourable physicochemical properties, such as high porosity, leading to a high specific surface area, as well as excellent electrical and thermal conductivity.[43] The use of metal-supported nanoparticles, advantageous for their high catalytic activity, does, however, have some disadvantages in terms of material stability. These issues encompass nanoparticle agglomeration (sintering) or leaching, resulting from a weak interaction between the metal and carbon support, which leads to a reduction of active sites. Additionally, during the reaction, possible changes in the valence-state of the active species can occur, causing deactivation.[44] The presence of heteroatoms in the carbonaceous structure can address the stability issues of these materials, thereby improving catalytic performance. Several heteroatoms have been used as dopants, including *B, P, O, S* e *N*.[45] In this perspective the presence of nitrogen within the polymeric chains of chitin (with a C:N ratio of 8:1) is an interesting feature that can be harnessed in the field of environmental catalysis and in fact in

the literature, studies have been already reported regarding the use of this biopolymer in the synthesis of metal-free nitrogen-doped carbon catalysts. In a typical *N*-doped carbon based material we can define different type of nitrogen groups such as pyridinic, pyrrolic and graphitic groups.[46] The pyridinic group is a types of nitrogen that is doubly coordinated, typically found at the edge or within vacancies of graphitic domains. It contributes to the π-system with a single p-electron, and its lone pair gives it a basic character. On the other hand, pyrrole nitrogen is a three-fold coordinated nitrogen atom located in a pentagonal ring. When substituted in graphene, pyrrole acts as an electron localizer and behaves as a 2-position nucleophile. The structure of graphitic nitrogen is still a topic of ongoing discussion. [46] Current theoretical models describe this species as a three-fold coordinated nitrogen atom that substitutes a carbon atom in a planar configuration, but this species is also ascribed to a positively charged tetrahedric nitrogen atom intermolecularly interacting with anionic functional groups.[46]
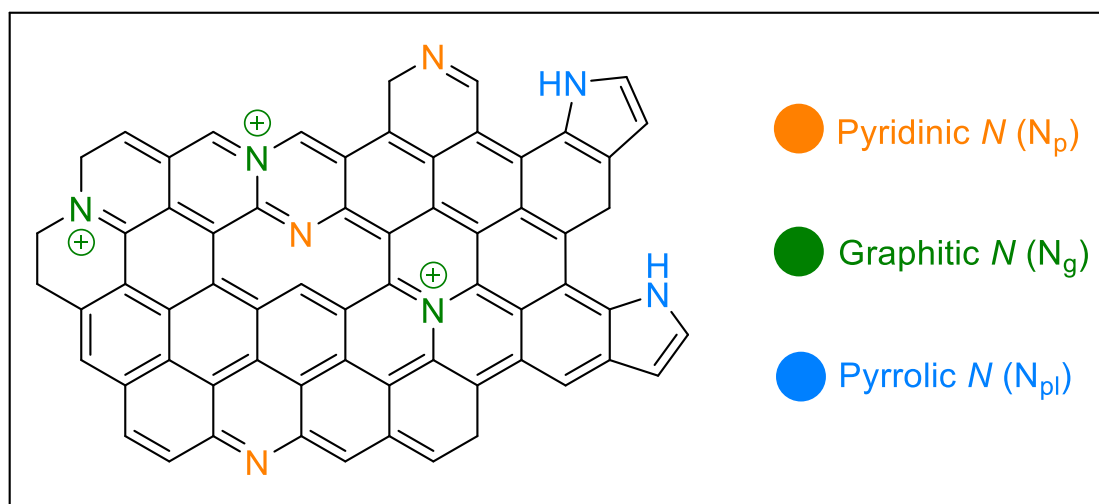
Figure 6: different type of N which can be found in a typical N-doped carbon based material.

Thanks primarily to the presence of pyridinic surface groups that impart basicity to the material, studies can be found in the literature regarding the use of chitin in the synthesis of metal-free nitrogen-doped carbon catalysts, where nitrogen serves as an active site in base-catalyzed reactions, thereby avoiding the use of toxic and costly heavy metals.[45,47] Furthermore, other reported examples involve the use of chitin-derived *N*-doped carbons as a support for metal deposition.[48–50] In these cases, the presence of nitrogen favours the deposition of metal nanoparticles. Both graphitic and pyridinic nitrogen are sp^2 hybridized and act as electron acceptors, withdrawing electron density from the carbon matrix. However, graphitic nitrogen has 2 electrons in the p$_z$ orbital

and serves as a nitrogen dopant in the material, with one electron occupying an anti-bonding π* molecular orbital. These characteristics make graphitic nitrogen electron-rich and prevent the formation of a direct nitrogen-metal bond due to the high electrostatic repulsion with metal nanoparticles.[43] On the contrary, pyridinic nitrogen shares only one electron with the π system of the support, allowing for the direct coordination of metal nanoparticles. This is facilitated by the σ-donation of nitrogen to the metal and a possible back-donation of the metal to the now free π* orbital of the support.[43,46] In this way, pyridinic nitrogen not only may promote the proper dispersion of active sites (similar to graphitic nitrogen) but also enhances the stability of the catalytic systems by acting as an anchoring site to prevent metal leaching. Due to these promising characteristics, in this work, the synthesis and characterization of catalytic systems involving palladium nanoparticles supported on nitrogen-doped carbons have been explored. Chitin obtained from shrimp waste was used as a precursor for these materials. The catalytic performances of these samples were further investigated in the Suzuki-Miyaura and Heck reactions.

SUZUKI-MIYAURA AND HECK CROSS COUPLING REACTIONS

Cross-coupling reactions are a typical class of organic chemistry reactions that have garnered significant interest in the scientific community due to the possibility to form new C-C bonds between two substrates, enabling the synthesis of increasingly complex organic molecules. The pharmaceutical sector, in particular, has greatly benefited from these reactions. In 2006, for instance, 11% of the reactions applied in three multinational pharmaceutical companies (AstraZeneca, Pfizer, and GlaxoSmithKline) were cross-coupling reactions.[51] Some well-known examples include the Heck-Mizoroki, Suzuki-Miyaura, Sonogashira, Stille, and Buchwald-Hartwig (hetero-coupling C-N) reactions. Generally, all of these reactions involve the formation of C-C bonds between unsaturated (sp^2 or sp^3) carbons and originally emerged from the use of Palladium (Pd) in homogeneous catalysis, although there are now studies in the literature exploring the use of other metals such as Pt, Cu, Au, Fe, and Ni.[52] Typically, these reactions involve two types of substrates: an organometallic species (such as organoborates or organostannates) and an organic electrophile (aryl or alkyl halide). The high selectivity and versatility with various substrates have made these reactions extensively studied over the years, and similarities in various mechanisms have been observed. A typical generic cross-coupling reaction usually consists of the following steps:[53]

- Oxidative addition of an alkyl/aryl halide to Pd(0), yielding a Pd(II) organo complex. This step is typically the rate-determining step.

- Transmetalation, involving the replacement of the halide ligand coordinated to Pd with an aryl/alkyl ligand.
- Reductive elimination, where the Pd(0) catalyst is regenerated, forming the C-C bond between the two organic species.
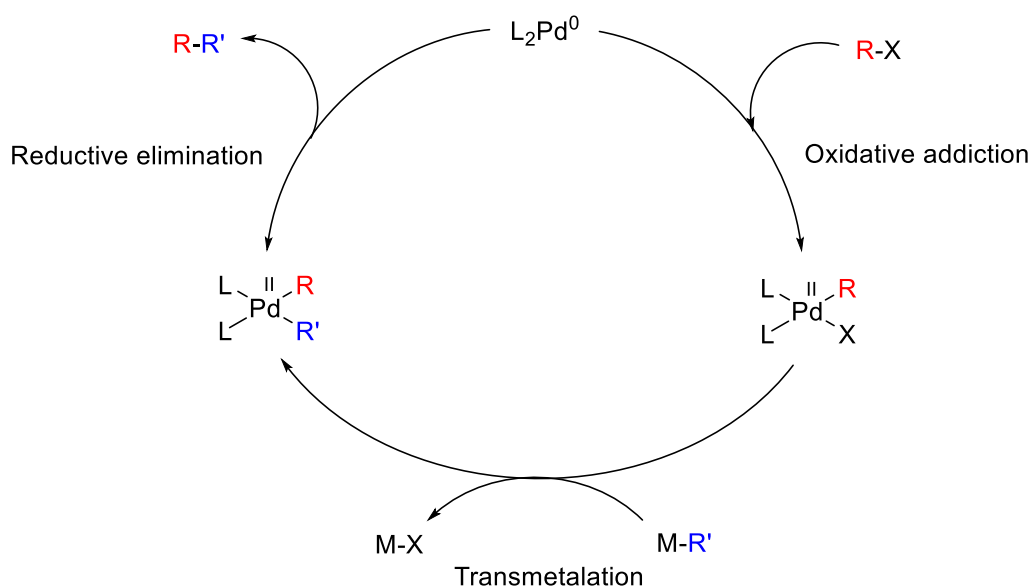
Scheme 1: Simplified catalytic cycle for a generic cross-coupling reaction.

Mechanistic studies have been conducted for homogeneous catalysis starting from Pd complexes. The most commonly used ligands are phosphines, which generate a $Pd(PR_3)_4$ complex of Pd(0). Even if Pd(II) complexes with halides ($PdCl_2$) or acetate ($Pd(OAc)_2$) are also widely used.[54] In these cases, Pd is reduced in situ in the presence of a promoting base, such as phosphines, alkoxides, triethylamine, or ethylene, to form catalytically active zerovalent species.[54,55] *N*-heterocyclic carbenes (NHCs) are also gaining strong popularity as replacements for phosphines. This is because the strong Pd-NHC bond limits ligand dissociation, increasing the complex's stability. Additionally, good σ-donation facilitates the oxidative addition step, and significant steric hindrance accelerates the reductive elimination step.[56,57]

To avoid difficulties in catalyst separation, there has been significant research development in the use of efficient supported heterogeneous catalytic systems, varying both the metallic component and the support material.[58] Among all metals, palladium remains the most commonly used. Regarding the investigated supports, metallic oxides such as alumina (Al_2O_3), silica (SiO_2) and titania (TiO_2) have been employed.[59] For the Heck reaction, Huang et al. developed a Pd/SiO_2 catalyst through calcination from a metallic precursor, achieving good results in the coupling between

bromobenzene and styrene (80% yield, 135°C, 4 hours, in dimethylacetamide).[60] Climent et al. synthesized Pd nanoparticles supported on alumina, silica, and titania and tested these systems in the synthesis of the raspberry-scented fragrance 4-(p-methoxyphenyl)butan-2-one through a Heck cross-coupling. Among the three supports, titania proved to be the most effective with an 80% yield.[61]

Moreover, for the Suzuki reaction, Hossain et al. obtained and tested materials composed of Pd nanoparticles supported on alumina nanorods in the coupling between 3-bromoanisole and 4-carboxyphenylboronic acid, achieving good conversion rates and recyclability.[62] Ncube et al. generated catalysts consisting of dendrimers containing Pd nanoparticles encapsulated in a porous SiO_2 support, which were then tested in the Suzuki reaction between iodobenzene and phenylboronic acid, yielding quantitative results at 110°C after 1 hour in dimethylformamide (DMF).[63]

Other studied supports include carbonaceous and magnetite-based materials. Liu et al. synthesized Pd-supported systems on activated carbon using an innovative method involving argon glow discharge plasma reduction, without the use of reducing agents. This led to excellent results in the Suzuki cross-coupling between 4-bromotoluene and phenylboronic acid (98% yield, 60°C, 30 minutes, K_2CO_3 in EtOH:H_2O = 1:1) and the Heck reaction between iodobenzene and styrene (93% yield at 120°C for 4 hours), despite the use of less eco-friendly solvents like DMF.[64] Ghorbani et al. synthesized catalytic systems where Pd is supported on magnetic magnetite particles through S-methylthiourea. Despite the laborious synthesis procedure, the added value of this material is the easy separation using an external magnet after the reaction, and the excellent stability. Such catalyst achieved good yields in the cross-coupling between iodobenzene and butyl acrylate even after multiple cycles (95% yield, 120°C, 90 minutes in DMF), although the use of toxic DMF negatively impacts the sustainability of the reaction. In addition, in the Suzuki reaction, the aforementioned material exhibited excellent properties for the coupling between iodobenzene and phenylboronic acid (96% yield, 50°C, 30 minutes in H_2O).[65]

Although less common in the literature, other transition metals have been also used for C-C cross coupling reactions, either as free nanoclusters or supported nanoparticles.[58] Recently, Hosseini-Sarvari et al. synthesized a nickel catalytic system supported on TiO_2 to promote Suzuki cross-coupling for the formation of biaryl compounds, achieving good yields (60-100%), albeit with room for improvement in reaction times (6-24 hours), using $CeCO_3$ as a base at 80°C in a mixture of MeOH/H_2O.[66]

Given the excellent characteristics of Pd and the above-mentioned *N*-doped carbon support, this study focuses on Heck-Mizoroki and Suzuki-Miyaura reactions through a heterogeneous catalysis strategy, employing catalytic materials based on low-loading metallic Pd supported on *N*-doped carbons derived from chitin. The significant potential of these reactions prompted the American chemist Richard F. Heck, along with the Japanese chemists Ei-ichi Negishi and Akira Suzuki, to be awarded the Nobel Prize in Chemistry in 2010 for their contributions to "Palladium-catalyzed cross couplings in organic synthesis".[67]

HECK-MIZOROKI REACTION MECHANISM

The Heck-Mizoroki reaction (or Heck reaction) differs from common cross-coupling reactions in that it involves the formation of a C-C bond between an unsaturated aryl/alkyl halide and an alkene in the presence of a base and a Pd catalyst.[68] This reaction has the advantage of not requiring the preparation of organometallic compounds (such as organostannanes used in the Stille reaction, which are highly toxic). Consequently, the transmetallation step is absent from its mechanism. The mechanistic study of this reaction is not straightforward and strongly depends on the reaction conditions. Since the reaction begins with an oxidative addition, it is necessary to have electrically and sterically unsaturated catalytic species. In the simplest case, starting with the $Pd(PPh_3)_4$ species, it is accepted that this species exists in an equilibrium where it undergoes dissociation, losing two phosphine ligands to form the catalytically active $Pd(PPh_3)_2$ species.[53,69]

At this point, it's possible to define a catalytic cycle that includes the following steps:

1. Oxidative Addition: The aryl/alkyl halide (RX) undergoes oxidative addition to Pd(0), oxidizing it to Pd(II) and forming a stable square-planar species with 16 electrons. It has been demonstrated that this reaction occurs through a concerted-like mechanism involving a three-centre transition state.[70] There are two stages: associative and oxidative. In the first stage, there is σ-donation from the carbon-halogen (C-X) bond to Pd, leading to elongation of the C-X bond. In the second stage, there is electron density back-donation from Pd to the σ* C-X antibonding orbital, breaking the C-X bond completely and completing the oxidative addition. This mechanism typically results in a cis product, although isomerization to the thermodynamically more stable trans species often occurs.[53]
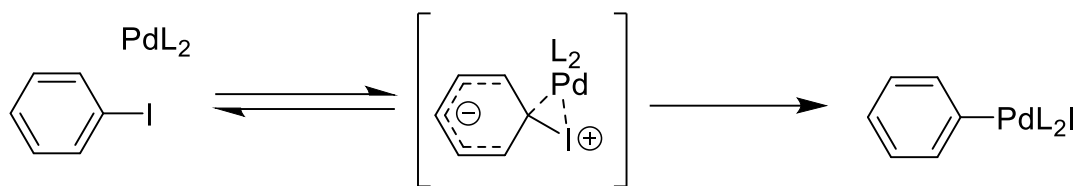
Scheme 2: Oxidative Addition.[53,70]

2. Olefin Insertion: The olefin inserts itself into the R group coordinated to Pd without changes in oxidation state or coordination number.

3. Beta-Hydride Elimination: This step leads to the formation and dissociation of the product, generating a Pd(II) hydride complex. To facilitate this step, all bonds between Pd and hydride must be on the same plane, allowing hydride to approach the metal center. Stereoselectively, this step forms a trans olefin.

4. Reductive Elimination: This step regenerates the Pd(0) catalytic species. The reaction is promoted by a base that is essential for catalyst regeneration, capturing the formed hydrogen halide (HX). Therefore, the base needs to be added in stoichiometric amounts.[53]
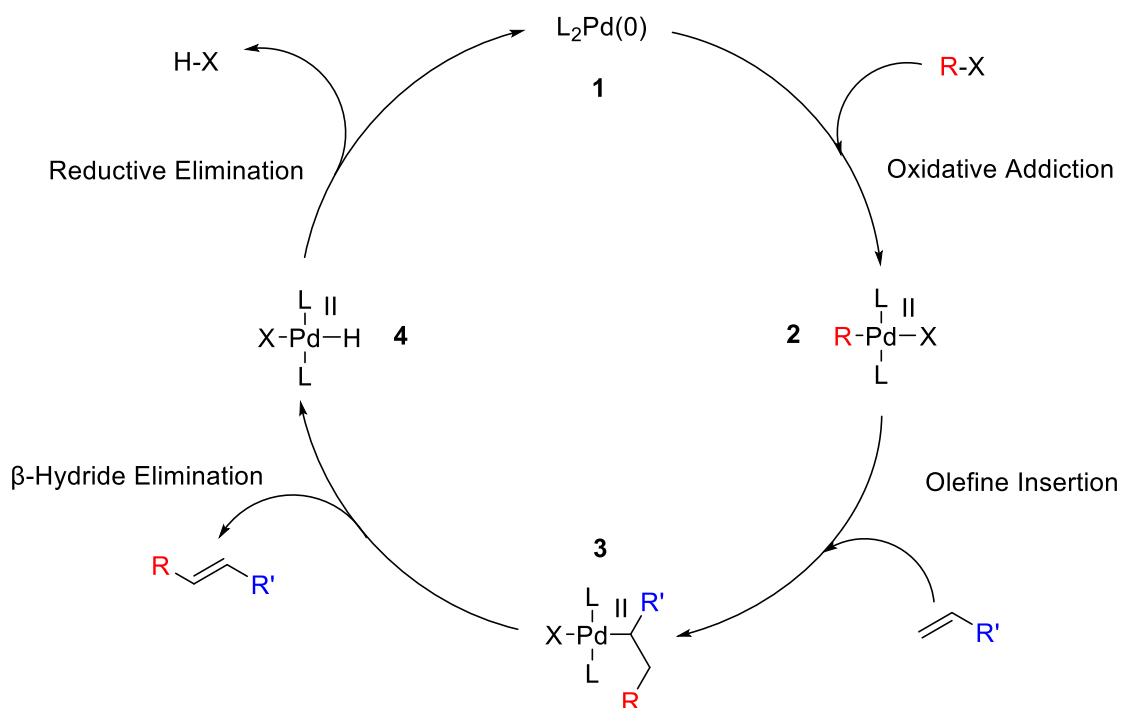
Scheme 3: Simply mechanism for Heck-Mizoroki cross-coupling reaction.[53]
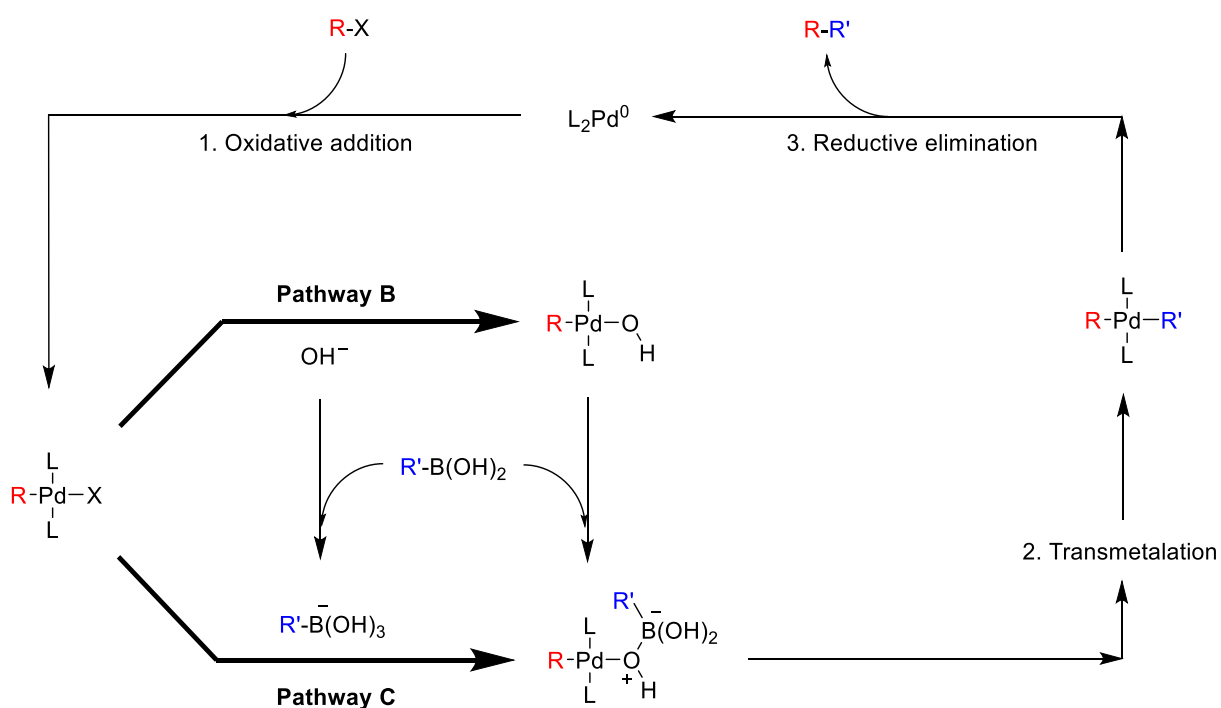
SUZUKI-MIYAURA REACTION MECHANISM

This cross-coupling reaction forms new C-C bonds from an aryl/alkyl halide and an aryl boronic acid.[71] Organoboron compounds have the advantage of being non-toxic and have gradually replaced other organometallic agents RM (where M is Mg, Zr, Si, Sn, Cu) used in other reactions.[54] Similar to the Heck-Mizoroki reaction, through homogeneous catalysis, this reaction begins with a Pd(0) complex in the presence of a base, whereas heterogeneous catalysis involves the use of Pd-supported catalysts. The role of the base has been pivotal in elucidating the reaction mechanism, which proceeds through the following steps:

1. Oxidative Addition of RX: The aryl/alkyl halide (RX) undergoes oxidative addition to the Pd(0) species, oxidizing it to Pd(II). This step is similar to the Heck-Mizoroki reaction and shares the same considerations. There are studies where, depending on the solvent, the mechanism of oxidative addition can be either concerted with a three-centre transition state (as seen previously) or of the SN2 type (nucleophilic attack of Pd on the C sp^2 with the departure of the halide, which then coordinates trans to the aryl/alkyl group).[72,73] The reduced reactivity of the aryl halide with increasing electronegativity of the halogen, as observed experimentally, is explained by the mechanism of oxidative addition. The higher the electronegativity of the halogen, the more stabilized the molecular orbital of the C-X bond (bond dissociation energies for Ph–X: Cl: 96 kcal/mol; Br: 81 kcal/mol; I: 65 kcal/mol), making the σ-donation that initiates oxidative addition less favourable.[74,75]

2. Transmetallation: This step involves the replacement of the halide coordinated to Pd with the organic component R' of the aryl boronic acid. The role of the base is crucial because the presence of an anionic nucleophilic species (such as alkoxide RO- or hydroxide OH-) is required for the success of the reaction.[71] This species can either be formed in situ or represented by the base itself. For example, in Suzuki reactions in anhydrous organic solvents, the addition of water, which subsequently reacts with a base to generate the hydroxide ion, promotes the reaction.[76] This step has been the subject of various computational studies as at least three mechanisms have been hypothesized:[77]

    a. Transmetallation without Base: Transmetallation occurs without the aid of a base. Computational and experimental studies suggest that this is the least likely mechanism because it involves excessively high energy barriers.

    b. Base-Mediated Nucleophilic Attack: In this mechanism, a base in solution forms a nucleophile (usually RO- or OH-) that directly replaces the coordinated halide,

followed by the coordination and transmetallation of the aryl boronic acid. This mechanism has been ruled out by computational calculations due to the inability to find an appropriate transition state, although kinetic studies confirm this mechanism.[78] According to computational calculations, the coordination of OH- (or RO-) to the phosphine (which oxidizes) coordinated to Pd and the subsequent migration of the OH- group to the metal center, causing the decoordination of the halide and the formation of a hydride species that completes transmetallation with the aryl boronic acid, is more feasible. However, this pathway is less likely because the oxidation of the phosphine is typically one of the causes of catalyst degradation. This is also confirmed by experimental observations showing that in the presence of boronic acids, the amount of oxidized phosphine is very low.[77]

c. Base-Mediated Boronate Formation: In this mechanism, a base in solution forms a nucleophile (usually RO- or OH-) that adds to the boron (a Lewis acid) of the aryl boronic acid, forming a reactive anionic species (boronate) that is more nucleophilic and carries out transmetallation. This mechanism, with the most linear energy profile, is the most likely one and is supported by experimental observations.

3. Reductive Elimination: In this step, the catalytic Pd(0) species is regenerated with the formation of a new C-C bond between the two substrates.

Scheme 4: Simply mechanism of Suzuki-Miyaura cross-coupling reaction.[79]

In addition to the main Suzuki-Miyaura cross-coupling reaction, it is necessary to consider possible side reactions that need to be controlled:[80]

- Homocoupling of Two Aryl Boronic Acids: This can occur in the presence of oxygen. In this case, oxygen coordinates to Pd, forming a peroxo-complex. This species interacts with the first aryl boronic acid, leading to the formation of an intermediate. In the presence of water, this intermediate coordinate the aryl group and a hydroxide to Pd. Subsequently, a transmetallation reaction occurs between a second aryl boronic acid and the hydroxide on Pd, resulting in the formation of boric acid and a complex. Through reductive elimination, the catalyst is regenerated to its initial state, forming the homocoupling product.[81]
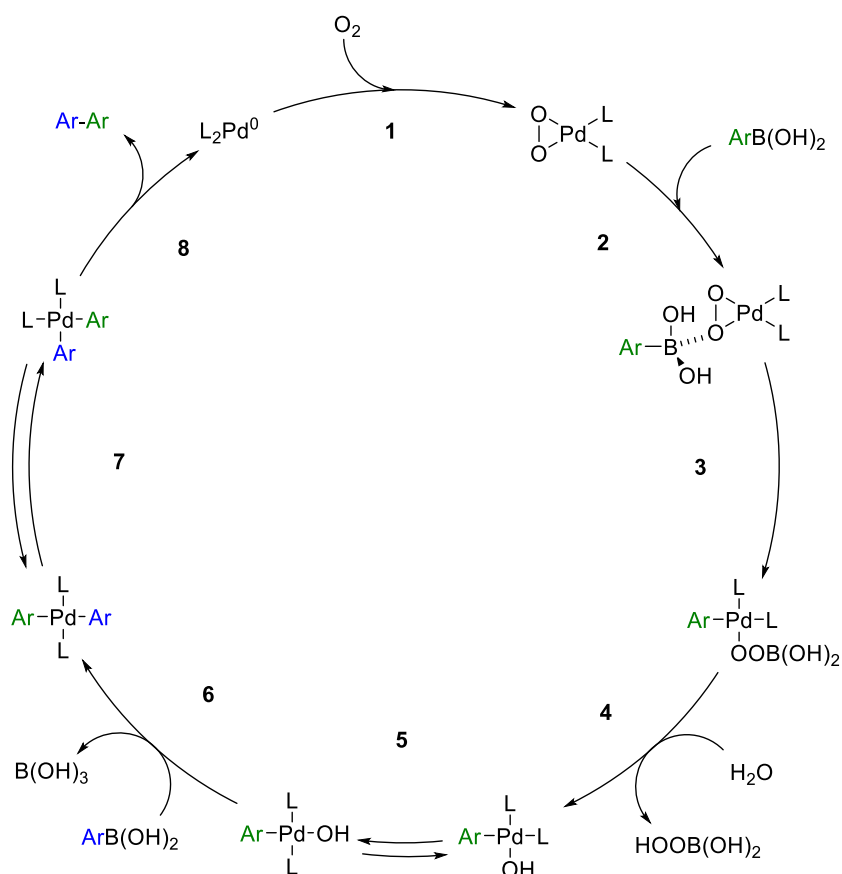
Scheme 5: Catalytic cycle of homocoupling side reaction between two Aryl Boronic Acids.[81]

- Protodeboronation of Aryl Boronic Acid: This can occur through various mechanisms under both acidic and basic conditions.[82]

- Hydrodehalogenation of Aryl Halide: This side reaction becomes more significant with stronger bases used in the reaction. It occurs in the presence of a nucleophile, typically an

alkoxide, which can be formed in situ or act as the base. After the oxidative addition step, substitution of the halide coordinated to the metal with the alkoxide can occur. Subsequent β-hydride elimination leads to the formation of a carbonyl compound and a hydride complex of Pd. The final reductive elimination forms the dehalogenated product.[83,84] These processes are illustrated in the scheme 6.
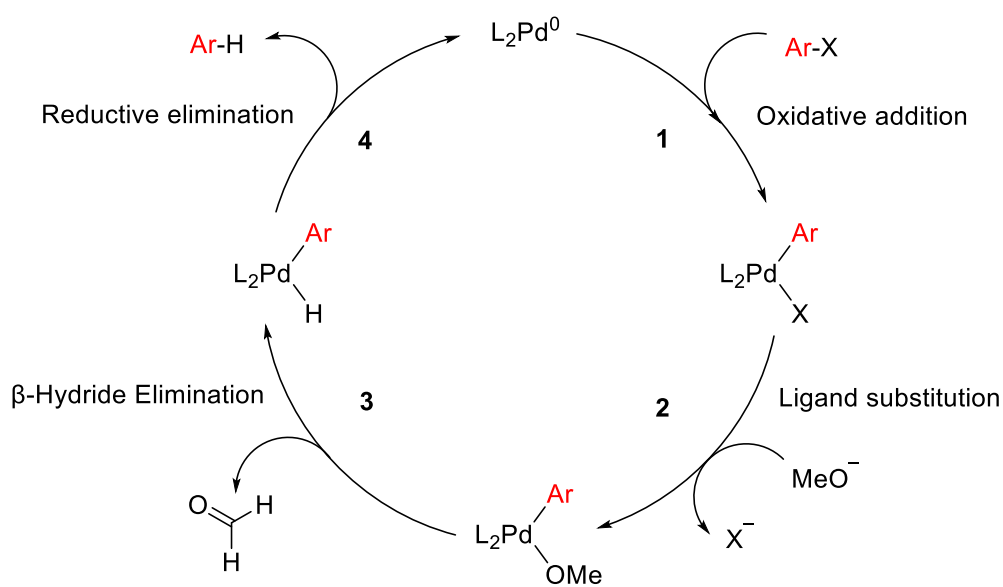
Scheme 6: Possible mechanism of Hydrodehalogenation side reactionof Aryl Halide.[83]

These side reactions can reduce the yield of the desired Suzuki-Miyaura cross-coupling product and need to be carefully managed during the reaction.

## MECHANOCHEMISTRY: A SUSTAINABLE OPPORTUNITY

The first principle of green chemistry focuses on preventing waste generation.[6,9] To quantify the amount of waste generated in a production process, Roger A. Sheldon introduced the Environmental Factor (E-Factor or simply EF). This is defined as the kilograms of waste produced per kilogram of product obtained from a given process.[85] EF takes into account not only the waste generated during synthesis but also all the substances used in the work-up phase until the product is ready for use. Therefore, it is one of the most important green metrics, parameters designed to help us quantify the "greenness" of a process and objectively compare different syntheses. An analysis of EF in the main areas of the chemical industry reveals that the petrochemical industry has the lowest EF value (EF < 0.1), primarily because it uses well-established technologies that have allowed the optimization of all process stages over time. In contrast, the pharmaceutical industry

has the highest EF (EF = 25-100) and appears to be the "dirtiest" sector.[85] One of the reasons explaining this result is related to the use of solvents. In the synthesis of an Active Pharmaceutical Ingredient (API), multiple reaction steps are typically carried out in batch processes, often using different solvents. Large quantities of materials are used in each reaction step to work up the product, which needs to be isolated in an extremely pure form. All these steps significantly increase solvent consumption (and consequently EF), which can account for 80-90% of the total mass used in the synthesis process, posing a significant environmental challenge.[86] In fact, it is estimated that 50% of total greenhouse gas emissions and 60% of energy consumption in API synthesis come from solvent usage.[87] As well, other areas related to cosmetics or food industries have the same solvent issues.[88,89] As the main sector involved, the pharmaceutical industry has been a pioneer in developing solvent selection guidelines to minimize environmental pollution caused by solvents.[90] Moving towards a future of sustainability and circular economy, catalysis (especially heterogeneous catalysis) is an excellent tool, but it is not enough. To reduce waste production, it is also necessary to work on reducing solvent consumption, by eliminating (wherever possible) or minimizing their use.

In this context, mechanochemical reactions offer a thrilling opportunity. Mechanochemistry is defined by IUPAC as a chemical reaction that is activated by the direct absorption of mechanical energy, through grinding, abrasion or fracture,[91] increasing the surface area and the contact between reactants, hence accelerating the rate of the reaction. Additionally, they occur at high local pressures and temperatures due to the kinetic energy input, making it easier to surpass the activation energy required for product formation.[92] These features allow to carry out reactions in solvent-free conditions or as a tool to assist extraction protocols under the minimum amount of solvent.[48,93] There is a wide range of applications of this new solvent-free chemistry, ranging from the synthesis of high-value-added chemicals to the design of advanced nanomaterials.[48,94,95] The instruments typically used include various types of mills such as:[95]

- Mixer mills, which employ cylindrical flasks oscillating horizontally, resulting in high impact forces between the ball bearing and the curved ends of the flask;
- Planetary mills, which use a spinning vessel on an oppositely spinning sunwheel, providing high centrifugal and frictional forces on the materials;
- Drum mills;
- Cryomills, designed for cryogenic grinding.

However, this instrumentation often limits reactions to batch processes and can pose difficulties in scaling up, confining their use mainly to the laboratory. In this context, mechanochemical technologies for continuous-flow processes have emerged. An example is the employment of twin-screw extruders, which not only allows a better control of reaction conditions but is also more suitable for industrial processes.[92,96] Literature studies demonstrate that this technology can significantly reduce the environmental footprint, as measured by the Life Cycle Assessment (LCA) of an Active Pharmaceutical Ingredient (API), in terms of E-factor and solvent usage, thus drastically reducing production costs.[97] Furthermore, depending on the instrumentation and by appropriately modifying grinding conditions (screw speed, residence time, material quantity), different results can be obtained, increasing productivity towards a specific product.[48]
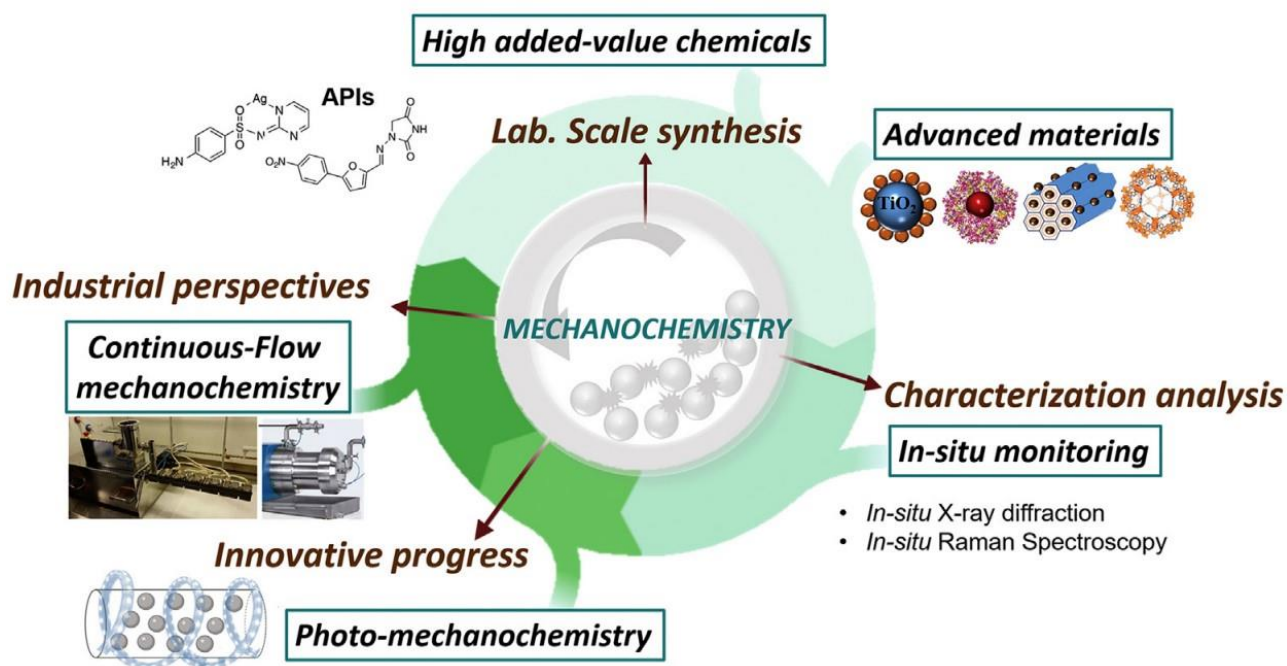
Figure 7: Schematic representation of different applications of mechanochemical technique.[92]

Considering the aforementioned premises, in this study, the biomass-derived catalytic materials prepared in this work were also tested in the Suzuki-Miyaura reaction under solvent-free conditions employing a twin-screw extruder. Additionally, new catalytic materials were synthesized through a mechanochemical approach, characterized, and tested. The results obtained were finally compared with the conventional method in solution to provide a comprehensive overview and draw final conclusions.

SCOPE OF THE THESIS

In summary, the main objectives of this thesis are outlined in the following paragraphs. Specifically, this work focuses on:

- *Valorisation of Fishery Waste*: This research aims to valorise waste from the seafood industry by utilizing chitin derived from shrimp shells, following a circular economy approach.

- *Green Synthesis of Heterogeneous Catalysts*: Aligned with one of the 12 principles of green chemistry, one of the goals of this thesis is to use chitin for the synthesis of heterogeneous catalysts composed of chitin-derived *N*-doped carbons functionalized with varying loadings of Pd nanoparticles. These catalysts can be easily recovered after use, thus reducing overall waste generation in chemical processes. These catalytic systems are synthesized using non-toxic and non-polluting methods, including impregnation (Method A) and solution methods (Method B). Additionally, catalytic systems are synthesized using a twin-screw extruder through a mechanochemical procedure, eliminating the need for solvents.

- *Characterization of Catalytic Systems*: Comprehensive characterization of the synthesized catalytic systems, including those produced using conventional Methods A and B, as well as those obtained via mechanochemistry, is conducted using a multi-technique approach, including XRD, XPS, TEM, SEM, and N_2-physisorption analysis.

- *Evaluation of the Catalytic Performance*: Evaluation of the catalytic performance of the systems formed through Methods A and B in Heck-Mizoroki and Suzuki-Miyaura reactions conducted in batch mode, with a focus on optimizing reaction conditions.

- *Mechanochemically-assisted Suzuki-Miyaura Reactions*: Testing of the prepared catalytic systems in Suzuki-Miyaura reactions using an extruder in a solvent-free mechanochemical procedure.

- *Catalyst Stability Study*: Conducting catalyst stability tests in the Heck-Mizoroki reaction with the best-performing catalyst by performing multiple recycling experiments.

Given these objectives, the overarching aim of this thesis is to contribute to the advancement of sustainable and efficient catalytic systems while simultaneously addressing the issue of waste management in chemical processes.

EXPERIMENTAL

MATERIAL AND EQUIPMENT

All chemicals employed during the reactions and the synthesis of catalysts were commercially available compounds sourced from Sigma-Aldrich and are presented in Table 1. If not otherwise specified, reagents and solvents were employed without further purification. Gas Chromatography-Mass Spectrometry (GC-MS, Electron Ionization (EI), 70 eV) analyses were performed on a HP5-MS capillary column (L = 30 m, Ø = 0.32 mm, film = 0.25 mm). GC (flame ionization detector; FID) analyses were performed with an Elite-624 capillary column (L = 30 m, Ø = 0.32 mm, film = 1.8 mm). All reactions were performed in duplicate to verify reproducibility.

Quantification analysis to determine conversion values was performed by ^{1}H-NMR in the Bruker Avance III HD 400 WB equipped with a 4 mm CP/MAS probe, employing deuterated chloroform. Furthermore, the identification of the obtained products was performed by GC-MS in the Agilent 7820 A GC/5977B High Efficiency Source (HES) MSD.

Table 1. Chemicals employed in this work.

REAGENTS	MOLECULAR WEIGHT (u.m.a.)	SOLVENTS	MOLECULAR WEIGHT (u.m.a.)
Iodobenzene	204.02	H_2O	18.02
4-iodoacetophenone	246.05	Methanol	32.04
4-iodoaniline	219.03	Ethanol	46.07
4-iodoanisole	234.04	γ-Valerolactone	100.12
3-iodobenzonitrile	229.02	Acetonitrile	41.05
Bromobenzene	157.01	Ethyl acetate	88.11
3-Bromotoluene	171.04	Methyl-THF	86.13
4-Bromotoluene	171.04	BASES	MOLECULAR WEIGHT (u.m.a.)
4-chloroiodobenzene	238.46	Triethyl amine	101.19
4-chlorotoluene	126.59	Potassium carbonate	138.21
4-chloronitrobenzene	157.56	Sodium carbonate	105.99
Phenylboronic acid	121.93	OTHER	MOLECULAR WEIGHT (u.m.a.)
p-tolilboronic acid	135.96	Chitin	221.21*
m-tolylboronic acid	135.96	2-propanol	60.10
4-metoxyphenylboronic acid	151.96	ethylene glycol	62.07
Methylacrylate	86.09	Pd(OAc)$_2$	224.50
Ethylacrylate	100.12	EDTA	292.24

*Referred to molecular weight of the strucural unit N-acetilglucosamine

SYNTHESIS OF CATALYTIC MATERIALS

N-doped carbon-supported Pd nanoparticles were synthesized with different amounts of Pd precursor, to achieve loadings of 1%, 2.5% and 5% (w/w). In order to reach these concentrations during the synthesis, 0.1, 0.25 and 0.5 mmol of Palladium acetate ($Pd(OAc)_2$) were employed, respectively. According to the procedure in the article of Rodriguez-Padron et al.[50], catalytic systems were obtained employing two different protocols: impregnation and solution methods, labelled respectively as procedure A and B.

A. *Impregnation method*. Firstly, the proper amount of $Pd(OAc)_2$ was dissolved in 2-propanol (15 mL) and subsequently, chitin (5 g) was added into the solution. The materials were left to age overnight at room temperature and further oven dried at 100 °C under vacuum. Finally, the samples were thermally treated at 500 °C (heating rate was 5 °C/min) for 1 hour under N_2 flow (10 mL min^{-1}). The catalytic samples achieved by this procedure were labelled as **Pd/CNi**.

B. *Solution method*. The proper amount of $Pd(OAc)_2$ was dissolved in 2-propanol (60 mL), together with EDTA (1 g). Subsequently, chitin (5 g) was added to the mixture, which was kept under stirring for 9 h at 80 °C under reflux. The suspension was filtered and the so-obtained solid was dried at 100 °C overnight and, finally, heated at 500 °C for 1 h, according to the conditions previously described. The catalytic sample achieved by this procedure was labelled as **Pd/CNs**.

The resulting materials were ground to powder (particle size <200 µm) and stored in the oven (70 °C, 15 mbar) until further use. The yield of the obtained materials was ca. 35 ± 5%, based on the total weight of chitin and the metal precursor used.

CHARACTERIZATION OF CATALYTIC MATERIALS

The crystalline structure of the samples was investigated by X-ray diffraction (XRD) in a D8 Advance diffractometer from Bruker® AXS, using the X-ray source of the Cu Kα radiation, coupled to a LynxEye detector, and monitoring the 2θ within 8–80° at a rate of 0.08° min^{-1}.

The chemical composition on the surface of the solids was examined using X-ray Photoelectron Spectroscopy (XPS) with a Physical Electronics VersaProbe II Scanning XPS Microprobe. This equipment uses a monochromatic X-ray Al Kα radiation source under a vacuum of 10−7 Pa. The

binding energies were calibrated to the C1s peak from adventitious carbon at 284.8 eV. High-resolution spectra were recorded using a concentric hemispherical analyzer at a constant energy pass of 29.35 eV over a 200 μm diameter analysis area. The pressure in the analysis chamber was maintained below $5 \times 10-6$ Pa. Data acquisition and analysis were performed using PHI ACCESS ESCA-F V6 software. A Shirley-type background was subtracted from the signals, and the recorded spectra were analyzed with Gauss–Lorentz curves to determine the binding energy of the atomic levels of different elements more accurately.

The textural properties, i.e., surface area, the volume of the pore and pore size, were determined from N_2 physisorption at 77 K, performed in an ASAP 2000 instrument from Micromeritics®. The samples were outgassed at 120 °C for 2 h. Then, adsorption–desorption isotherms were recorded at −196 °C. The specific surface areas were calculated by the BET method; the pore volumes were calculated from adsorption isotherms and the pore size distributions were estimated using the Barrett, Joyner and Halenda (BJH) algorithm available as built-in software from Micromeritics (Micromeritics Instrument Corporation (Norcross, GA, USA)).

SEM-EDX images were acquired in a JEOL-SEM JSM-7800 LV scanning microscope. Transmission electron microscopy (TEM) was performed to observe the size and shape of the particles in a JEOL 2010 operated at an acceleration voltage of 200 kV and with a FEI Tecnai G2 system, equipped with a charge-coupling device (CCD) camera. Samples were ground and then suspended in ethanol, followed by dipping of a holey-carbon coated copper grid of 300 mesh which was left to dry under air for a few minutes prior to recording.

The exact amount of Pd presented in the catalytic systems was obtained through ICP-OES analysis carried out in the Avio 550 Max ICP-OES Optical Emission Spectrometer.

CATALYTIC EXPERIMENTS

Catalytic experiments were carried out in sealed test tubes. In a typical Heck-Mizoroki cross coupling reaction, 10 mg of the catalyst was added, followed by iodobenzene (1 mmol, 112 μl), ethyl acrylate (1.5 mmol, 160 μl), and triethyl amine (1 mmol, 140 μl) in the stated order. Subsequently, γ-Valerolactone (GVL, 2 ml) was introduced into the mixture. The solution was then sealed and stirred at 125 °C for 4 hours. After the reaction, the catalyst was separated from the solution through filtration. Quantification analysis to determine conversion values was performed by ^{1}H-NMR, employing deuterated methanol. Furthermore, the identification of the obtained products was performed by GC-MS in the Agilent 7820 A GC/5977B High Efficiency Source (HES) MSD.

In a typical Suzuki-Miyaura cross coupling reaction, 10 mg of the catalyst was added, followed by potassium carbonate (K_2CO_3, 0.5 mmol, 70 mg), iodobenzene (0.25 mmol, 26 μl) and phenylboronic acid (0.35 mmol, 43 μl), in the stated order. Subsequently, ethanol (3 ml) was introduced into the mixture. The solution was then sealed and stirred at 80 °C for 4 hours. After the reaction, the catalyst was separated from the solution through filtration. Quantification analysis to determine conversion and selectivity values was performed by gas chromatography (GC) using a flame ionization detector (FID). The measurements were accomplished in the Agilent 6890 N gas chromatograph (capillary column HP-5, 60 mL min^{-1} N_2 carrier flow, 20 psi column top head pressure). The identification of the obtained products was performed by GC-MS in the Agilent 7820 A GC/5977B High Efficiency Source (HES) MSD.

MECHANOCHEMICAL APPROACH: EXPERIMENTAL

SYNTHESIS OF CATALYTIC MATERIALS

The materials were synthesized using a mechanochemical extrusion method. This involved the use of chitin (5 g), Pd(Ac)$_2$ (0.5 mmol), and ethylene glycol (15 mL). The mixture was extruded in a ZE 12 HMI Twin-Screw Extruder (Three Tec, Seon, Switzerland) at a temperature of 200 °C and a speed of 50 rpm. The resulting material was then dried in an oven at 100°C under vacuum overnight before being used in catalytic tests. Additionally, a thermal treatment was performed at 500°C for 1 h under a flow of N_2 (10 mL/min) for further comparison. The heating rate for this process was 5 °C.

The synthesis process was also carried out with the addition of Na_2CO_3 (0.5 mmol) under the previously described conditions.

CATALYTIC EXPERIMENTS

A typical CF-Mechanochemical Suzuki-Miyaura cross-coupling reaction was carried out to evaluate the performance of the catalysts. The reaction was conducted under continuous flow conditions using a ZE 12 HMI extruder from Three Tec. The reaction involved iodobenzene (2 mmol), PhB(OH)$_2$ (3 mmol), K_2CO_3 (4 mmol), and the chosen catalysts (40 mg). The mass loading, temperature, time of reaction, and speed of rotation of extruder were optimized. The conversion and selectivity were determined using GC-FID after an extraction with a minimum amount of ethanol, while the product structures were identified using GC-MS.

RESULTS AND DISCUSSION

SYNTHETIC APPROACH

Two strategies were employed to attempt the incorporation of palladium nanoparticles onto the chitin matrix, which would serve as a source of carbon and nitrogen. The first approach (referred to as method A) involved the impregnation of chitin at room temperature with a minimal quantity of 2-propanol containing palladium acetate ($Pd(OAc)_2$). The second approach (Method B) entailed dispersing chitin in a larger volume of 2-propanol (70 mL), which also contained palladium acetate. The mixture was then maintained at 80 °C with continuous stirring for a duration of 9 hours. In both protocols it was employed the proper amount of $Pd(OAc)_2$ in order to achieve Pd loadings of 1%, 2.5% and 5% leading to catalytic systems labelled as **1Pd/CNi**, **2.5Pd/CNi**, **5Pd/CNi** for those obtained with method A, and **1Pd/CNs**, **2.5Pd/CNs**, **5Pd/CNs** for those obtained with method B, respectively. Method A, while environmentally friendly owing to its minimal solvent usage, does have drawbacks, such as lack of homogenous distribution and limited control over particle size. Conversely, Method B employs a deposition-precipitation technique, providing superior control over nanoparticle morphology, size, and dispersion. The subsequent sections will dive into the results obtained from each method and provide a comparative analysis. *N*-doped carbon systems were chosen as support materials based on recent studies that suggest enhanced stability of metal entities due to metal-nitrogen interactions. To ensure optimal dispersion of the nanoparticles, EDTA was employed as a metal complexing agent in method B. Chitin extracted from shrimp shells was selected as a sustainable source of nitrogen and carbon due to its abundant availability. Despite its low solubility, which presents challenges in various applications, this work proposes a strategy to harness its potential, thereby adding value to a significant byproduct of the seafood supply chain, in alignment with the principles of a circular economy.
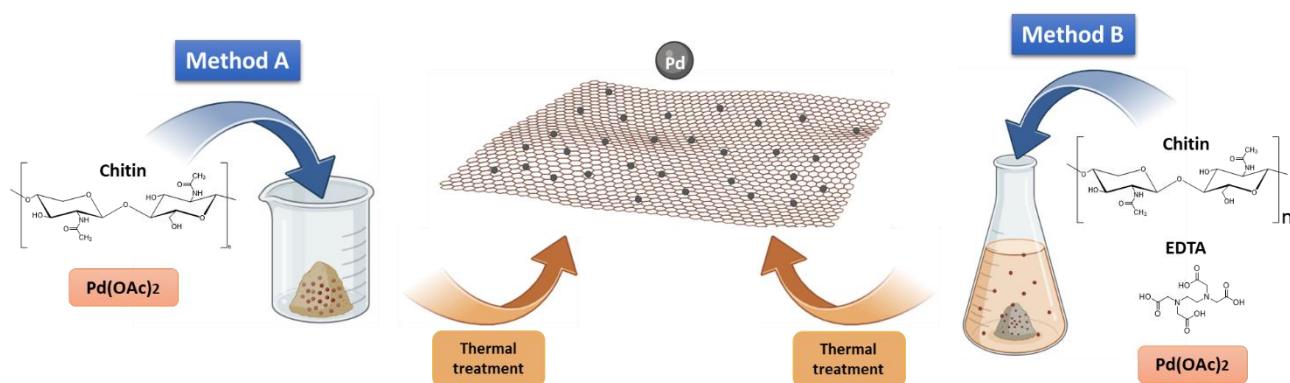
Figure 8: Schematic representation of the synthetic strategies considered for the preparation of Pd/CN materials.

MATERIALS CARACTERIZATION

The characterization of the catalytic systems was accomplished through a multi-technique approach, with the majority of the characterization analyses being conducted at the Department of Inorganic Chemistry at the University of Malaga, Spain, which has well-stablished collaborations with our group at Ca' Foscari University. This department has well-established collaborations with our group at Ca' Foscari University.

The crystal structure and arrangement of the synthesized materials were examined through XRD analysis, as depicted in Figure 9. Notably, all the XRD patterns of the materials displayed consistent characteristics. A common signal observed was a broad band around 24.0°, indicating the presence of amorphous carbon, particularly on the (002) crystallographic plane associated with stacked graphene-like sheets.[98] All the sample displayed sharp and well-defined signals located at 39.9°, 46.5°, and 67.9° corresponding to the (111), (200), and (220) planes of Pd(0) with a face-centred cubic crystal structure.[99] The expected gradual decrease in signal intensity with decreasing Pd loading was confirmed by the XRD spectra. The XRD pattern of the **Pd/CNs** materials seem to exhibit slightly broader peaks, mostly noticeable in the sample with a higher loading. This observation could suggest smaller sizes of the Pd metal nanoparticles in the samples obtained through method B compared to those obtained with method A. To validate this hypothesis, we conducted microscopic analysis on the two samples where the difference was most pronounced (**5Pd/CNi** and **5Pd/CNs**).
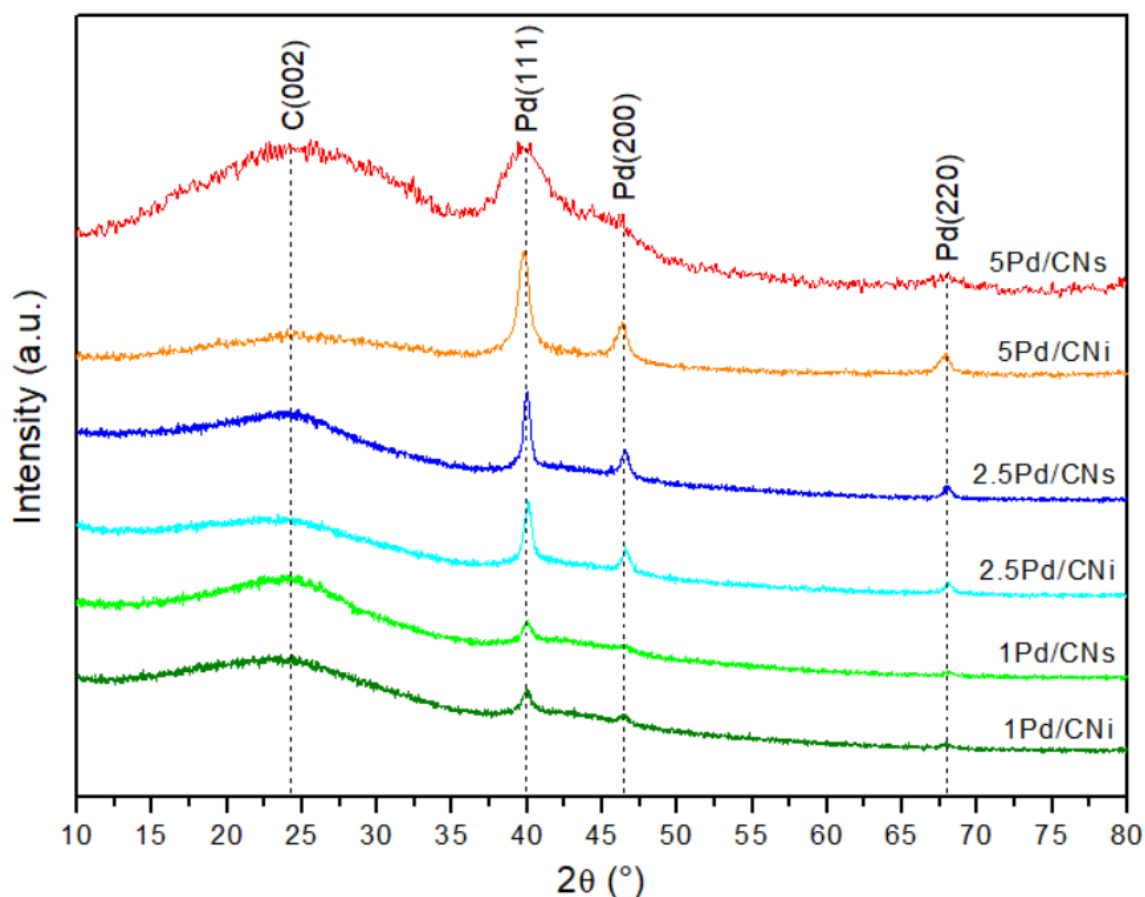
Figure 9: XRD analysis of catalytic systems obtained with method A and B.

The morphology of the catalytic materials, containing a 5% Pd loading, was analysed using TEM, and the resulting micrographs are presented in Figure 10. Both **5Pd/CNi** (Figure 10A) and **5Pd/CNs** (Figure 10B) exhibited highly uniform and well-dispersed palladium nanoparticles supported on a laminar *N*-doped carbon matrix. Remarkably, the average diameter of the nanoparticles was notably smaller for the sample prepared using Method B. Specifically, **5Pd/NCi** exhibited an average radius of (11.3 ± 1.0) nm, whereas **5Pd/NCs** displayed a much smaller average radius of (2.6 ± 1.0) nm. These findings corroborate the hypothesis presented in the XRD analysis, underscoring the substantial influence of the synthesis method on the ultimate morphology of the samples. These results are consistent with previous reports in the literature and confirm that the solution-based method can yield superior control over the size and morphology of the prepared nanoparticles.
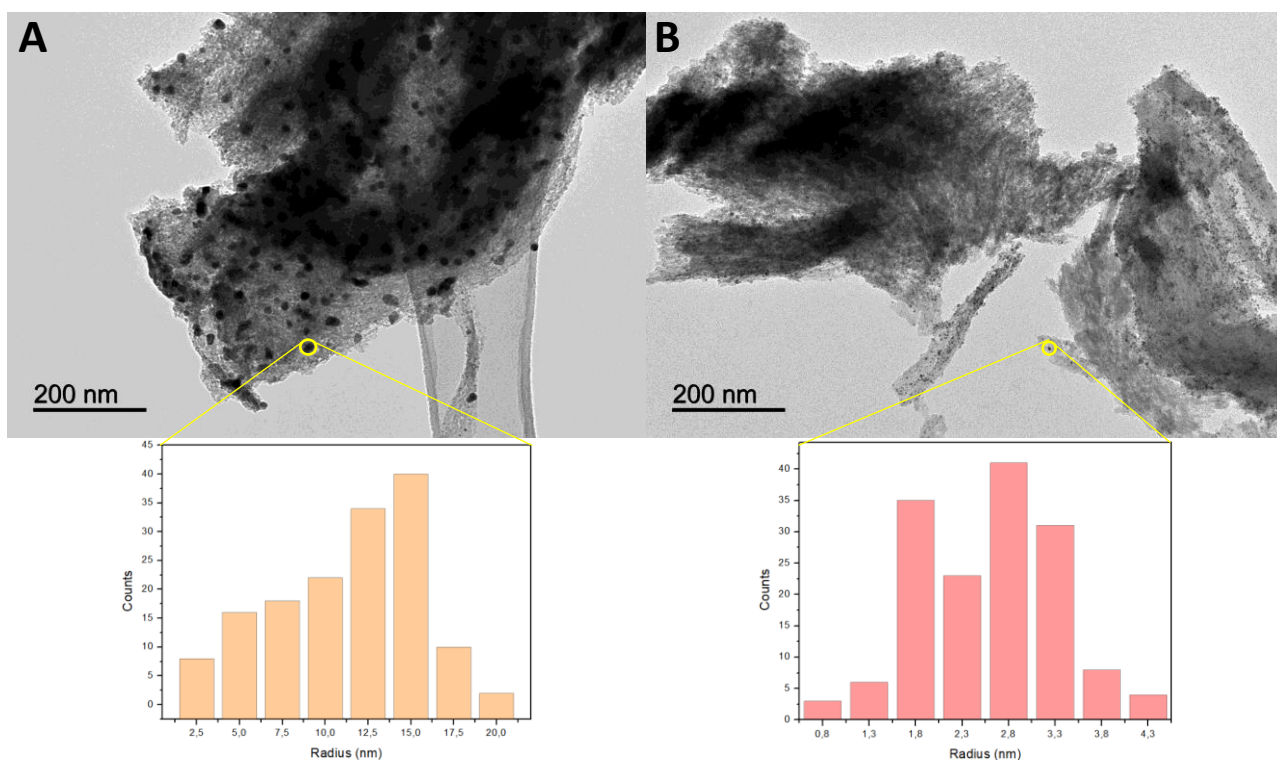
Figure 10: TEM analysis of catalysts **5Pd/CNi** and **5Pd/CNs** with the respectively distribution of pores size.

Further insights into the morphology and elemental composition of the samples were gained through SEM-mapping analysis (Figure 11), which validated the successful incorporation of palladium entities into the *N*-doped carbon matrix. SEM-mapping measurements confirmed the presence of carbon, nitrogen, oxygen, and palladium in both catalytic samples, with all elements being uniformly distributed in each case. Additionally, SEM images of **Pd-N/Ci** and **Pd-N/Cs** samples, as shown in Figure 11A and 11F, revealed a 3D-irregular arrangement with certain porosity and a rugose-like morphology.
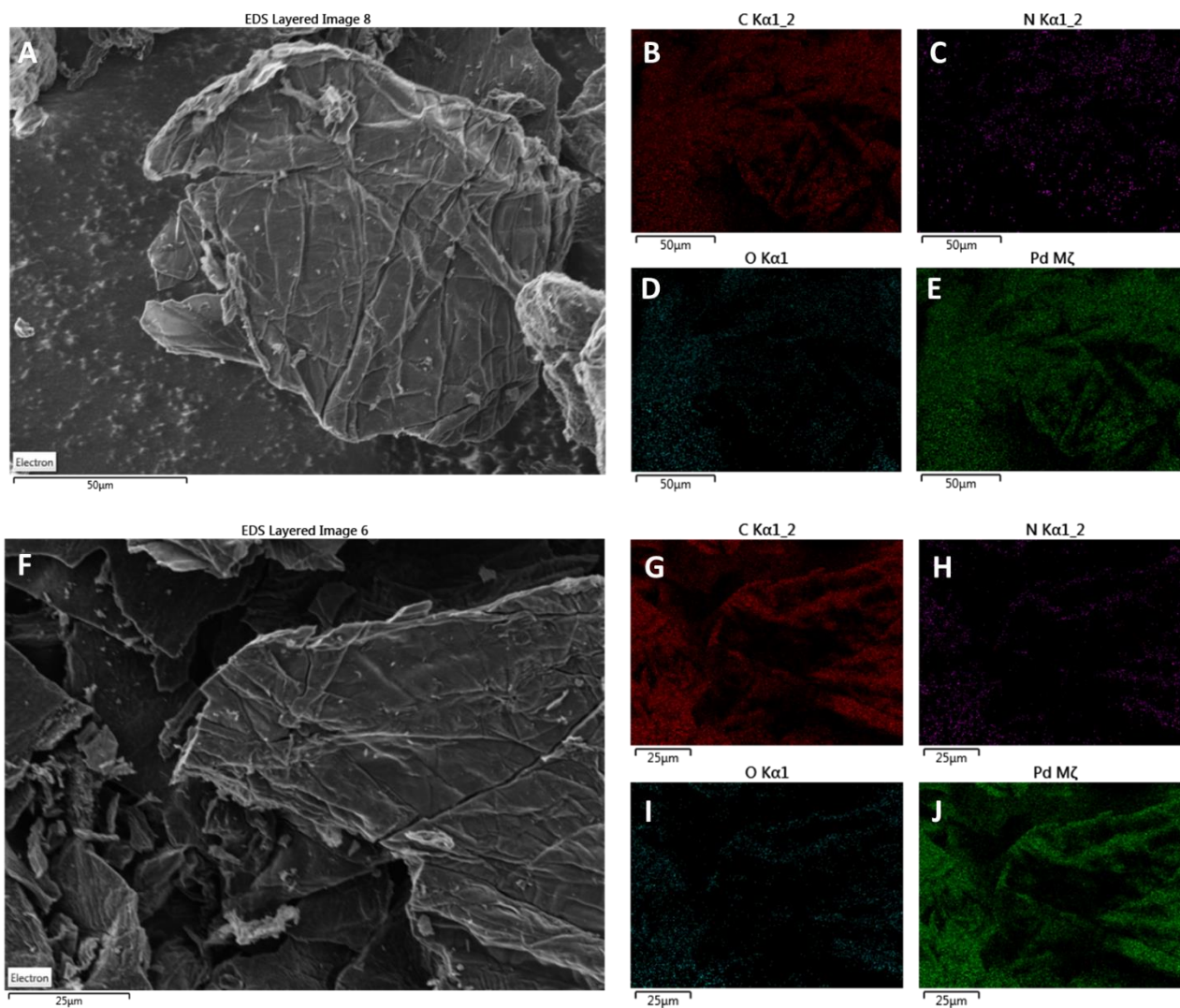
Figure 11: SEM-mapping micrographs of **Pd/CNi** and **Pd/CNs** materials. SEM images of **Pd/CNi** (A) and **Pd/CNs** (F). SEM-mapping results of **Pd/CNi** for carbon (B), nitrogen (C), oxygen (D) and palladium (E). SEM-mapping results of **Pd/CNs** for carbon (G), nitrogen (H), oxygen (I) and palladium (J).

The textural properties of the samples were examined using N_2 physisorption measurements. To determine whether and how porosity, surface area, and pore size vary with different catalytic loadings, we conducted a study using materials with the lowest and highest loadings—specifically, 5% and 1% Pd. Additionally, to explore potential differences attributed to the catalyst synthesis methodology, we included materials obtained through impregnation (Method A) and solution (Method B) in our analysis.

Firstly, as can be observed in Table 2, all the examined samples exhibit mean pore size diameters between 3.6 and 6 nm, classifying them as mesoporous materials.[45,50,100] This classification is further confirmed by experimental physisorption profiles that fit typical Type IV isotherms associated with mesoporous materials, showing adsorption behavior similar to the Brunauer-Emmett-Teller (BET)

isotherm (Type II) but with hysteresis due to capillary condensation. In this study the pore volume and the mean pore size diameter were calculated employing the Barret-Joyner-Halenda (BJH) model, which considers not only the Kelvin radius but also the monolayer thickness, giving a more realistic response.
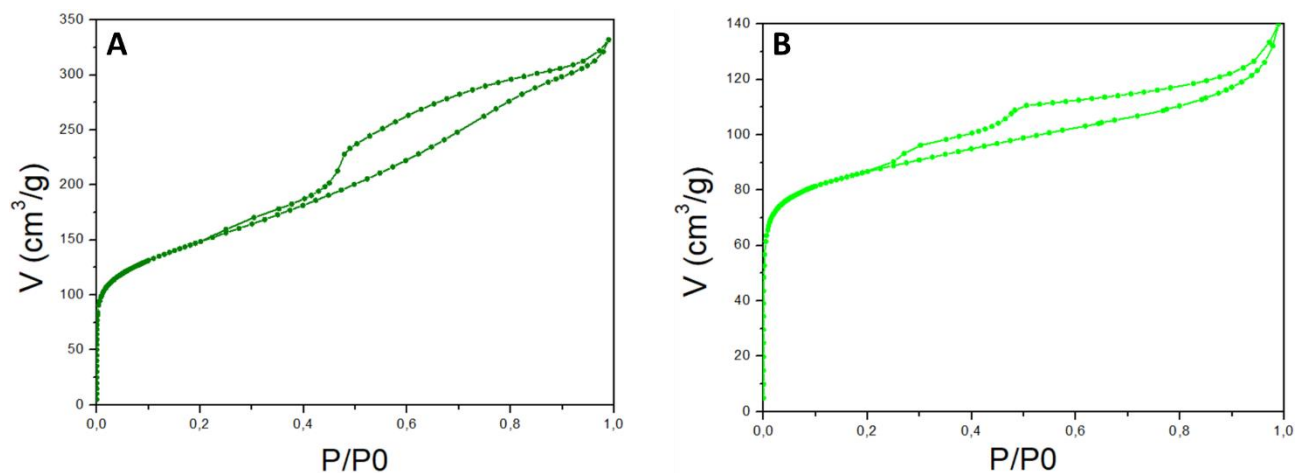
Figure 12: Representative N_2 physisorption of catalytic systems 1Pd/CN obtained with method A (Figure 12A) and B Figure 12B).

In particular, **5Pd-N/Ci** and **5Pd-N/Cs** catalysts exhibit similar mean pore size diameters (4.3 nm and 4.0 nm, respectively), surface area values (300 m^2/g and 311 m^2/g, respectively), and pore volume values (0.25 m^3/g and 0.28 m^3/g, respectively) (Table 2, entry 2 and 3). For comparison, chitin was treated under similar calcination conditions, and the textural properties of the resulting *N*-doped carbon are also provided in Table 2, entry 1. These results could suggest that the textural characteristics of the samples were primarily influenced by the carbon-nitrogen matrix and the calcination protocol, while the metal entities and their incorporation strategies had a minimal impact.

However, unexpectedly divergent values were observed for the materials modified with 1 wt.% of palladium. Specifically, **1Pd/CNi** displayed smaller mean pore sizes but larger surface area and pore volume (3.6 nm, 526 m^2/g, and 0.48 cm^3/g, respectively). In contrast, the **1Pd/CNs** catalytic system exhibits larger mean pore sizes while maintaining a higher surface area but with a lower pore volume (6 nm, 402 m^2/g, and 0.19 cm^3/g, respectively). Examining the average pore size in the **1Pd/CNi** and **1Pd/CNs** systems, we can postulate that in the instance of catalysts synthesized using Method A, Pd nanoparticles diffusion into the smaller pores is hindered by the limited solvent volume. Instead,

they tend to preferentially deposit within the larger pores. As a consequence, there is no pore occlusion, but rather a general reduction in pore size is observed.

In any case, these results demonstrated that, in general, the incorporation of Pd loading leads to an increased surface area of the material, in comparison with the metal-free counterpart. Recent studies have reported that the presence of Pd nanoparticles on a graphene-like support is responsible for creating nanoholes on the graphene sheets, thereby positively impacting the surface area and textural properties overall.[101] A similar hypothesis could be assumed in this case, in order to explain the higher surface area of the samples modified with 1 wt.% of palladium. However, this effect on the surface area is compensated when higher palladium loading (5% Pd materials) is used, most likely due to the partial occlusion of pores. Regardless these considerations, the materials retained excellent textural properties, which could further favour their catalytic performance as will be discussed in subsequent sections.

Table 2: Textural properties obtained by N_2-Physisorbtion of different synthesised catalytic system.

Material	S_{BET} (m^2/g)	D_{BJH} (nm)	V_{BJH} (cm^3/g)
C-N	320	3.9	0.35
5Pd/CNi	300	4.3	0.25
5Pd/CNs	311	4.0	0.28
1Pd/CNi	526	3.6	0.48
1Pd/CNs	402	6.0	0.19

* S_{BET}: specific surface area was calculated using the Brunauer-Emmett-Teller (BET) equation. D_{BJH}: mean pore size diameter was calculated using the Barret-Joyner-Halenda (BJH) equation. V_{BJH}: pore volumes were calculated using the Barret-Joyner-Halenda (BJH) equation.

The chemical composition and surface properties of a catalytic material wield considerable influence over heterogeneous catalysis processes. To understand the chemical nature and elemental composition on the surface of prepared catalysts, XPS analyses were performed, and the results are illustrated in Figure 13 and Figure 14. In a manner akin to the analysis conducted for physisorption, in this instance, we have scrutinized representative materials obtained through both

Method A and B, with Pd loadings of 1% and 5%. XPS spectra consistently exhibited the presence of carbon, oxygen, nitrogen, and palladium on the surface of all catalyst materials. Specifically, the C1s XPS regions of the materials modified with 5 wt.% palladium loading (Figure 13A, 13E) were deconvoluted into five contributions situated at (284.3 ± 0.2) eV, (285.7 ± 0.2) eV, (287.2 ± 0.2) eV, (288.6 ± 0.2) eV and (290.0 ± 0.2) eV, attributed to C–C/C=C bonds from graphitic and/or aromatic carbon, C–OH, C–N/C–O, C=O and CO_3^{2+} species, respectively. Conversely, the latter contribution was absent in the case of the 1 wt.% palladium samples, exhibiting only four signals attributed to C–C/C=C bonds from graphitic and/or aromatic carbon, C–OH, C–N/C–O, and C=O. (Figure 14A and 14E). This observation suggests the likelihood of carbon dioxide formation resulting from the decomposition of the organic matrix, a phenomenon likely induced by the higher palladium content present in the samples with a 5 wt.% palladium loading.

The N1s XPS region (Figure 13B, 13F, 14B and 14F) showed two main bands typically attributed to pyridinic and pyrrolic nitrogen species, at (398.4±0.2) eV and (400.3±0.2) eV. It is worth noting that these N-functionalities, particularly pyridinic groups, could serve as active sites in base-catalysed reactions, such as CO_2 fixation reactions.[47] Additionally, the presence of nitrogen entities could enhance the incorporation and dispersion of metal nanoparticles. Interestingly, graphitic N-groups were not found on the surface of these materials.

The O1s XPS spectra of the samples, shown in Figure 13C, 13G, 14C and 14G for the **5Pd-N/Ci**, **5Pd-N/Cs**, **1Pd/CNi** and **1Pd/CNs** samples, respectively, were deconvoluted into two main contributions. These components, located at (531.2±0.2) eV and (533.2±0.2) eV, are attributed to O-Metal bonds in metal oxides and to the presence of adsorbed H_2O in the catalyst structure, respectively.

Finally, the chemical nature of palladium entities on the catalyst surface was evaluated employing the Pd3d region of the XPS spectra (as shown in Figure 13D, 13H, 14D and 14H). The signals were deconvoluted into four contributions located at (335.1 ±0.2) eV, (336.2±0.2) eV, (340.3±0.2) eV and (341.5±0.2) eV. In particular, the signals at approximately (335.1 ±0.2) eV and (340.3±0.2) eV were associated with Pd3$d_{5/2}$ and Pd3$d_{3/2}$ of Pd (0), respectively; while the band shoulders contributions located at binding energy values of (336.2±0.2) eV and (341±0.2) eV indicated the presence of Pd (II) species of palladium oxide on the catalyst surface. By analysing the XPS data in conjunction with the XRD results, it becomes evident that the synthesized nanoparticles primarily consist of a metallic Pd (0) core, while the surface exhibits partial oxidation.
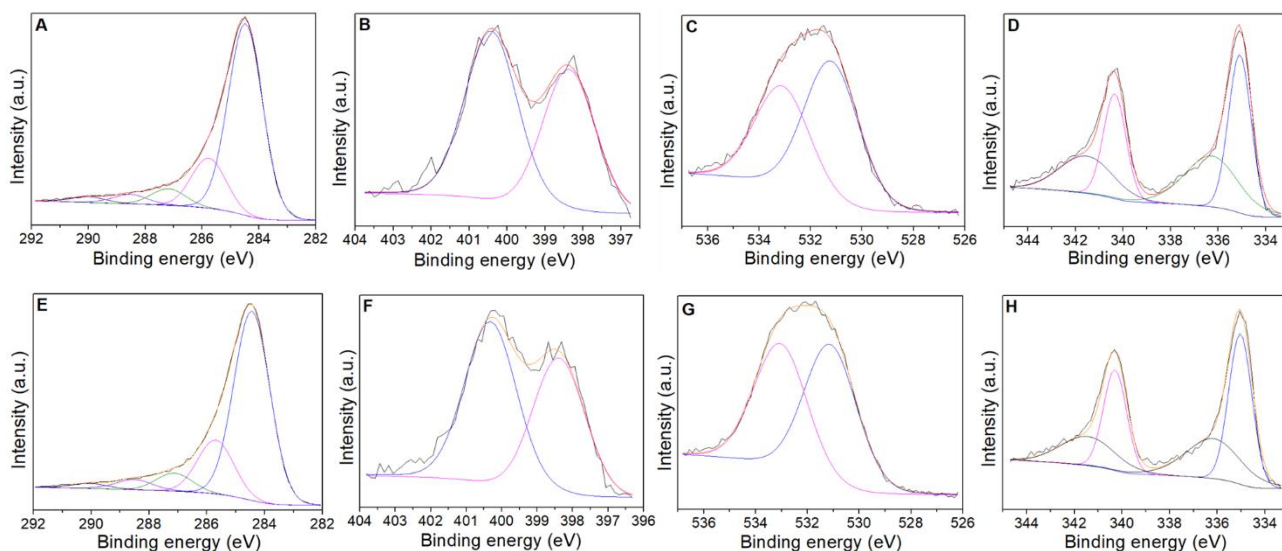
Figure 13: XPS spectra of **5Pd/CNi** (A-D), **5Pd/CNs** (E-H). For each catalytic system, it is represented in this order the C1*s* (A, E), N1*s* (B, F), O1*s* (C, G) and Pd3*d* (D, H) XPS regions.
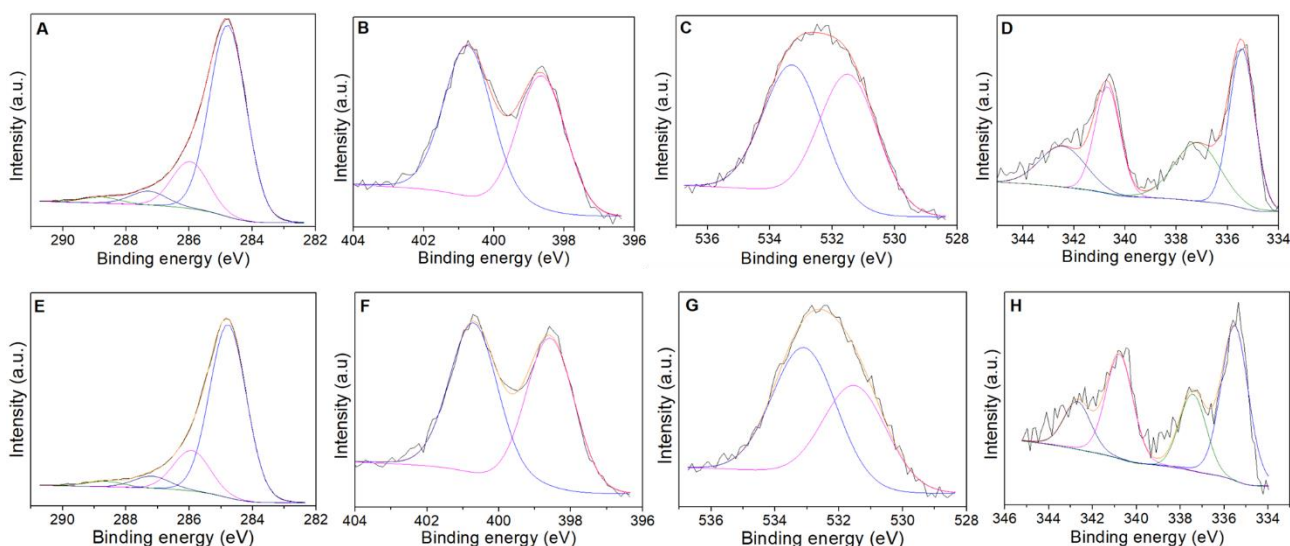
Figure 14: XPS spectra of **1Pd/CNi** (I-N), **1Pd/CNs** (O-R). For each catalytic system, it's represented in this order the C1*s*, N1*s*, O1*s* and Pd3*d* XPS regions.

XPS quantification analysis was carried out to ascertain the metal content on the catalysts' surface, and the findings are detailed in Table 3. Furthermore, ICP measurements were conducted to determine the palladium concentration in the bulk samples, as also documented in Table 3. The weight percentage of total palladium found for the bulk material, as confirmed by ICP-OES results, was consistent with the expected percentages based on the amounts of metal and carbon precursors employed in each synthetic methodology (A and B). Notably, the palladium concentration on the surface, as assessed via XPS, was slightly higher in comparison to the ICP-OES

data. These results likely indicate a uniform dispersion of the metal entities within the materials, with a higher concentration residing on the surface of the carbonaceous materials.

Table 3: XPS Binding energy and Palladium concentration according to XPS and ICP-OES results.

Sample	Pd (0) $3d_{5/2}$/eV	Pd (II) $3d_{5/2}$/eV	Pd wt.% (XPS)	Pd wt.% (ICP-OES)
5Pd-N/Ci	335.1	336.4	7.5	5.4
5Pd-N/Cs	335.1	336.2	7.6	4.9
1Pd-N/Ci	335.1	336.4	1.5	1.1
1Pd-N/Cs	335.1	336.2	1.6	1.1

CATALYCIC ACTIVITY

The previously synthesized and characterized catalytic systems were tested in two cross-coupling reactions: the Heck-Mizoroki and Suzuki-Miyaura reactions. A comprehensive analysis of their catalytic performance will be presented in the subsequent sections.

HECK-MIZOROKI REACTION

In the Heck reaction, the following components were added in the specified sequence: 10 mg of the catalyst, 1 mmol of iodobenzene, 1.5 mmol of ethyl acrylate, 1 mmol of triethylamine, and 2 ml of GVL, all in an open-air vial. The Heck reaction typically requires relatively high temperatures, and in the literature, polar aprotic solvents with high boiling points have commonly been employed to dissolve the involved reagents. Solvents such as DMF, DMA, or N-methylpyrrolidone are frequently used for this purpose.[102] However, these solvents are toxic, and they pose disposal challenges when they dissolve in water. In this regard, GVL can be an interesting alternative due to its comparable polarity and boiling point (207°C), along with the added benefit of being non-toxic and derived from biomass.[102] Considering such premises, GVL was chosen as solvent in this work. The initial reaction conditions were determined based on two articles by Perosa et al. and Strappaveccia et al..[102,103] The reaction products were identified via GC-MS, where secondary products were rarely observed, confirming the high selectivity of these types of cross-coupling reactions.

Quantification analysis of the reaction, in order to determine the conversion of iodobenzene to the cross-coupling product (ethyl cinnamate) was achieved using ^{1}H-NMR spectroscopy, with deuterated chloroform as solvent. This approach has been used in an article by Melchiorre et al. (see Figure 15).[104] In that study, by analyzing ^{1}H-NMR spectra, they identified a characteristic signal of iodobenzene at around 7.5 ppm (labeled as b) and one characteristic signal of ethyl cinnamate at around 7.1 ppm (labeled as a), allowing the calculation of conversion using the equation displayed below. For the yield, a known quantity of mesitylene was used as a standard, and the equal relaxation time (and therefore signal) of protons with different chemical environments was exploited, following the procedure previously described by Rigo et al., properly modified for the reaction under consideration.[105]

$$Yield\ (\%) = 100 \times \frac{\left(\dfrac{3 \times Nstd \times AHa}{5 \times AHs}\right)}{N_0}$$

Equation 1: N_{std}: amount of internal standard (mesitylene, mol); AHa: integral of the area corresponding to the signal of product (5H); AHs: integral of the area corresponding to the signal of internal standard (3H); N_0: amount of iodobenzene at t_0 (mol).

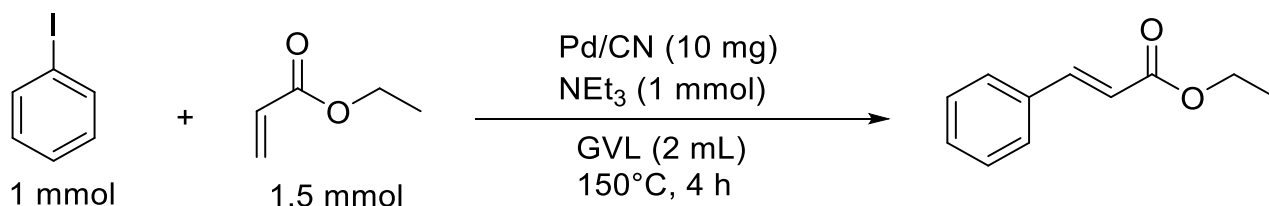$$Conversion\ (\%) = \left(\frac{\int b}{\int a + \int b}\right) \times 100$$

Equation 2: a: area of characteristic signal of iodobenzene; b: area of characteristic signal of ethyl cinnamate.
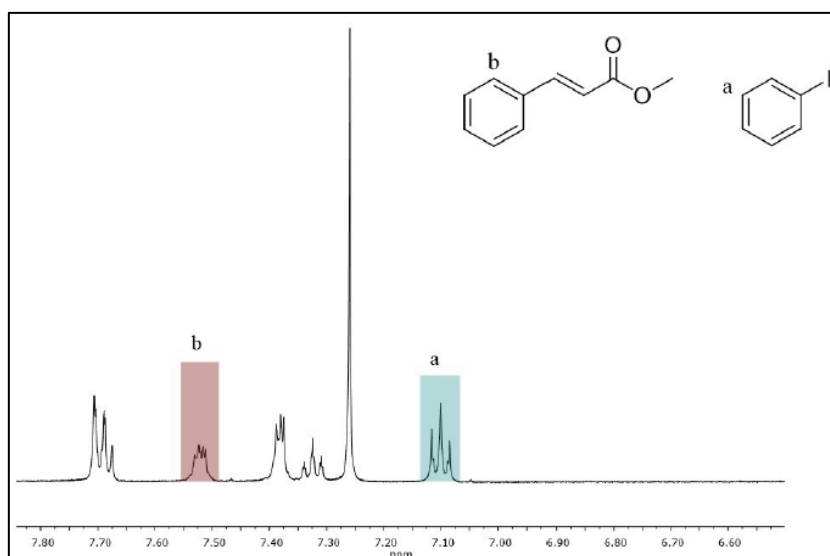
**Figure 15**: Characteristics signals of ethyl cinnamate and iodobenzene in H^1-NMR spectra.[104]

OPTIMIZATION OF PARAMETERS

Scheme 7: Heck-Mizoroki reaction considered.

Catalyst screening. Initially, a catalyst screening was carried out at 150°C for 4 hours to determine the influence of the Pd loading on the conversion and selectivity of the investigated reaction. Also, the commercial catalyst Palladium on carbon with a loading of 5% w/w (**5Pd/C**) was tested. Gratifyingly, all the tested catalysts exhibited complete conversion and yielded quantitative results. Therefore, the **1Pd/CNi** catalytic system was selected for further optimization, primarily due to its low metal loading and the environmentally friendly nature of Method A. To assess the progress of the reaction in the absence of Pd, two control experiments were conducted either in absence of any catalytic system or by using the metal-free nitrogen-doped carbon support. In both cases, minimal to no conversion were observed.
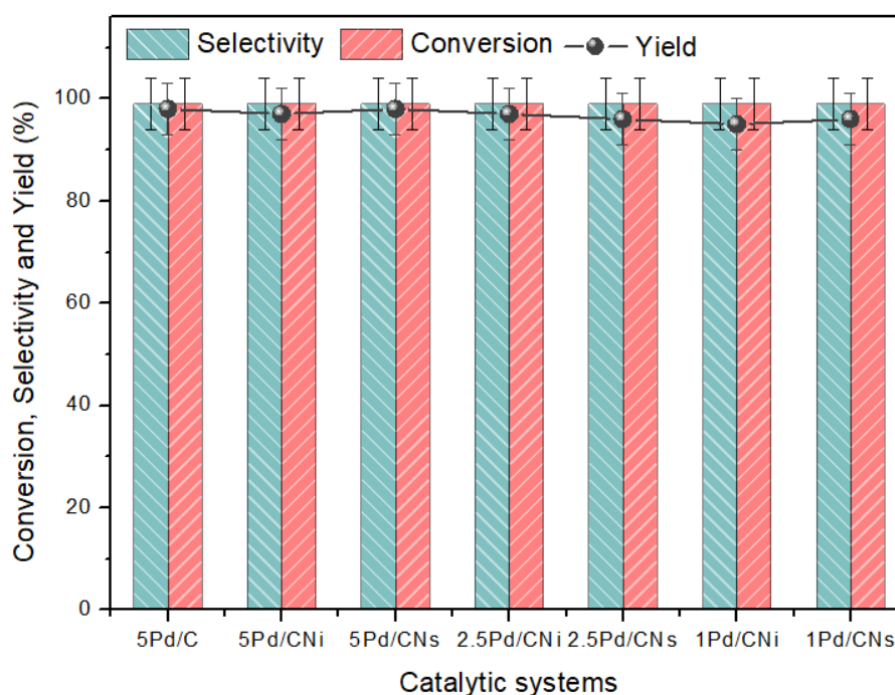

Figure 16: Catalytic screening of Heck-Mizoroki cross-coupling reaction. Iodobenzene (1 mmol), ethyl acrilate (1.5 mmol), NEt₃ (1.5 mmol), catalyst (10 mg), GVL (2 ml), 150°C, 4 hours.

Base analysis. In the Heck reaction, the use of a base plays a pivotal role by facilitating the final step of the catalytic cycle, which involves the reductive elimination of HX. This step leads to the regeneration of the catalytically active metallic Pd species. Therefore, a study was conducted to determine the influence of the base nature on the catalytic performance and on the reaction progress. Among the bases tested, including triethylamine (NEt$_3$), K$_2$CO$_3$ e Na$_2$CO$_3$, almost no significant differences were observed, unlike in the Suzuki reaction (as will be described in the following sections). Therefore, further investigations regarding the base quantity were carried out, in particular using NEt$_3$. Although the catalytic cycle consumes the base, which must be introduced in at least stoichiometric amounts relative to the limiting reagent, the objective was to investigate whether the inherent basicity of the support, primarily attributed to the presence of pyridinic N, could potentially compensate for and reduce the necessary quantity of added base. Unfortunately, no significant influence from the support was observed. In fact, when the reaction was conducted without NEt$_3$, no conversion was detected. Instead, the reaction achieved complete conversion when 1 mmol of base was used, being hence chosen as optimal for subsequent tests.
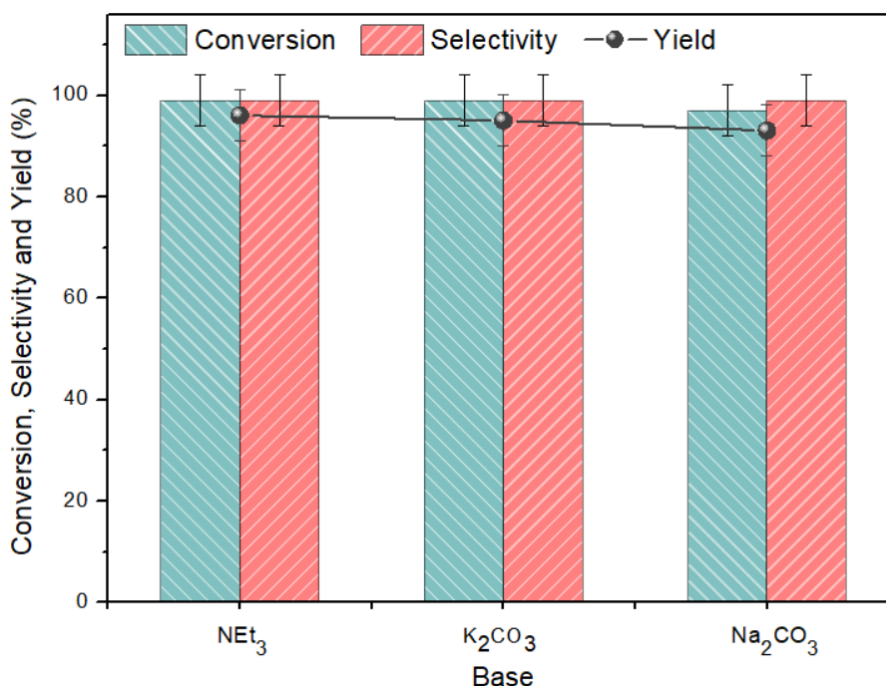

Figure 17: Different bases tested in Heck-Mizoroki reaction. Iodobenzene (1 mmol), ethyl acrilate (1.5 mmol), base (1.5 mmol), **1Pd/CNi** (10 mg), GVL (2 ml), 150°C, 4 hours.
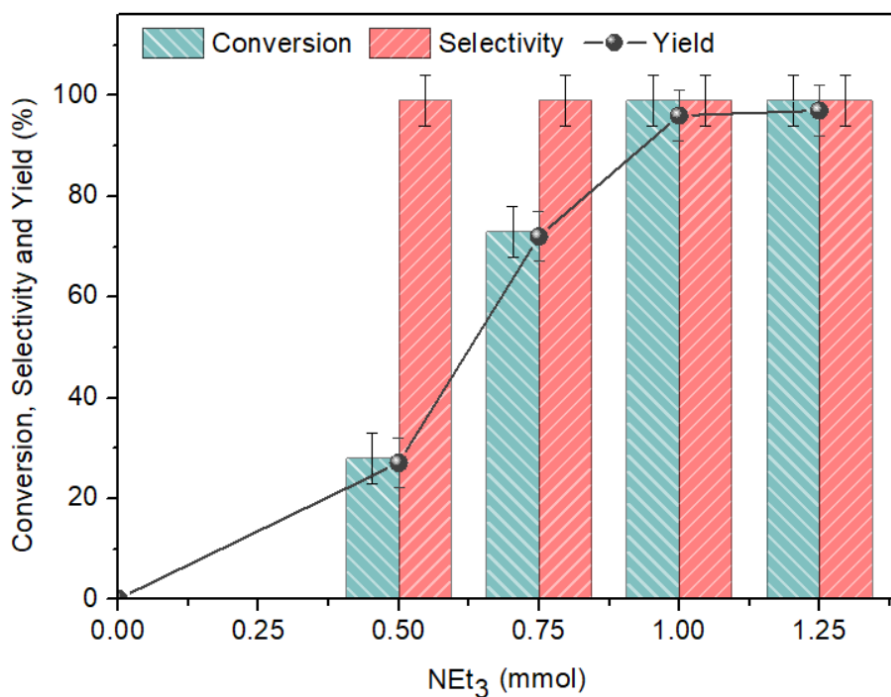
Figure 18: Different base amount tested in Heck-Mizoroki reaction. Iodobenzene (1 mmol), ethyl acrylate (1.5 mmol), **1Pd/CNi** (10 mg), GVL (2 ml), 150°C, 4 hours.

Temperature optimization. Subsequently, the optimization of temperature was carried out. Tests were conducted at 50, 75, 100, 110, 125, and 150 °C, achieving quantitative yield by performing the reaction at 125 °C. Non-significant conversion was detected at 50°C (<5%), while at 75°C the conversion reached 52%. As a high conversion (93%) was obtained at 100 °C, a test at an intermediate temperature of 110 °C was also performed; however, no significant differences were observed compared to the test conducted at 100 °C (same conversion of 93%). The Heck reaction typically requires elevated temperatures, and the results obtained align with those found in the literature.[72,102,106] Therefore, 125 °C was chosen as the temperature for further studies.
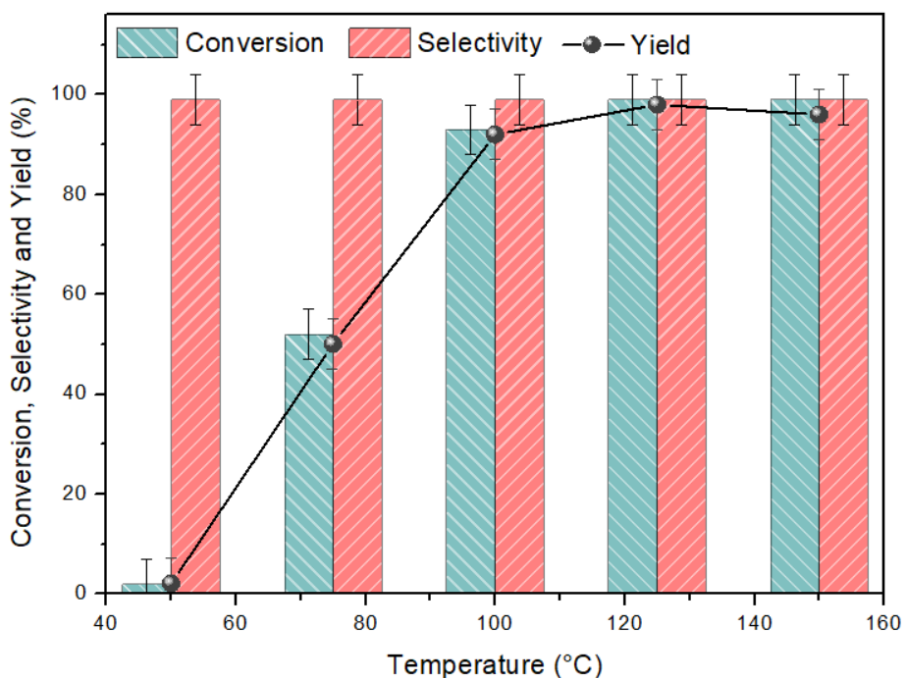
Figure 19: Temperature optimization of Heck-Mizoroki reaction. Iodobenzene (1 mmol), ethyl acrilate (1.5 mmol), NEt$_3$ (1 mmol), **1Pd/CNi** (10 mg), GVL (2 ml), 4 hours.

Time optimization. The study of reaction time was conducted at 0, 0.5, 1, 2, 3, and 4 h. During the first 30 minutes, almost no conversion was detected (<5%). Instead, after 1 h a yield of 60% was achieved. As expected, the conversion gradually increased, reaching values of 83% and 93% after 2 and 3h, respectively. Quantitative conversion was only achieved after 4 h.
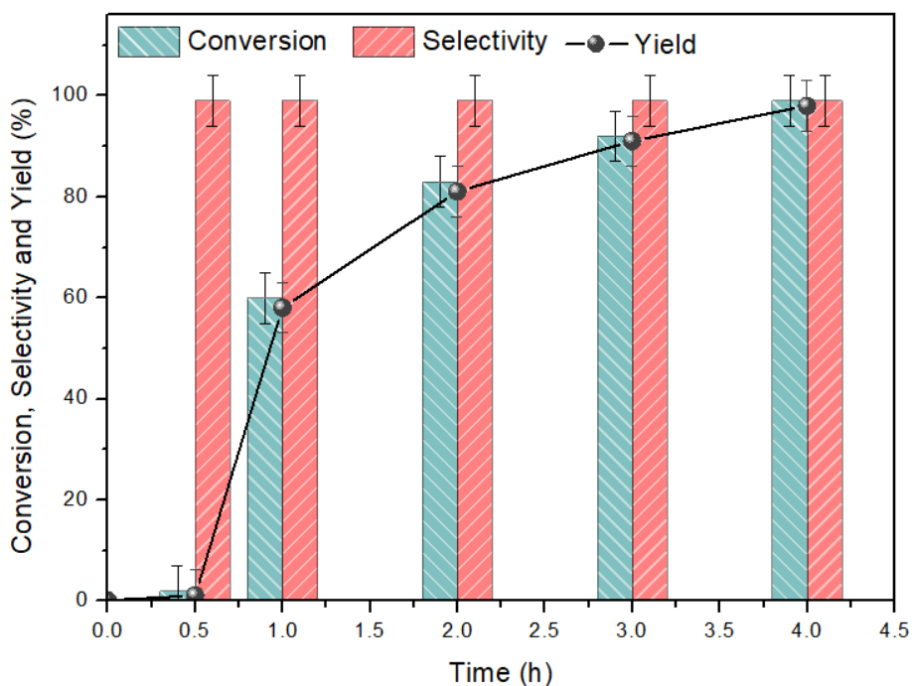
Figure 20: Time optimization of Heck reaction. Iodobenzene (1 mmol), ethyl acrilate (1.5 mmol), NEt$_3$ (1 mmol), **1Pd/CNi** (10 mg), GVL (2 ml), 125°C.

Solvent screening. After optimizing the reaction conditions, the influence of the solvent on the conversion of iodobenzene was examined. Various alternatives to GVL were tested, all with good polarity and different boiling points. In cases where the solvents boiling point was lower than the required reaction temperature (125°C), the reactions were conducted in pressurized reactors (autoclaves). Moreover, when feasible based on the solvent signal, the conversion of iodobenzene was assessed using GC-FID. The results indicate that GVL was found to be as the most favourable solvent for this type of cross-coupling, underscoring its position as a remarkable substitute for hazardous solvents such as DMF or DMA. The reaction proceeded with conversion values ranging from 60% to 70% for all solvents, with polar solvents performing notably well. Among them, ethanol exhibited the highest performance with a conversion rate of 76%, while less polar solvents, such as Methyl-THF, yielded a conversion rate of 58%. Considering that the oxidative addition step serves as the rate-determining step, a characteristic that holds true for most cross-coupling reactions, it's noteworthy that a solvent with higher polarity can effectively stabilize the highly polarized three-center transition state. This, in turn, facilitates and promotes the reaction. In water, despite good conversion (70%), the selectivity was only 60% toward ethyl cinnamate due to partial hydrolysis of the ester to the corresponding carboxylic acid (cinnamic acid). Finally, the neat reaction showed promising results with a conversion of 77%.
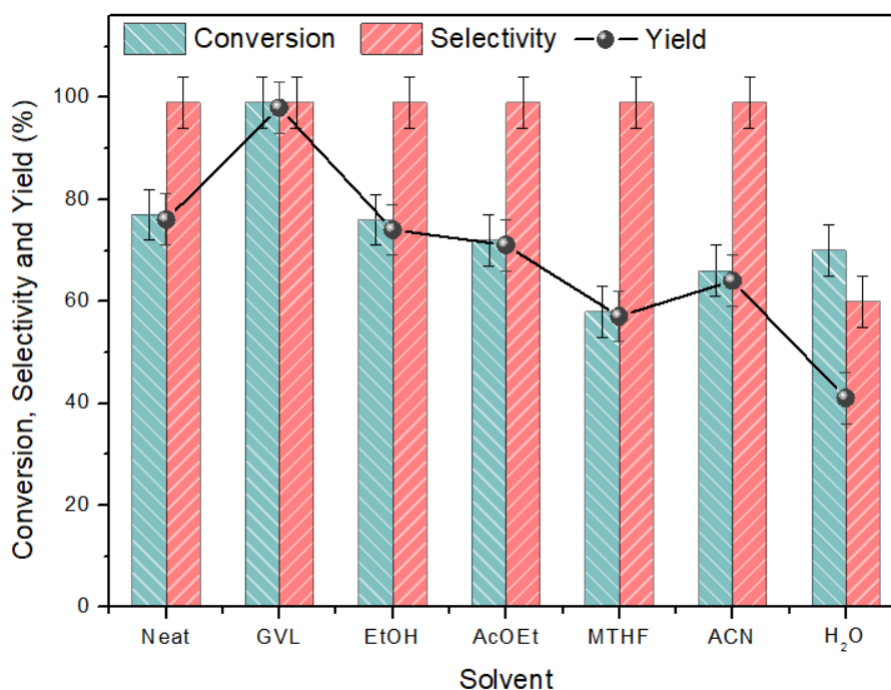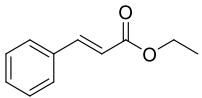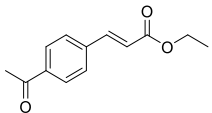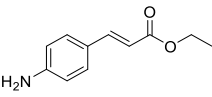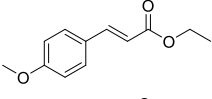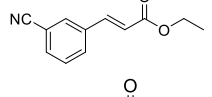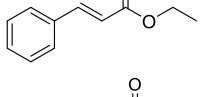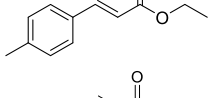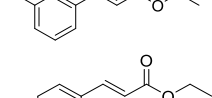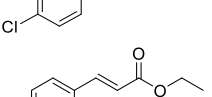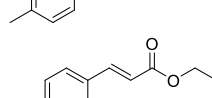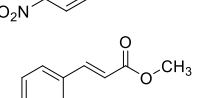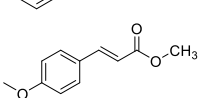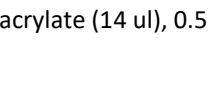

Figure 21: Solvent screening of Heck-Mizoroki reaction. Iodobenzene (1 mmol), ethyl acrilate (1.5 mmol), NEt$_3$ (1 mmol), **1Pd/CNi** (10 mg), 125°C, 4 hours.

SUBSTRATE SCOPE

Following the establishment of the optimal reaction conditions, investigations into substrate scope were carried out. In instances where the solvent signal did not coincide with that of the limiting reagent, the conversion was assessed using GC-FID.

Table 4: Substrate scope. Reaction conditions: aromatic halide (1 mmol), alkene (1.5 mmol), NEt$_3$ (1 mmol), **1Pd/CNi** (10 mg), 125°C, 4 hours.

Entry	Aryl halide	Alkene	Cross-coupling Product	Conversion (%)
1	iodobenzene	Ethyl acrylate		100
2	4-iodoacetophenone	Ethyl acrylate		71.5
3	4-iodoaniline	Ethyl acrylate		61.5
4	4-iodoanisole	Ethyl acrylate		80
5	3-iodobenzonitrile	Ethyl acrylate		74.4
6	Bromobenzene	Ethyl acrylate		0
7	4-Bromotoluene	Ethyl acrylate		0
8	3-Bromotoluene	Ethyl acrylate		0
9*	4-cloro-1-iodobenzene	Ethyl acrylate		0
10	4-clorotoluene	Ethyl acrylate		0
11	4-Cl-nitrobenzene	Ethyl acrylate		0
12	Iodobenzene	Methyl acrylate		64
13	4-iodoanisole	Methyl acrylate		80

*Employed 0.09 mmol (21 mg) of 1-chloro-4-iodobenzene, 1.5 eq. of ethyl acrylate (14 ul), 0.5 ml of GVL, 1 eq. of NEt$_3$ (13 ul), 125°C, 4h.

Upon analyzing the results, it was substantiated that the reactivity of aromatic halides is significantly higher for iodine-substituted compounds in comparison to bromo- or chloro-substituted counterparts, a phenomenon commonly observed in cross-coupling reactions.[53] This discrepancy is attributed to the weaker nature of the I-C bond when contrasted with C-Br and C-Cl bonds, rendering it more susceptible to cleavage during the initial oxidative addition step—often the rate-determining stage in the catalytic cycle. Moreover, there appears to be some steric hindrance imparted by the aryl halide, as evidenced by the superior performance of iodobenzene relative to other disubstituted aryls. Notably, 4-Iodoanisole exhibited the best results after iodobenzene, achieving a conversion rate of 80%. Conversely, the lower conversion observed with 4-iodoaniline might be attributable to the coordinating effect of the amino group, which has the potential to coordinate with Pd, thereby hindering the progression of the catalytic cycle. The obtained results were compared to other chitin-based catalytic systems reported in the literature. Yiun Du et al. synthesized a Pd catalyst supported on composite nanofibers of chitosan (an important deacetylated derivative of chitin) and sodium polyacrylate. This material was evaluated for catalyzing the coupling reactions between iodobenzene and n-butyl acrylate, as well as between iodobenzene and methyl acrylate. Remarkably, it achieved yields of 95% and 98%, respectively, within a mere 3-hour timeframe. However, these experiments used a large excess of base (NEt$_3$) and N,N-dimethylacetamide (DMA) as a solvent, which is both toxic and environmentally detrimental.[106]

A similar catalytic system composed of Pd metal nanoparticles deposited on chitosan nanofibers and poly(vinyl alcohol) was developed by Zeyu Ye et al. and tested in the coupling reaction between iodobenzene and methyl acrylate, yielding good results. However, in this case as well, an excess of base and non-green solvents like dimethyl sulfoxide (DMSO) were employed. Additionally, a much larger quantity of catalyst (50 mg of catalyst with 1.5% of Pd loading for 0.7 mmol of substrate) was required compared to what was used in this thesis.[107]

Pei et al. deposited Pd nanoparticles on chitin microspheres and tested this material for the coupling between iodobenzene and styrene, obtaining a yield of 79% of the desired product using NEt$_3$ as base in a DMF/H$_2$O solvent mixture at 80 °C for 10 h.[108] A similar reaction was studied by Jin et al. using catalysts composed of Pd supported on chitin nanocrystals. The reaction led to quantitative conversion only after 24 hours at a temperature of 90°C.[109] Finally, Strappaveccia et al. conducted the cross-coupling between iodobenzene and ethyl acrylate under conditions similar to those in this work but using a commercial 10%-Pd/C catalyst. The results obtained were like those obtained in

this thesis. Therefore, the catalytic systems obtained through the valorization of seafood industry waste could be a greener alternative to commercial systems in this type of reaction.[102]

Table 5: Heck cross-coupling reaction between iodobenzene and different alkenes with catalytic systems based on chitin.

	Alkene	Catalyst	Solvent	Base	Time (h)	T(°C)	Yield (%)	Ref.
1	Ethyl acrylate	**1Pd/CNi**	GVL	NEt$_3$	4	125	100	This work
2	Methyl acrylate	Pd@CS/PAAS	DMA	NEt$_3$	3	110	98	[106]
3	n-buthyl acrylate	Pd@CS/PAAS	DMA	NEt$_3$	3	110	95	[106]
4	Methyl acrylate	Pd-CS/PVA	DMSO	NEt$_3$	3	110	95	[107]
5	Styrene	Pd/chitin-Ar	DMF/H$_2$O	NEt$_3$	10	90	78.8	[108]
6	Styrene	PdNP@ChNC	ACN/H$_2$O	K$_2$CO$_3$	24	90	100	[109]
7	Ethyl acrilate	10%-Pd/C	GVL	NEt$_3$	2	125	90	[102]

RECYCLE OF CATALYST

After identifying the optimal reaction conditions and conducting the substrate scope, the Heck-Mizoroki cross-coupling between iodobenzene and ethyl acrylate was considered to assess the stability of the **1Pd/CNi** catalytic system through multiple cycles. The reaction was carried out at 125°C for 4 hours, employing 1 mmol of iodobenzene, 1.5 mmol of ethyl acrylate, 1 mmol of NEt$_3$, 10 mg of catalyst in 2 ml of GVL. To perform the various recycling experiments, the reaction mixture was centrifuged at the end of each reaction, separating the supernatant from the precipitate. The precipitate was washed three times with acetone in a centrifuge, and the recovered catalyst was used for the subsequent cycles. After the first reaction, three additional cycles were carried out, achieving excellent conversions, although there was a slight decrease in conversion in successive cycles. Specifically, conversions of 99%, 91%, and 87% were obtained for the 1st, 2nd, and 3rd cycles, respectively. This could be attributed to several factors, including potential catalyst leaching,

sintering of the metallic nanoparticles, or adsorption of organic moieties on the catalyst surface. These phenomena may be more pronounced at higher temperatures.

Therefore, a potential future direction for this research could involve investigating the catalyst stability under milder conditions, such as those typically encountered in the Suzuki-Miyaura reaction, where the catalyst is expected to maintain nearly unchanged conversion values.
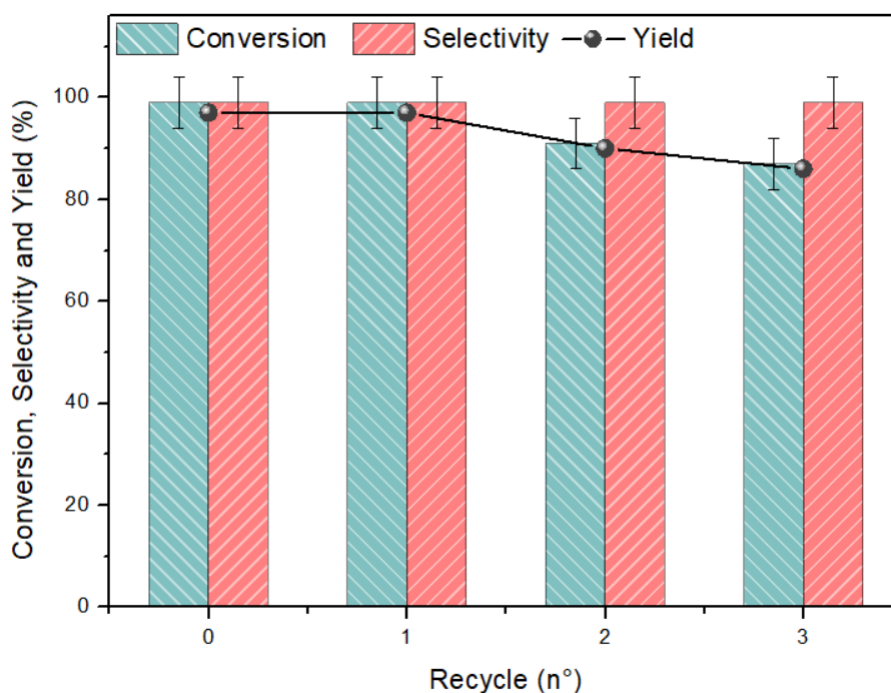
Figure 22: Recycle test in Heck-Mizoroki reaction. Iodobenzene (1 mmol), phenylboronic acid (1.5 mmol), NEt$_3$ (1 mmol), **1Pd/CNi** (10 mg), GVL (2 ml), 125°C, 4h.

In any case, to gain a deeper understanding of these results, the recycled catalyst, referred to as **R-1Pd/CNi**, was subjected to analysis to investigate any potential changes in its crystal structure, morphology, chemical composition, and surface properties. To achieve this, XRD, XPS, and N$_2$ physisorption analyses were performed.

XRD analysis revealed that both the fresh **Pd/CNi** and **R-1Pd/CNi** materials exhibited similar patterns. In both cases, a signal at around 24.0° was observed, indicating the presence of amorphous carbon, especially on the (002) crystallographic plane associated with stacked graphene-like sheets. Additionally, both samples displayed signals at 39.9° and 46.5° (broad, yet still discernible from noise), corresponding to the (111) and (200) planes of Pd(0) with a face-centred cubic crystal structure. However, as shown in Figure 23, the XRD spectrum of the **R-1Pd/CNi** catalytic system exhibits lower signal intensities compared to the fresh sample. This could be attributed to certain

Pd leaching under the reaction conditions used in the Heck reaction, or to the adsorption of organic moieties, overlap with the Pd signals. Another possible hypothesis is a structural reorganization during the reaction that leads to an increase in the amorphous component (with a loss of crystallinity) of the catalyst. Nevertheless, it is noteworthy that these phenomena have a minor effect, considering the excellent catalytic activity of the material, which maintains outstanding conversions.
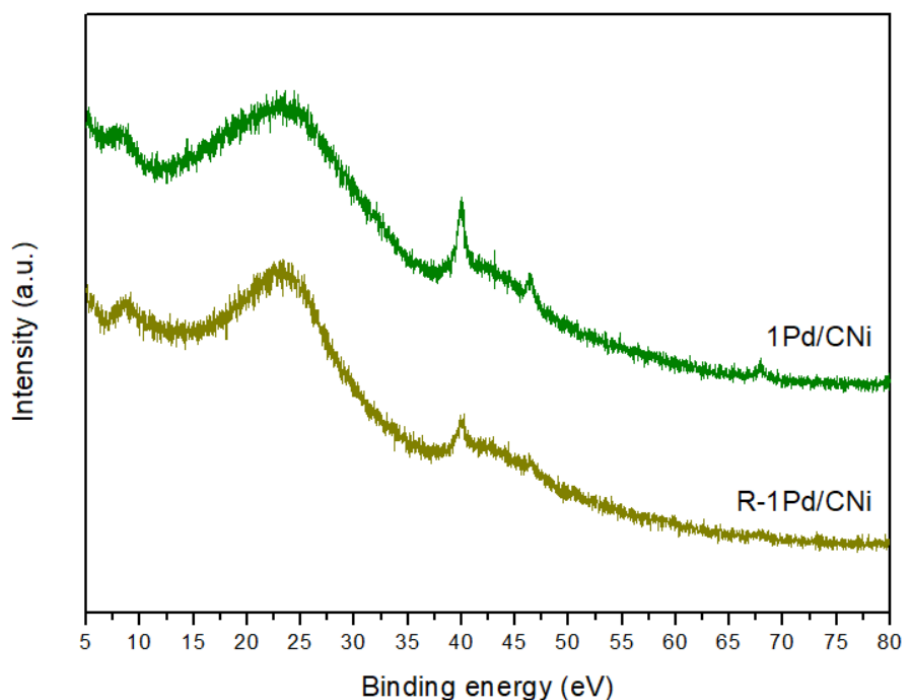
Figure 23: XRD analysis of catalytic systems **1Pd/CNi** and **R-1Pd/CNi.**

The morphology of the catalytic materials, containing a 1% Pd loading, was analysed using TEM, and the resulting micrographs are presented in Figure 24. Both **1Pd/CNi** and **R-1Pd/CNi** exhibited highly uniform and well-dispersed palladium nanoparticles supported on a laminar *N*-doped carbon matrix. As shown, the fresh and spent catalysts did not show significant differences in morphology, consistent with the maintenance of excellent catalytic activity. The mean particle size was determined to be (12.1 ± 1) nm and (13.6 ± 1) nm for the **1Pd/CNi** and **R-1Pd/CNi** materials, respectively. TEM-mapping further reveals, in addition to the Pd nanoparticles, the presence of C, O, and N, all uniformly dispersed within the sample.
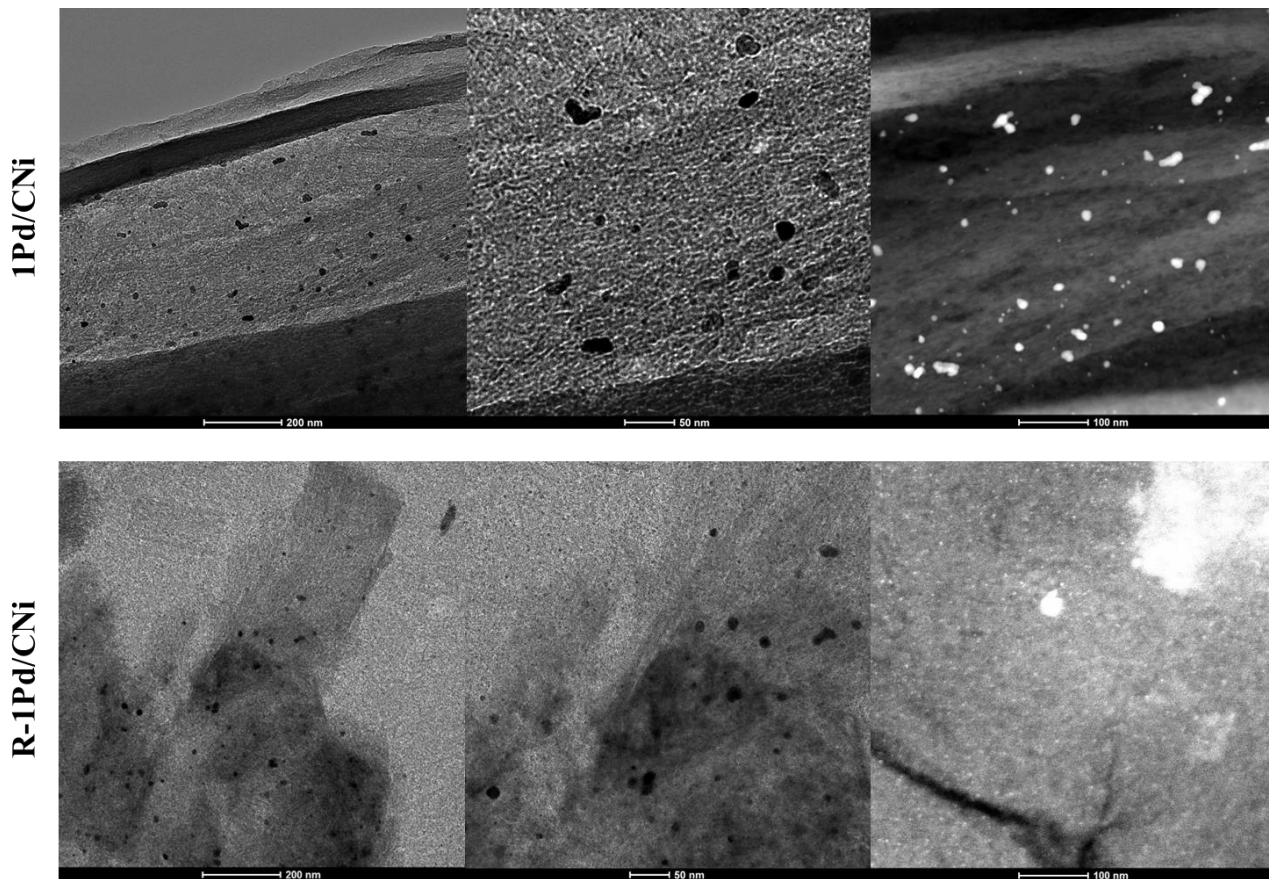
Figure 24: TEM micrograph of **1Pd/CNi** and R-**1Pd/CNi** at 200, 50 and 100 nm, respectively.
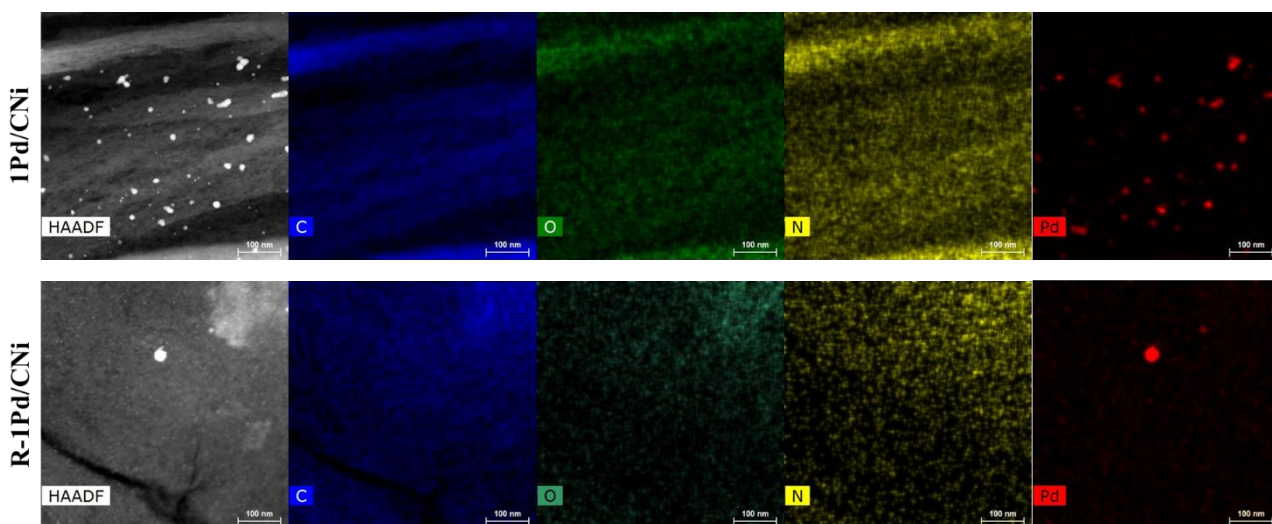
Figure 25: TEM mapping of C, O, N, Pd of **1Pd/CNi** and R-**1Pd/CNi**.

The textural properties of the samples were investigated using N_2-physisorption measurements. As depicted in Figure 26, the shape of the isotherm remained consistent, yielding a Type IV with a Type II hysteresis loop, indicating a mesoporous behaviour. However, in the recycled material, a reduction in the total pore volume (0.38 cm^3/g instead of 0.48 cm^3/g) and consequently a decrease

51

in surface area (395 m^2/g instead of 526 m^2/g) were observed. This observation could lend stronger support, over other hypotheses, to the idea that after the reaction there is an adsorption of organic molecules on the catalyst, resulting in the occlusion of smaller pores during the reaction. This is also corroborated by the slight increase in the mean pore size (3.8 nm instead of 3.6 nm).

Table 6: Textural properties obtained by N$_2$-Physisorbtion of **1Pd/CNi** and **R-1Pd/CNi**.

Material	S$_{BET}$ (m^2/g)	D$_{BJH}$ (nm)	V$_{BJH}$ (cm^3/g)
1Pd/CNi	526	3.6	0.48
R-1Pd/CNi	395	3.8	0.38

* S$_{BET}$: specific surface area was calculated using the Brunauer-Emmett-Teller (BET) equation. D$_{BJH}$: mean pore size diameter was calculated using the Barret-Joyner-Halenda (BJH) equation. V$_{BJH}$: pore volumes were calculated using the Barret-Joyner-Halenda (BJH) equation.
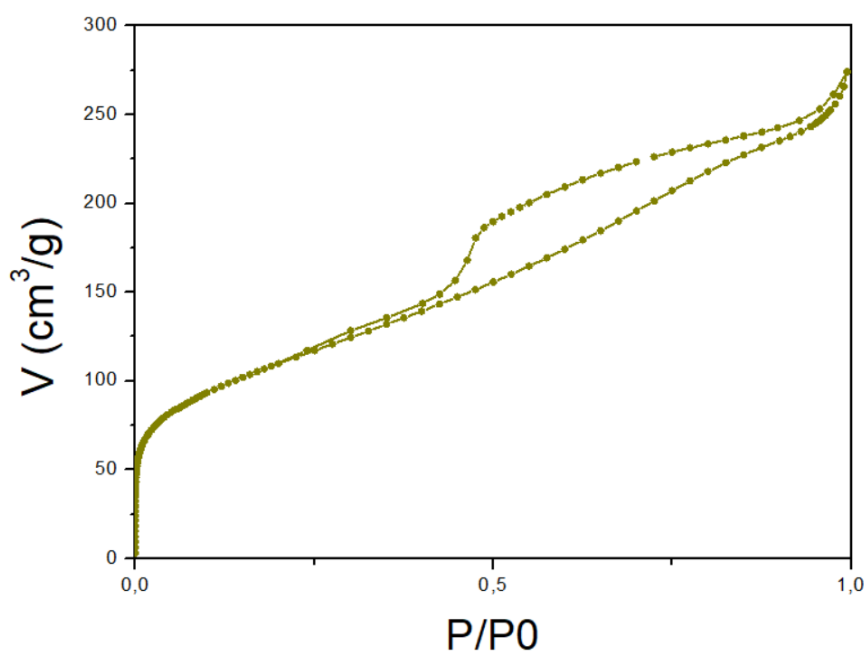
Figure 26: N$_2$ physisorption of catalytic systems **R-1Pd/CNi.**

The chemical composition and nature on the catalysts surface were examined through XPS analyses. The spectra obtained for the **R-1Pd/CNi** material, as displayed in Figure 27, are similar to those of the corresponding **1Pd/CNi** catalytic system; therefore, similar conclusions can be drawn. An apparent difference can be observed in the analysis of the Pd3d region of the XPS spectra (as shown in Figure 27) where the deconvolution of the signal into four components, located at (335.1 ±0.2)

eV, (336.2±0.2) eV, (340.3±0.2) eV, and (341.5±0.2) eV, results in more intense signals related to Pd(II). While in the **1Pd/CNi** catalytic system, the Pd(0): Pd(II) ratio on the surface is approximately 3:1, in the recycled catalytic system, this ratio decreases to approximately 1:1, indicating partial oxidation of the catalyst during the reaction. Taking into account the results of XRD, it can be concluded that the catalyst, when considering both the core and the surface, maintains a general prevalence of metallic Pd.
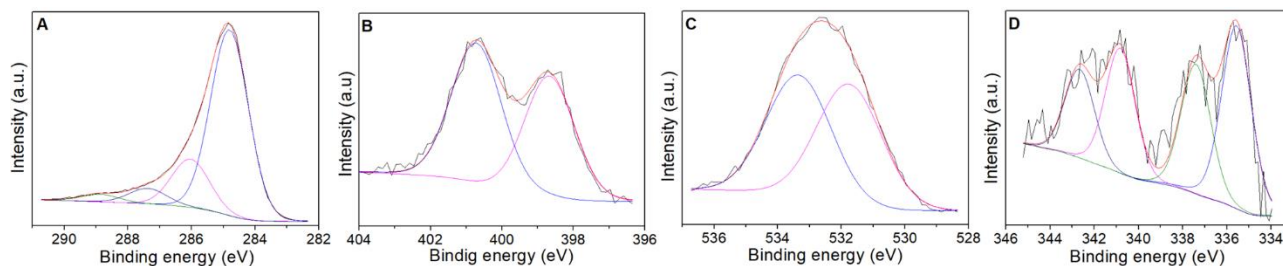
Figure 27: XPS spectra of **R-1Pd/CNi.** It's represented in this order the C1s, N1s, O1s and Pd3d XPS regions.

SUZUKI-MIYAURA REACTION

The catalytic systems were additionally tested in the Suzuki-Miyaura cross-coupling between iodobenzene and phenylboronic acid. In a sealed vial, the following reagents were introduced in the following order: 10 mg of catalyst, 0.5 mmol of potassium carbonate (70 mg, 1.5 eq.), 0.25 mmol of iodobenzene (26 ul, 1 eq.), 0.35 mmol of phenylboronic acid (43 mg, 1.5 eq.), and 3 ml of ethanol used as a solvent. The mixture was then stirred at 75°C for 4 h. The initial reaction conditions were based on an article by García-Suárez et al. Nonetheless, due to challenges associated with low catalyst dispersion and the solubility of the products in water, an alternative environmentally friendly solvent was contemplated—one that could be derived from biomass, like ethanol. This choice aligns with the recommendations provided in the CHEM21 project's solvent guide (Chemical Manufacturing Methods for the 21st Century Pharmaceutical Industries).[110] The reaction products were identified through GC-MS. Conducting the reaction in an open vessel under an air atmosphere resulted in the formation of a small amount of the homocoupling product between two phenylboronic acids. However, this was consistently a minor occurrence, emphasizing the synthesized catalytic systems' impressive ability to maintain high selectivity even when the reaction is conducted in such conditions. Quantification was performed using GC-FID with a calibration curve using an internal standard (mesitylene, 25 ul) for both the product (biphenyl) and the limiting reagent (iodobenzene).

OPTIMIZATION OF PARAMETERS
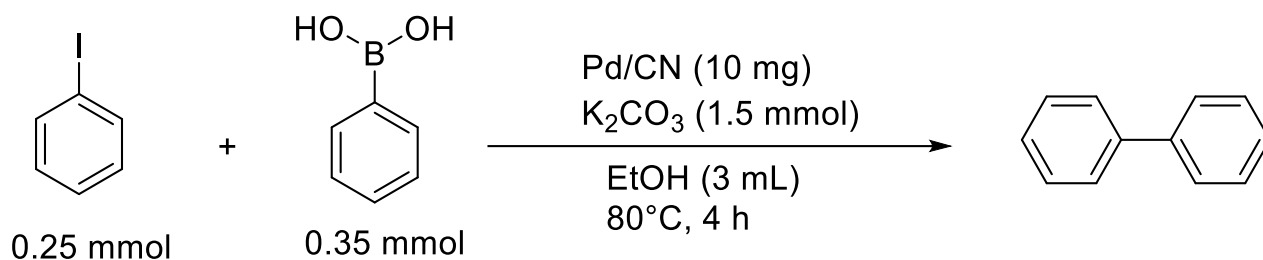
Scheme 8: Suzuki-Miyaura cross coupling reaction considered.

Catalyst screening. Similar to the Heck-Mizoroki reaction, a catalyst screening was initially conducted to determine the influence of the Pd loading on the reaction progress. The reaction, carried out under 75°C conditions for 4 h, resulted in quantitative yields with all catalytic systems. Two control experiments were performed, one in absence of catalyst and one by using the N-doped carbonaceous support. However, in both cases, no conversion was observed, confirming the essential role of Pd in promoting these types of reactions. Therefore, for subsequent studies, the material with the lowest catalytic loading, synthesized using the most sustainable protocol (method A), was chosen, namely **1% Pd/CNi**.
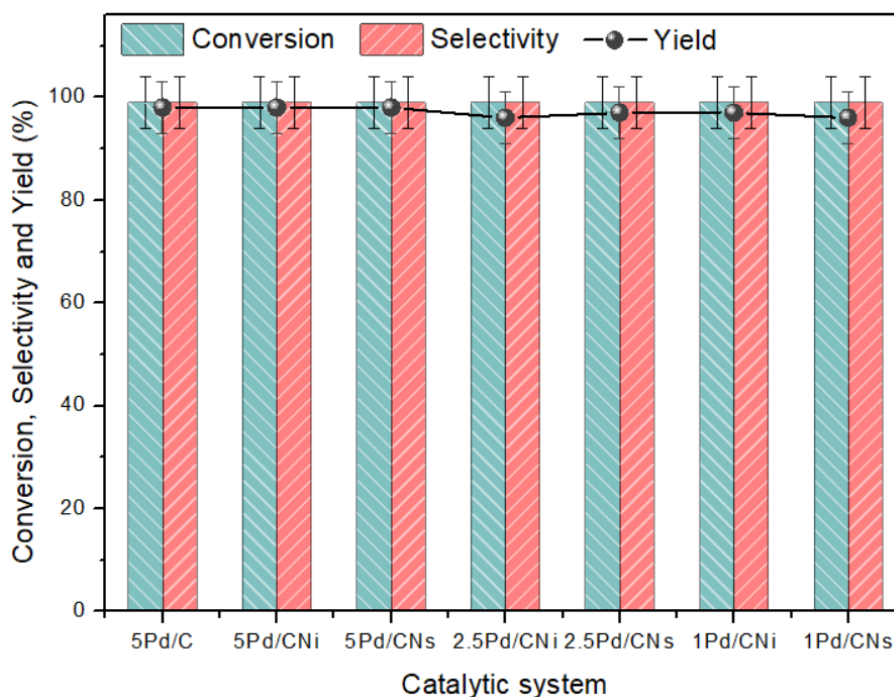
Figure 28: Catalytic screening of Suzuki-Miyaura cross-coupling reaction. Iodobenzene (0.25 mmol), phenylboronic acid (1.5 eq.), K2CO3 (2 eq.), catalyst (10 mg), EtOH (3 ml), 75°C, 4 hours.

Temperature optimization. With this catalytic system, efforts were made to optimize the reaction temperature. Experiments were conducted at 25, 50, and 75°C (just below the boiling point of ethanol). Temperature plays a crucial role in increasing the reaction yield. At room temperature, no conversion was observed, but the difference between 50 and 75°C was significant, leading to an increase of the biphenyl yield from 57% to 100%. This result aligns with other studies in the literature, which indicate that 80°C is the optimal temperature to boost the product yield.[75] Despite this temperature being slightly outside the green window (0-70°C) defined by the pharmaceutical industry in the CHEM21 project, conducting the reaction just below the reflux condition allows for up to a five-fold reduction in energy consumption. According to the same guidelines, this approach helps meet the operational conditions that a process should aim for (green flag).[111]
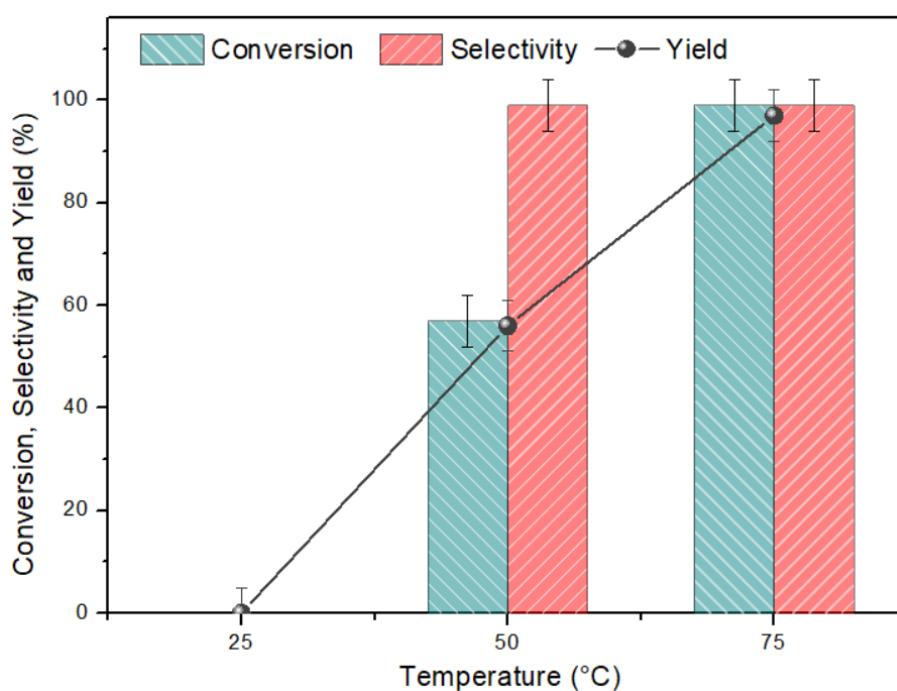
Figure 29: Temperature optimization of Suzuki-Miyaura cross-coupling reaction. Iodobenzene (0.25 mmol), phenylboronic acid (1.5 eq.), K_2CO_3 (2 eq.), **1Pd/CNi** (10 mg), EtOH (3 ml), 4 hours.

Time optimization. With these results in hand, a study on reaction time was conducted. The findings indicate that the reaction initiates quite early, with around 30% conversion observed after just 30 minutes. The plateau was reached after approximately 2 hours, with a yield of 92%, and complete conversion (and yield) was achieved only after 4 h of reaction.
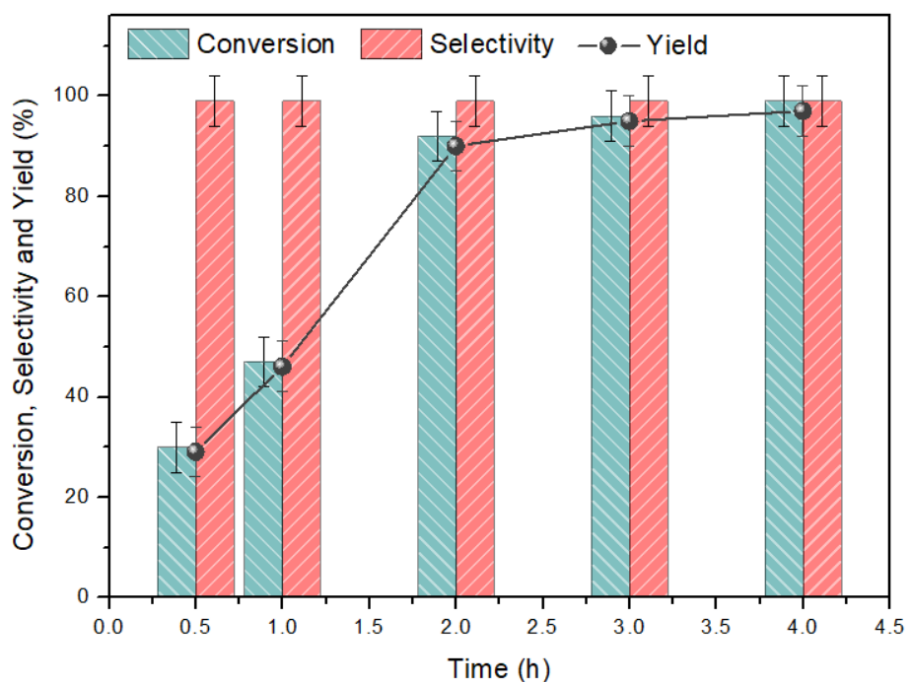
Figure 30: Time optimization of Suzuki-Miyaura cross-coupling reaction. Iodobenzene (0.25 mmol), phenylboronic acid (1.5 eq.), K2CO3 (2 eq.), **1Pd/CNi** (10 mg), EtOH (3 ml), 75°C.

Solvent screening. In the literature, various solvents are reported for cross-coupling reactions. Generally, in such reactions where compounds with significantly different chemical and physical properties are involved, the choice of solvent is crucial to bring all these substances into contact and allow the diffusion of reagents near the active site of the heterogeneous catalyst.[72] For these reasons, polar aprotic solvents are often used. In Suzuki reactions, the solvent plays a more critical role as it can act as a nucleophile (having previously reacted with the base or not) and interact either with the catalyst or the arylboronic acid during the transmetallation step.[79] This is why studies in polar protic solvents like H_2O and alcohols, or mixtures of protic-aprotic solvents (e.g., DMF/H_2O), can be found in the literature.[75] In this work, ethanol was selected to address these considerations comprehensively, although other solvents were also tested, such as H_2O, acetonitrile (ACN), methanol, ethyl acetate (AcOEt), methyl-THF, and γ-Valerolactone (GVL). From the results obtained, there is a noticeable difference between polar protic solvents like ethanol and methanol, which give quantitative yields, compared to the others, which provide yields equal to or below 10%. This can be explained by considering the role of the base in the reaction. The carbonate, albeit weakly, induces a deprotonation equilibrium of ethanol (or methanol), forming a strong nucleophile that can activate the arylboronic acid or the catalytic species after the oxidative addition step, thus promoting the reaction. With the other solvents, this does not occur, and the mild conditions may not be sufficient to overcome the activation barrier of the transmetallation step. Among these

results, water provides intermediate yields (40%). In that case, the reaction product, typically insoluble in water, is brought into solution by diluting the reaction mixture with ethanol. Additionally, during the reaction, unlike in the other solvents, in water, the catalyst does not effectively disperse but remains more aggregated, indicating poor hydrophilicity. In this scenario, the reagents encounter difficulties in diffusing to the interface with the active site located on the catalyst's surface, primarily because of reduced wettability.
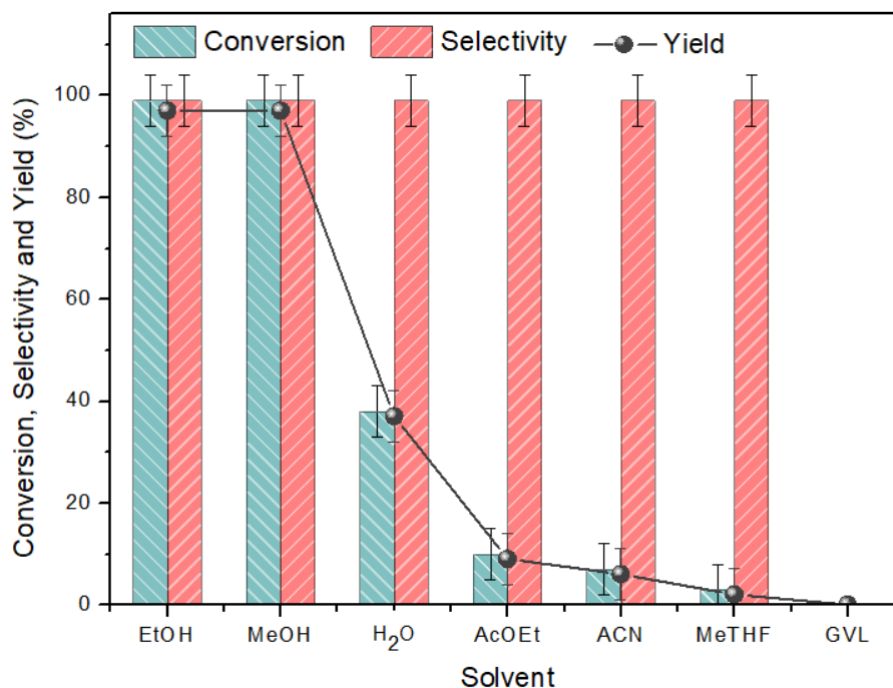

Figure 31: Solvent screening of Suzuki-Miyaura cross-coupling reaction. Iodobenzene (0.25 mmol), phenylboronic acid (1.5 eq.), K2CO3 (2 eq.), **1Pd/CNi** (10 mg), solvent (3 ml), 75°C, 4 hours.

Base analysis. With these conditions, the role of the quantity and type of base within the Suzuki reaction was investigated. Although it does not play a primary role as in the Heck cross-coupling, it was observed that the base is essential in the Suzuki reaction as it can either directly activate the phenylboronic acid to an organoboronate species or deprotonate the protic solvent (alcohol or H_2O) to form the nucleophile, which (depending on the studies) either activates the arylboronic acid or replaces the halide coordinated to Pd, forming a less stable species that completes the transmetallation phase. Initially, a study was conducted to determine which of NEt_3, Na_2CO_3, e K_2CO_3 yielded the best results in terms of yield under the reaction conditions described above. The results show profoundly different behavior when changing the base. Indeed, with K_2CO_3, a quantitative yield is obtained, while with Na_2CO_3, only 55% yield is achieved. This behavior is

explained by the lower strength of the ionic pair formed between K^+ and CO_3^{2-} compared to Na^+ and CO_3^{2-}. In this way, the carbonate is more "free" and exhibits greater basicity, promoting the reaction. The results obtained with NEt_3 were more unexpected (although very low conversion is also found in the studies of Miyaura and Suzuki), but they can be explained by its different coordinating capacity compared to K_2CO_3. Assuming that the reaction mechanism follows the initial substitution of the base with the halide coordinated to palladium and the subsequent transmetallation of the formed species with phenylboronic acid, the significantly higher coordinating capacity of the amine can induce a more stabilized species, thus stopping the catalytic cycle. Even considering the effect of carbonate in the deprotonation equilibrium of ethanol to form ethoxide, a better nucleophile, the coordinating capacity and concentration (as it is an equilibrium shifted slightly towards the alkoxide) of the latter is still much lower than that of NEt_3. Once it was established that K_2CO_3 is the more suitable base to promote the reaction, tests at different concentrations of the base were performed. In these tests, it was found that even when used in sub-stoichiometric quantities, K_2CO_3 can promote the reaction to quantitative yield. To verify the possible basicity of the support, a test was conducted in the absence of a base. However, similarly to the Heck-reaction, also in this case low to negligible conversions were reached (yield: 4%).
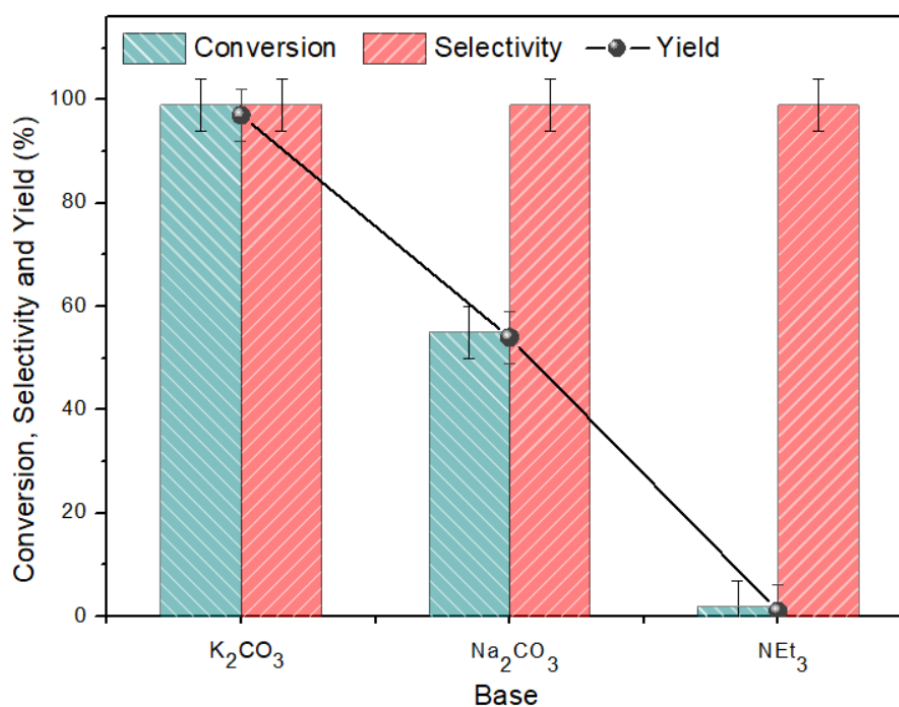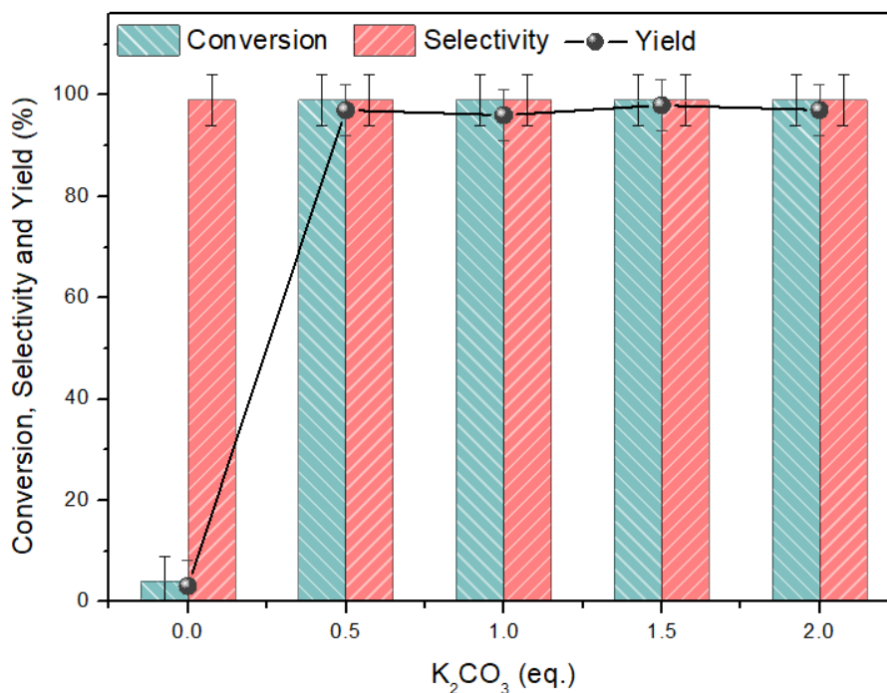

Figure 32: Different bases tested in Suzuki-Miyaura cross-coupling reaction. Iodobenzene (0.25 mmol), phenylboronic acid (1.5 eq.), base (2 eq.), **1Pd/CNi** (10 mg), EtOH (3 ml), 75°C, 4 hours.
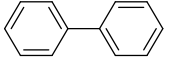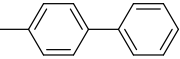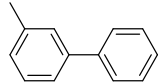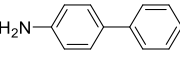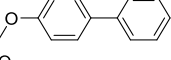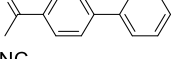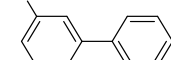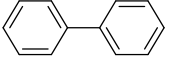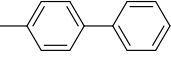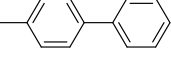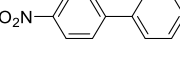
Figure 33: Different base amount tested in Suzuki-Miyaura cross-coupling reaction. Iodobenzene (0.25 mmol), phenylboronic acid (1.5 eq.), **1Pd/CNi** (10 mg), EtOH (3 ml), 75°C, 4 hours.

SUBSTRATE SCOPE

With these optimized conditions, a substrate scope was conducted. Various aryl halides and arylboronic acids were tested. The results indicate, similar to the Heck-Mizoroki reaction, a significant difference in reactivity between iodinated aryls and bromo- and chloro-substituted aryls. These differences are attributed to the weaker halogen-carbon bond, which favors the initial oxidative addition step. Within the iodinated aryls, there are marked differences based on the substituents on the aromatic ring. Since the aromatic ring acts as an electrophilic reagent in the cross-coupling, electron-donating substituents will hinder the reaction (as seen with 4-iodoanisole and even more so with 4-iodoaniline), while electron-withdrawing substituents will promote the reaction (as observed with 4-iodoacetophenone or 3-iodobenzonitrile). For the same aryl halide (iodobenzene), excellent results were obtained by varying the arylboronic acid, with higher reactivity observed for boronic substrates with electron-donating substituents in the para position on the benzene ring. Regarding selectivity, despite the reaction occurring in the presence of air, less than 5% of the homocoupling product is obtained, demonstrating that this catalytic system effectively controls potential side reactions.

Table 7: Substrate scope. Reaction conditions: aryl halide (0.25 mmol), arylboronic acid (1.5 eq.), K2CO3 (0.5 eq.), **1Pd/CNi** (10 mg), ethanol (3 ml), 75°C, 4 hours.

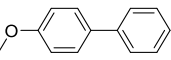| Entry	Aryl halide	Arylboronic acid	Cross-coupling Product	Conversion (%)	Selectivity (%)
1	iodobenzene	Phenylboronic acid		99	99
2	iodobenzene	*p*-tolilboronic acid		99	95
3	iodobenzene	*m*-tolilboronic acid		91	97
4	iodobenzene	4-metoxyphenylboronic acid		95	96
5	4-iodoaniline	Phenylboronic acid		18	99
6	4-iodoanisole	Phenylboronic acid		47	99
7	4-I-acetophenone	Phenylboronic acid		99	99
8	3-I-benzonitrile	Phenylboronic acid		96	99
9	Bromobenzene	Phenylboronic acid		6	99
10	4-Bromotoluene	Phenylboronic acid		4	99
11	4-Chlorotoluene	Phenylboronic acid		0	
12	4-Cl-nitrobenzene	Phenylboronic acid		3	99

Similarly to what was done for the Heck reaction, the results obtained were compared with other catalytic systems recently synthesized in the literature. Khosravi et al. synthesized and tested catalytic systems based on Pd supported on porous carbon beads with two different stabilizing agents, triphenylphosphine (TPP) and trioctylphosphine (TOP). In the cross-coupling between iodobenzene and phenylboronic acid (PhB(OH)$_2$), good yields (between 70% and 90%) were obtained in water after 4 hours at 65°C. The results are approximately in line with those of this study. However, it is worth to mention that the catalyst preparation method turns out to be much more energy-intensive and resource-consuming, involving heat treatments at 1500 °C, additional oxidants (H$_2$O$_2$), or less green solvents like THF and pentane..[112]

Mhaldar et al. prepared a heterogeneous Pd(II) catalyst through the initial functionalization of a composite cellulose-alumina support with 2-aminopyridine, followed by complexation of Pd(OAc)$_2$ onto the formed material. The cross-coupling reaction between iodobenzene and phenylboronic acid resulted in non-quantitative yields (72%) in 3 hours at 80°C in ethanol, using potassium

carbonate as a base and 40 mg of catalyst with a 1% loading. The yield increased to 95% in one hour using DMF as a solvent, which is a toxic, polluting compound with a high boiling point and miscible in water, being hence a persistent pollutant in wastewater and is therefore generally avoided.[113]

Jiang et al. synthesized catalytic systems based on Pd nanoparticles supported on activated carbons that were previously functionalized with thiol and amine groups to enhance material stability. The cross-coupling test was conducted at 80 °C for 1 h in a mixture of H_2O/Ethanol with K_2CO_3 as the base, and the material exhibited excellent performance using 40 mg of catalyst (yield 100%). However, the catalyst synthesis phase is rather labor-intensive and involves the use of strong acids (40% HNO_3) and non-green solvents (toluene).[114]

Li et al. synthesized heterogeneous catalysts where the polyimidazolium support, through its carbene groups, coordinates with Pd, resulting in a stable and well-dispersed system. This material was tested in the cross-coupling between iodobenzene and phenylboronic acid, leading to quantitative conversion in 3 h at 60 °C. The only drawback relates to the solvent used, which was a mixture of DMF/H_2O at a 1:1 ratio, and these components can be challenging to separate.[115] This information is summarized in Table 5.

Table 8: Different catalytic system for Suzuki cross-coupling reaction between Iodobenzene and phenylboronic acid, employing K_2CO_3 as base.

Entry	Catalyst	Solvent	Time (h)	T(°C)	Yield (%)	Ref.
1	**1Pd/CNi**	Ethanol	4	75	100	This studio
2	Pd(TPP)/MB-H_2O_2	H_2O	4	65	79	[112]
3	Pd(TOP)/MB-1500	H_2O	4	65	90	[112]
4	Pd-AMP-Cell@Al_2O_3	Ethanol	3	80	72	[113]
5	Pd-AMP-Cell@Al_2O_3	DMF	1	80	95	[113]
6	SH-Pd/AC	H_2O/Ethanol	1	80	100	[114]
7	Pd-PPc-4	DMF/H_2O	3	60	99	[115]

MECHANOCHEMICAL APPROACH: RESULTS AND DISCUSSION

SYNTHETIC APPROACH

The catalysts were prepared using an extrusion process, as outlined in Figure 34. The experimental parameters were selected based on prior experience of the Green Organic Synthesis Group (GOST) with the mechanochemical synthesis of nanomaterials.[95,116,117] A mixture of palladium acetate (0.50 mmol, 112 mg), ethylene glycol (15 mL, 0.26 mol), and chitin (5 g) was fed into a mini-extruder (ZE 12 HMI extruder from Three Tec). Ethylene glycol was employed as a green reducing agent, according to some recent reports in the literature.[118] Ethylene glycol viscosity enables the formation of a paste-like mixture. The extruder was heated to 190 ˚C and the conveying screws were set to 50 rpm at a torque of around 2 Nm. The resulting material in the form of small cylindrical pieces (approximately 1 mm diameter) was collected and used, directly or after a thermal treatment at 500 °C under N_2 atmosphere, as catalyst for a C-C bond forming reaction, specifically Suzuki-Miyaura cross-coupling between iodobenzene and phenylboronic acid.

In a variation of this procedure, Na_2CO_3 (53 mg, 0.5 mmol) was added to the reaction mixture to enhance the basic properties of the sample. The four prepared materials were labelled as **P-5Pd/CN-ex** and **5Pd/CN-ex** for the catalysts obtained without and with thermal treatment in the absence of a base, respectively, while the labels **P-5-Pd/CN-ex-Na$_2$CO$_3$** and **5Pd/CN-ex-Na$_2$CO$_3$** were used for the catalysts obtained without and with thermal treatment in the presence of Na_2CO_3, respectively.

Figure 34: Schematic representation of the mechanochemically assisted synthesis of the catalytic materials.

MATERIALS CHARACTERIZATION

The crystal structure and arrangement of the samples were assessed through XRD analysis. The XRD patterns of the samples prior to thermal treatment are shown in Figure 35A, while Figure 35B presents the patterns for the thermally-treated samples.

The **P-5Pd/CN-ex** and **P-5Pd/CN-ex-Na₂CO₃** materials exhibited the characteristic diffraction peaks of chitin at approximately 10, 20, 21, 23, and 26°, corresponding to the (020), (110), (120), (101), and (130) crystallographic planes, respectively.[119,120] A broad peak observed between 20° and 30° likely indicated the presence of amorphous carbon formed during the mechanochemical synthesis at 190°C. Moreover, it was observed a signal at 39.2° which indicates the successful reduction of Pd (II) leading to the formation of Pd(0) nanoparticles. As shown in Figure 35B, the broad signal at approximately 24.0° was attributed to the (002) crystallographic plane associated with stacked graphene-like sheets, indicating the formation of amorphous carbon.[98] The sharp and well-defined peaks at 40.1, 46.6, and 68.1° were attributed to the (111), (200), and (220) crystallographic planes of palladium, respectively, confirming the presence of Pd(0).[50,121,122]
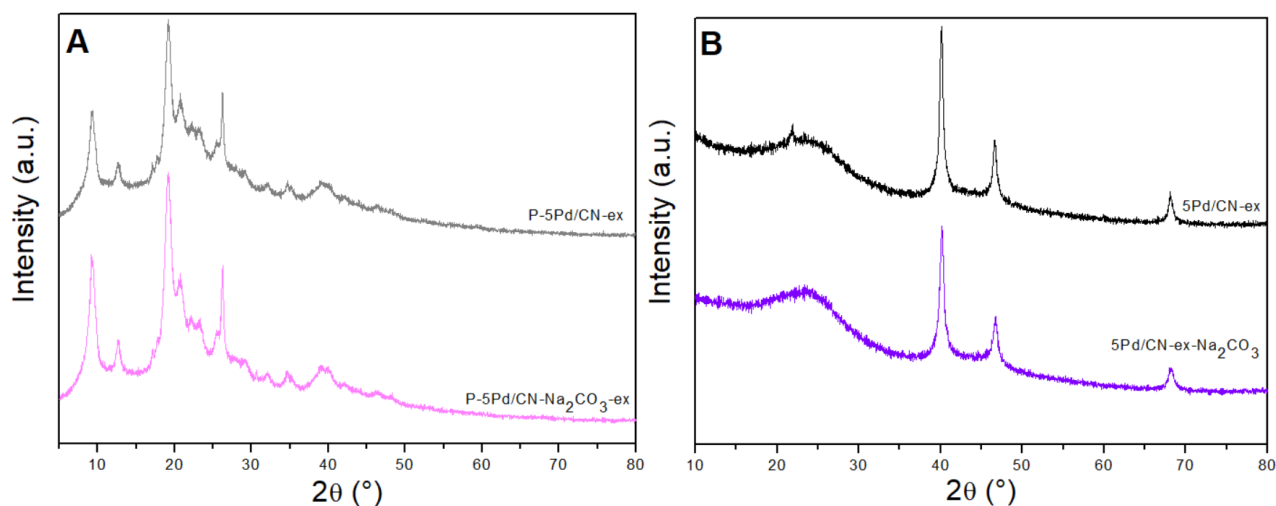
Figure 35: XRD pattern of the catalytic systems before (A) and after (B) thermal treatment.

The thermally treated samples, both with and without the base, were further characterized. The particle size of the catalytic systems was determined from XRD diffraction patterns using the Scherrer equation (Table 9).[123,124] The calculated particle sizes were (14.9 ± 0.5) nm and (10.3 ± 0.5) nm for **5Pd/CN-ex** and **5Pd/CN-ex-Na₂CO₃**, respectively. The presence of Na_2CO_3 in the mechanochemical synthesis of the catalyst appears to have influenced the dimension of the obtained nanoparticles, leading to smaller particle size. These results suggest that either a repulsive effect of sodium cations or the coordination of carbonate to palladium, both of which prevent possible agglomeration of nanoparticles during extrusion, result in a reduction in nanoparticle size. However, further studies are required to confirm these hypotheses.

Further investigations into the morphology of the catalytic systems were conducted through TEM microscopy (Figure 36). The micrographs showed that both samples exhibited highly uniform and well-dispersed palladium nanoparticles supported on a laminar *N*-doped carbon matrix. In addition, the average diameter of the nanoparticles was calculated, confirming the results obtained through the Scherrer equation. Indeed, the values obtained from the TEM analysis are (16.6 ± 1.0) nm and (10.0 ± 1.0) nm, respectively, for **P-5Pd/CN-ex** and **P-5Pd/CN-ex-Na₂CO₃**. In addition, TEM-mapping measurements confirmed the presence of carbon, nitrogen, oxygen, and palladium in both catalytic samples, with all elements being uniformly distributed in each case (Figure 37). In addition, for the sample **5Pd/CN-ex-Na₂CO₃,** also homogeneous distribution of Sodium can be observed, deriving by the incorporation of Na_2CO_3 into the material matrix during the synthesis.
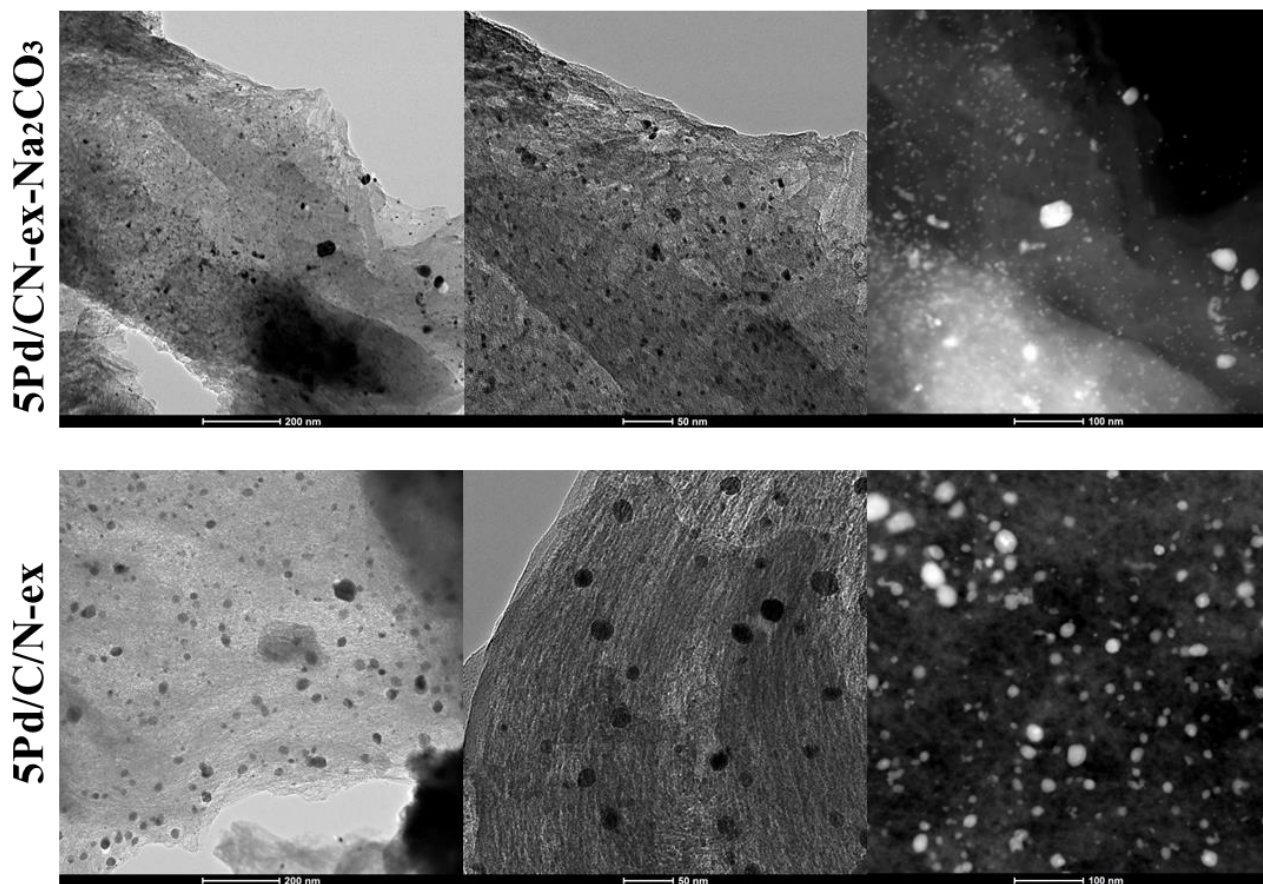
Figure 36: TEM micrograph of **5Pd/CN-ex** and **5Pd/CN-ex-Na₂CO₃** at 200, 50 and 100 nm, respectively.
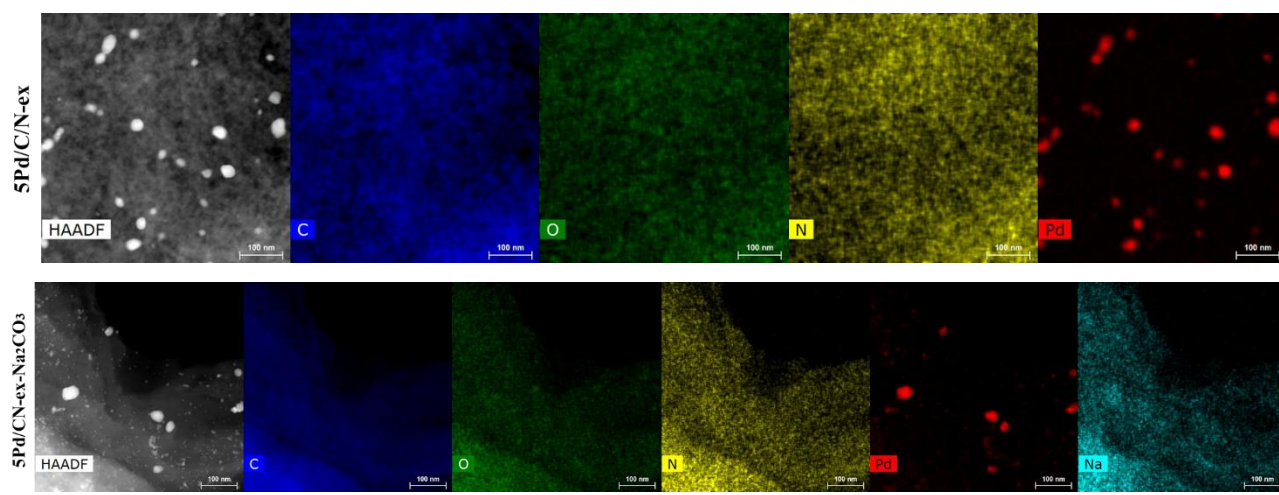
Figure 37: TEM mapping of C, O, N, Pd of **5Pd/CN-ex** and **5Pd/CN-ex-Na₂CO₃**.

The textural properties of the samples, including surface area, pore volume, and pore size, were examined by N_2-physisorption. Both materials showed physisorption isotherms type IV with type II adsorption hysteresis, indicative of the formation of a mesoporous materials. The Figure 38 displays a representative isotherm for **5Pd/CN-ex**. Similar to the catalysts obtained by method A and B, also

in this case surface area was calculated using the Brunauer-Emmett-Teller (BET) equation, while pore volumes and mean pore size diameter was calculated using the Barret-Joyner-Halenda (BJH) equation. Both samples exhibited a remarkably high surface area of 452 and 498 m^2g^{-1} for **5Pd/CN-ex** and **5Pd/CN-ex-Na₂CO₃**, respectively, demonstrating a significant improvement of the textural properties (in comparison, **5Pd/CNi** and **5Pd/CNs** have surface areas around 300 m^2/g). Finally, the range of pore diameter around 5.0 nm further confirmed the presence of mesoporous solids. In summary, these characterization studies validated the effectiveness of the mechanochemical protocol for the preparation of supported metal nanoparticles on mesoporous *N*-doped carbon-based matrix.[48] Finally, the palladium loading, determined by ICP-OES, was around 4 mg/g$_{catalyst}$ for both samples. The above is summarised in Table 9.
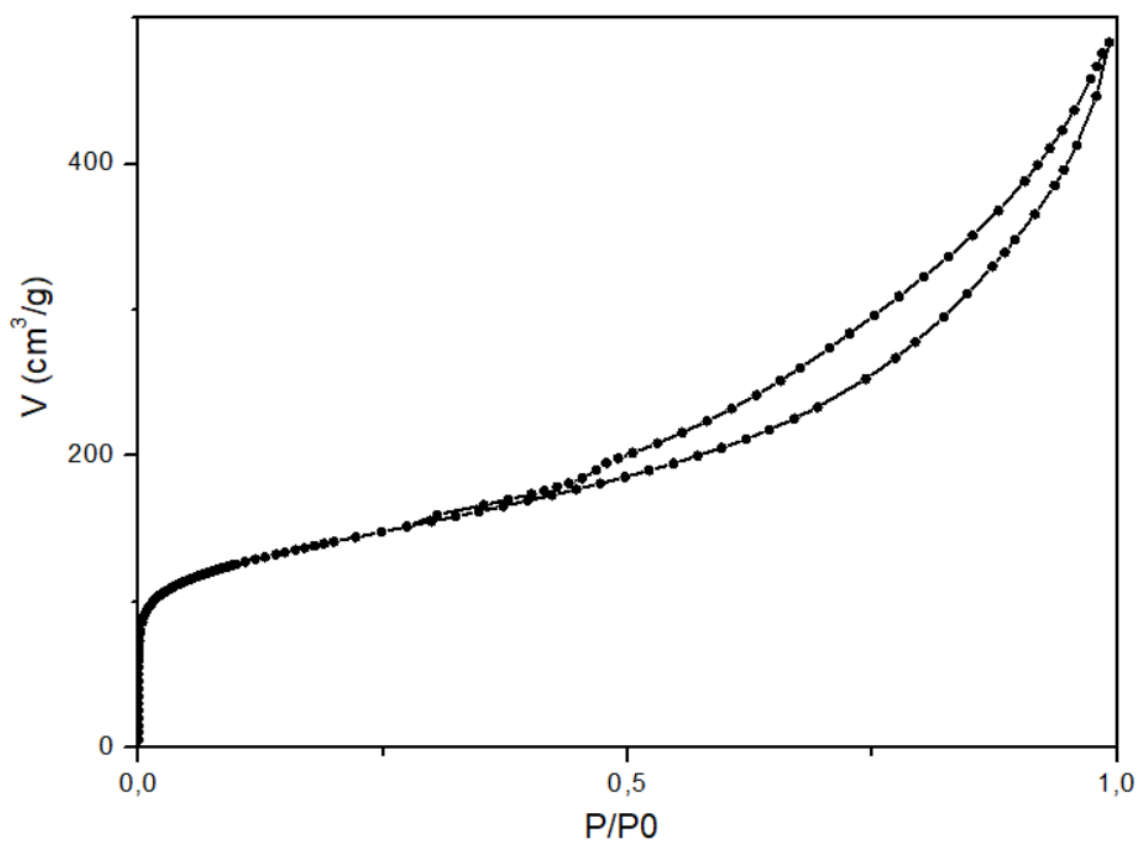
Figure 38: Representative isotherm for **5Pd/CN-ex**.

Table 9: Textural properties, particle size, and palladium content of the catalytic materials.

Material	S_{BET} (m²/g)	D_{BJH} (nm)	V_{BJH} (cm³/g)	Pd wt.% (ICP-OES)	Pd Particle Size (nm)
5Pd/CN-ex	498	4.9	0.61	4.3	14.9
5Pd/CN-ex-Na₂CO₃	452	5.3	0.53	3.9	10.3

* S_{BET}: specific surface area was calculated using the Brunauer-Emmett-Teller (BET) equation. D_{BJH}: mean pore size diameter was calculated using the Barret-Joyner-Halenda (BJH) equation. V_{BJH}: pore volumes were calculated using the Barret-Joyner-Halenda (BJH) equation. Pd concentrations were determined by ICP-OES and e Pd particle size was calculated using XRD analyses employing the Scherrer Equation.

Moreover, XPS analyses were conducted to gain insights into the surface chemical composition of the catalysts synthesized via the mechanochemical approach. As depicted in Figure 39, the spectra generally exhibit similar characteristics to those of materials obtained through more conventional methods A and B. However, for the samples prepared using Na_2CO_3, the surface of the catalytic material displays the presence of not only carbon, oxygen, nitrogen, and palladium but also sodium. In particular, the latter exhibited a distinct signal at (1071.4 ± 0.2) eV, indicating the presence of Na^+, most likely in the form of Na_2CO_3 (Figure 39I). C1*s* XPS regions (figure 39A and 39B) were deconvoluted into four contributions, located at (284.3 ± 0.2) eV, (285.7 ± 0.2) eV, (287.2 ± 0.2) eV and (288.6 ± 0.2) eV, attributed to C–C/C=C bonds from graphitic and/or aromatic carbon, C–OH, C–N/C–O and C=O species, respectively. Similar to the samples obtained through methods A and B, N1*s* XPS region (Figure 39B and 39F) showed the presence of two main bands at (398.4 ± 0.2) eV and (400.3 ± 0.2) eV, which are typically attributed to pyridinic and pyrrolic nitrogen species, respectively. Furthermore, O1*s* XPS region signals were deconvoluted into two contributions located at (531.2 ± 0.2) eV and (533.2 ± 0.2) eV, which are assigned to O-Metal bonds in metal oxides and to the presence of adsorbed H_2O in the catalysts structure, respectively. This behaviour aligns with that observed in the other synthesized samples. More interesting, an assessment of the chemical composition of the palladium entities on the catalysts surface, specifically for **5Pd/CN-ex** and **5Pd/CN-ex-Na₂CO₃**, was conducted based on the Pd3*d* XPS spectra. Notably, these spectra displayed marked distinctions from all other samples (refer to Figure 39D and 39H). In this case, the Pd3*d* XPS signals were deconvoluted into six distinct contributions. Four of these contributions correspond to the previously mentioned ones, located at (335.1 ± 0.2) eV and (340.3 ± 0.2) eV referred respectively to Pd3$d_{3/2}$ and Pd3$d_{1/2}$ of Pd (0), and at (336.2 ± 0.2) eV and (341.5 ± 0.2) eV

associated respectively to Pd3$d_{3/2}$ and Pd3$d_{1/2}$ of Pd(II) oxide. In addition to these signals, two additional contributions can be observed, located at (343.6 ± 0.2) eV and (338.3 ± 0.2) eV, indicating the presence of Pd-*N* bonds.[125]

It is interesting to note that mechanochemical synthesis promotes the formation of this bond, which differs from conventional syntheses using methods A and B. This enhanced interaction between the metal nanoparticles and the support is likely to result in greater catalyst stability against leaching phenomena, a persistent challenge in heterogeneous catalysis. During this work, XPS spectra were also collected for materials synthesized via mechanochemistry without undergoing the subsequent thermal treatment, labelled as **P-5Pd/CN-ex** and **P-5Pd/CN-ex-Na₂CO₃**. The spectra can be found in the appendix. The only notable differences were observed in the C1*s* XPS region, where there is a change in the relative intensity between the signals associated with C–C/C=C bonds from graphitic and/or aromatic carbon, C–OH, C–N/C–O, and C=O species. Indeed, before the thermal treatment, there is a prevalence of signals from C–N/C–O species and a 1:1 ratio between the signals of C–C/C=C species and C=O species. As expected, after the thermal treatment, the contributions from carbonyl carbons and C–N/C–O bonds decrease, with the consequent increase of the signals related to graphitic and/or aromatic carbon. The N1*s* XPS region also showed differences, exhibiting a single signal most likely associated with the amidic nitrogen of chitin, with a binding energy of (399.5±0.2) eV. Finally, the Pd3*d* XPS region exhibits the same four signals as the catalysts prepared using conventional methods. However, for the material obtained using Na₂CO₃, the ratio of Pd(0)/Pd(II) signals is shifted more towards Pd(0), indicating a probable promoter effect of the base in the reduction of the metal precursor during the mechanochemical treatment.
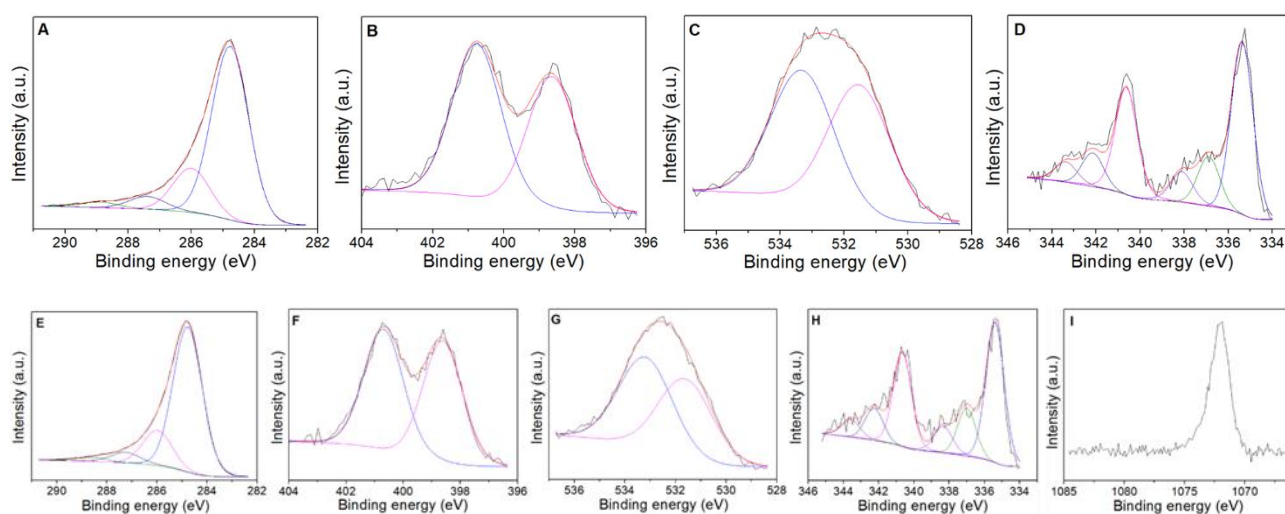
Figure 39: XPS spectra of **5Pd/CN-ex** (A-D) and **5Pd/CN-ex-Na₂CO₃** (E-I). For each catalytic system, it's represented in this order the C1*s*, N1*s*, O1*s* and Pd3*d* XPS regions. For **5Pd/CN-ex-Na₂CO₃** it's also available the Na1*s* region.

CATALYTIC ACTIVITY

The catalytic systems synthesized using conventional protocols (methods A and B) and those prepared through mechanochemical methods were tested in the Suzuki-Miyaura reaction between iodobenzene and phenylboronic acid, under solvent-free conditions, and conducted in the Twin Screw Extruder. This investigation aimed to explore the possibility of a mechanochemical influence on enhancing process efficiency. In this regard, conducting mechanistic studies would be interesting to discern whether and how the reaction mechanism undergoes alterations when performed in a solid state without the presence of solvents, which traditionally play a pivotal role in Suzuki reactions conducted in batch processes. In this direction, a plausible mechanism has been proposed in the literature by Pentsak and coworkers.[126] The authors conducted cross-coupling between various aryl halides and arylboronic acids under solvent-free conditions using a mechanochemical approach through ball milling. The proposed mechanism entails the generation of trace quantities of water within the solid mixture, brought about by the condensation of three molecules of arylboronic acid. Subsequently, the generated water can interact with the base (K_2CO_3) to form the hydroxide anion, which promotes the transmetalation step by either activating the arylboronic acid or by activating the palladium-based catalyst, thereby replacing the halide. Following the reductive elimination step, the product formation takes place. Additionally, four molecules of boric acid formed during the catalytic cycle under basic conditions can condense into potassium borate, with the release of water, which re-enters the catalytic cycle. This proposed mechanism is supported by experiments conducted with fluorinated arylboronic acids, which did not undergo trimerization and were oven-dried to remove network water. These experiments did not yield any conversion. However, upon the addition of trace amounts of water to these systems, there was a significant increase in the conversion to the cross-coupling product.[126]

Mass loading. Building upon the conditions previously optimized in batch reactions, the initial experiment focused on varying the mass introduced into the extruder. While this parameter may not hold particular significance in conventional batch reactions using solvents, it plays a pivotal role in mechanochemical processes. Increasing the mass within the extruder could enhance the mixing efficiency and boost the mechanical energy involved, thus promoting more efficient contact between the reagents. Consequently, after conducting some preliminary tests that demonstrated promising outcomes within an hour, the quantities of reagents were scaled-up, transitioning from 0.25 to 2 mmol for the limiting reagent (iodobenzene), while preserving the relative ratios between the different reagents in terms of equivalents. Using **5Pd/CNi** as catalytic system, two different

catalyst loading were tested: 20 mg and 40 mg. However, only slightly higher conversions were obtained for the latter case (an increase from 52% to 58% conversion). On the contrary, when maintaining a constant catalyst quantity of 40 mg and doubling the amount of reagents introduced (from 2 mmol to 4 mmol of iodobenzene), the conversion reached 93% within just one hour at 80°C. These preliminary results already highlight the advantages of the mechanochemical protocol, which include the elimination of solvents and the increased productivity compared to batch reactions. The catalytic systems **5Pd/CN-ex** and **P-5Pd/CN-ex** were also tested for comparison. After one hour at 80°C, it was observed an improvement in performance when using 2 mmol of the limiting reagent, as compared to the **5Pd/CNi** catalytic system, resulting in 73% and 81% conversions for the **P-5Pd/CN-ex** and **5Pd/CN-ex** catalysts, respectively. Similarly to the **5Pd/CNi** catalyst, when it comes to the mechanochemically-prepared materials, increasing the mass loading by doubling the amount of reagents while keeping the catalyst quantity the same led to a conversion rate of 95%. These results align with the previously observed trend. A summary of the results is shown in Table 10.

Table 10: Mass loading test. Phenyilboronic acid (1.5 eq.), K_2CO_3 (2 eq.), 80°C, 1h, rotation velocity of twin screw of 50 RPM. Selectivity was always >99%.

Entry	Iodobenzene (mmol)	Catalyst (mg)	Conversion (%)	Yield (%)
1	2	**5Pd/CNi** (20)	52	51
2	2	**5Pd/CNi** (20)	58	57
3	4	**5Pd/CNi** (40)	93	92
4	2	**P-5Pd/CN-ex** (40)	73	72
5	2	**5Pd/CN-ex** (40)	81	80
6	4	**5Pd/CN-ex** (40)	95	93

Catalyst screening. Once the optimal mass loading of 4 mmol of the limiting reagent had been established as defined earlier, a catalyst screening was conducted to identify the most productive catalytic system. The reaction was conducted in the extruder at 80°C for 1 hour, with the extruder twin screws rotating at a speed of 50 rpm. Satisfactory results were reached for all the tested catalytic systems, namely **1Pd/CNi**, **2.5Pd/CNs**, **5Pd/CNi**, **5Pd/CNs**, and **5Pd/CN-ex**, which yielded

conversions of 87%, 95%, 93%, 98%, and 95%, respectively. Based on these conversion values, it may appear that the **5Pd/CNs** system performs the best. However, to gain a more comprehensive view, the conversion was compared, also considering the amount of Pd employed. In terms of productivity, the catalytic systems yielded the following values: 8.70, 3.80, 1.96, 1.86, and 1.90 mol/(g_{Pd}h) for the **1Pd/CNi**, **2.5Pd/CNs**, **5Pd/CNi**, **5Pd/CNs**, and **5Pd/CN-ex** samples, respectively. Based on this analysis, the **1Pd/CNi** catalytic system emerges as the top-performing option, despite its 87% conversion. Additionally, with the aim of investigating whether the quantity of Na_2CO_3 introduced in the synthesis of the **5Pd/CN-ex-Na$_2$CO$_3$** catalyst could replace the K_2CO_3 base typically used in the reaction, tests with the catalytic systems **5Pd/CN-ex-Na$_2$CO$_3$** and **P-5Pd/CN-ex-Na$_2$CO$_3$** were conducted, in the absence of additional base. However, these tests did not yield significant conversions (<10%).
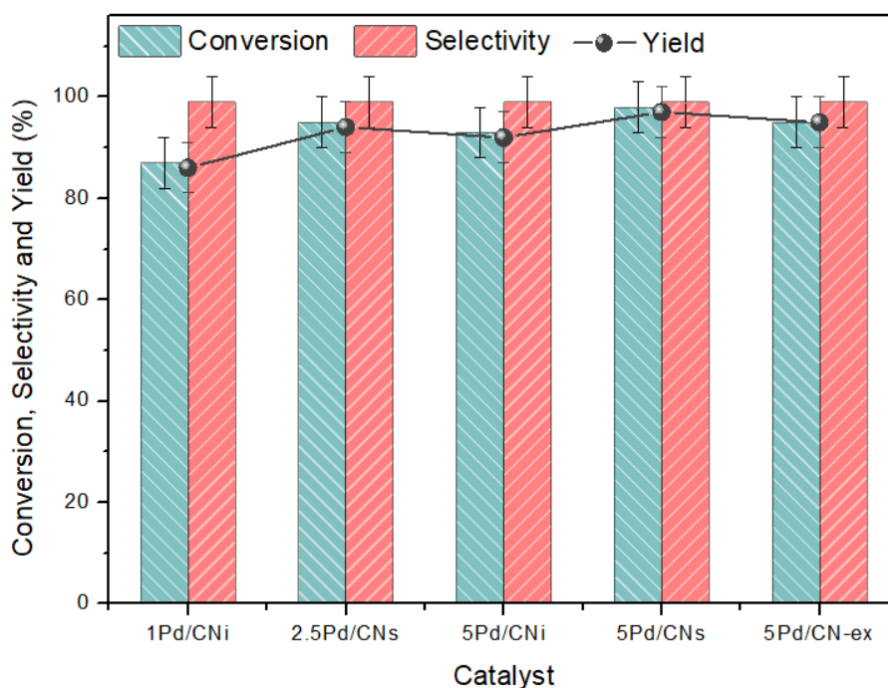
Figure 40: Catalyst screening of Suzuki-Miyaura reaction using mechanochemical protocol. iodobenzene (4 mmol), phenylboronic acid (1.5 eq.), K_2CO_3 (2 eq.), catalyst (40 mg), 50 rpm of velocity of twin screw, 80°C, 1 h.

Time and Temperature optimization. Finally, the operational conditions were optimized, specifically focusing on temperature, residence time, and rotation speed of the extruder twin screws. Tests conducted at rotation speeds of 50, 100, and 150 RPM gave rise to identical results, indicating that, in this case, the rotation speed does not significantly influence the synthesis of the product. More interestingly, studies on time and temperature were conducted. Using the **1Pd/CNi** catalytic system,

three experiments were carried out with reaction times of 0.5, 1, and 2 hours, resulting in conversions of 58%, 87%, and 93%, respectively. Considering productivity as one of the evaluative parameters, the optimal residence time was found to be 1 hour. Regarding temperature, experiments were conducted at room temperature (25°C), 50°C, and 80°C, resulting in conversions of 5%, 15%, and 87%, respectively. In this case, the importance of temperature in the success of the reaction was evident, with 80°C yielding the best results.
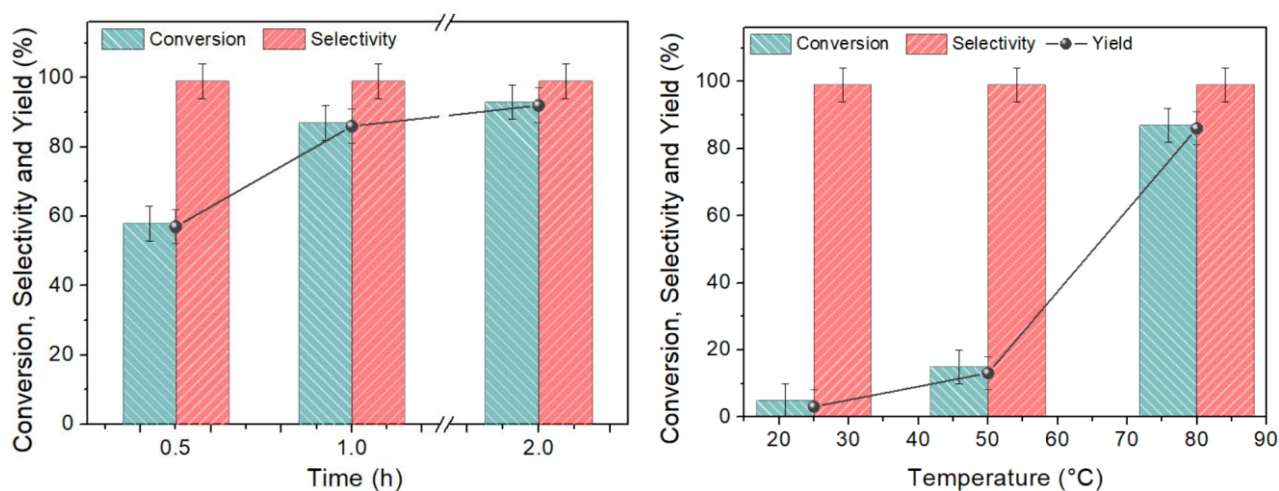
Figure 41: Time and Temperature optimization. Iodobenzene (4 mmol), phenylboronic acid (1.5 eq.), K_2CO_3 (2 eq.), **1Pd/CNi** (40 mg), 50 rpm of velocity of twin screw.

Comparation with literature. The optimal results obtained with the synthesized catalytic systems were compared to other case studies found in recent literature regarding Suzuki-Miyaura cross-coupling using mechanochemical protocols. Pickhardt et al. developed a liquid-assisted grinding (LAG) process using ball milling with Pd spheres to catalyze the Suzuki reaction between various substrates. In the reaction between iodobenzene (1 mmol) and phenylboronic acid (1 mmol), a base, K_2CO_3 (1g), and a minimal amount of ethanol are added.[127] This allows the reaction to proceed in one hour, achieving quantitative conversions. However, compared to the protocol presented here, their method requires the use of an additive (ethanol), albeit in small amounts. Without it, adequate conversions cannot be achieved even after 16 hours. Additionally, the use of ball milling restricts precise temperature control (not specified in the article) and confines the reaction to batch mode, unlike the extruder, which enables excellent temperature control and the development of more easily scalable continuous-flow processes at an industrial level.[92,96] Furthermore, the use of a 4g Pd sphere incurs significant costs compared to dispersing milligrams over a substrate.

Wohlgemuth et al. developed a protocol using a specific type of milling called resonant acoustic mixers (RAM), which utilizes acoustic resonance to impart kinetic energy to molecules.[128] In their study, a container covered with a layer of Pd allowed the achievement of a 90% yield in the cross-coupling product between iodobenzene and phenylboronic acid, in the presence of K_2CO_3 and a small amount of ethanol as an additive. In this case, similar limitations to the previous articles were observed.

Seo et al. used ball milling to synthesize a PEG-functionalized matrix with Pd phosphine complexes used to immobilize Pd from $Pd(OAc)_2$ added during the cross-coupling reaction between a bromoaryl compound and an arylboronic acid.[129] The reaction quantitatively produces the cross-coupling product after one hour at 45°C in the presence of water as a liquid additive and CsF as the base. However, besides the increased toxicity of the base used compared to simple potassium carbonate, the described process employs numerous auxiliary substances that inevitably increase the amount of generated waste. Additionally, although the stated temperature is 45°C, the authors heat the ball milling mixture to this temperature using a heat gun set to 70°C, raising doubts about temperature control and process scalability.

Pentsak et al. conducted the cross-coupling between 1-bromo-4-nitrobenzene and phenylboronic acid using ball milling, catalyzed by a composite of palladium nanoparticles supported on multi-walled carbon nanotubes (PdNP/MWCNT).[126] The reaction, conducted using potassium carbonate as the base, achieves a 91% conversion at 80°C, but it requires 6 hours to reach this level. These observations are summarized in Table 11.

Table 11: Different studies in the recent literature about Suzuki cross-coupling reaction using a mechanochemical protocol.

Entry	Catalyst	Reactor	Additive liquid (LAG)	Time (h)	Yield (%)	Ref.
1	**1Pd/CNi**	Extruder	No	1	99	This studio
2	Pd sphere	Ball milling	Ethanol	1	99	[127]
3	Pd layer	RAM	Ethanol	1	90	[128]
4	$Pd(OAc)_2$	Ball milling	H_2O	1	99	[129]
5	PdNP/MWCNT	Ball milling	No	6	91	[126]

CONCLUSION

In a context where green chemistry and process sustainability are gaining increasing importance, this thesis work has proposed a potential utilization of a product, chitin, derived from seafood industry waste, specifically from shrimp shells, in line with a circular economy perspective. This approach transforms what might be waste in one industry into a raw material in another industry, thus improving and optimizing the utilization of nature's resources. Chitin has been used by harnessing the amide groups present in its structure to create a nitrogen-doped support on which metals (in this case, Pd) can be deposited for the synthesis of heterogeneous catalysts. The presence of nitrogen in the structure, in this case from pyridinic and pyrrolic groups, is interesting because it can enhance the dispersion of metal nanoparticles and increase their interaction with the support, reducing undesired phenomena in heterogeneous catalysis such as leaching. In summary, six catalytic systems were synthesized using the impregnation method (Method A) and the solution method (Method B), each with varying Pd loads: **5Pd/CNi**, **2.5Pd/CNi**, **1Pd/CNi**, **5Pd/CNs**, **2.5Pd/CNs**, **and 1Pd/CNs**. Method A produces fewer waste by-products and is therefore more environmentally friendly, while Method B generally allows for a more homogeneous dispersion with smaller nanoparticle sizes. All catalytic systems were tested in two cross-coupling reactions, Heck-Mizoroki and Suzuki-Miyaura.

In the Heck-Mizoroki reaction, following various optimization tests including catalyst screening, base quantity, type of base, type of solvent, time, and temperature optimization, the best conditions identified in terms of conversion, selectivity, and yield were as follows: **1Pd/CNi** (10 mg), iodobenzene (1 mmol), ethyl acrylate (1.5 mmol), NEt_3 (1 mmol), GVL (2 ml), 125°C, 4h. These conditions led to nearly quantitative conversion and yields, with the extremely selective formation of the cross-coupling product (biphenyl). Subsequently, a substrate scope was carried out, revealing the ineffectiveness of the catalysts with aryl bromides and aryl chlorides. Finally, recycling tests of the catalyst were performed to assess its stability. The catalytic system was recovered at the end of each reaction through centrifugation. The results were encouraging as the catalytic activity remained high. However, there was a slight decrease in performance with an increasing number of cycles, which was attributed to various possible phenomena. In the future, it would be interesting to continue the study to determine whether this negative trend in catalytic activity continues with further cycles, as only three cycles were conducted in this work due to time constraints. Additionally, it is a future goal to conduct a similar study for the Suzuki-Miyaura reaction to observe if there are any influences from the elevated temperature conditions used in the Heck reaction.

In the Suzuki-Miyaura reaction, similar to what was done with the Heck cross-coupling, different catalytic systems underwent various optimization tests, including catalyst screening, base quantity, type of base, type of solvent, time, and temperature optimization. Through batch experiments, the best conditions were determined as follows: **1Pd/CNi** (10 mg), iodobenzene (0.25 mmol), phenylboronic acid (1.5 eq.), K_2CO_3 (0.5 mmol), Ethanol (3 ml), 75°C, 4h. Under these conditions, quantitative conversion and yields were achieved, selectively producing ethyl cinnamate, the cross-coupling product. In this case as well, substrate scope experiments indicated a drastic decrease in conversion when starting with aryl bromides or aryl chlorides. This decrease is attributed to the stronger carbon-halogen bond, which makes the initial oxidative addition step, typically the rate-determining step in these reactions, more difficult.

In the last phase of this study, starting from the Suzuki reaction between iodobenzene and phenylboronic acid, a mechanochemical protocol was developed. Catalysts based on Pd supported on an N-doped carbon matrix were synthesized through a mechanochemical approach, with and without heat treatment, resulting in **5Pd/CN-ex** and **P-5Pd/CN-ex**, respectively. In a similar manner, catalysts containing 0.5 mmol of Na_2CO_3 were also synthesized, labeled as **5Pd/CN-ex-Na$_2$CO$_3$** and **P-5Pd/CN-ex-Na$_2$CO$_3$**. For the systems **5Pd/CN-ex** and **5Pd/CN-ex-Na$_2$CO$_3$**, the appearance of a new signal in the Pd3*d* XPS region was observed, indicating the formation of a Pd-N bond, likely contributing to better catalyst stability against leaching. Using these new catalytic materials, along with those formed by methods A and B, mass loading tests were conducted, revealing a strong influence on conversion based on the amount of material introduced into the extruder. Subsequently, a catalyst screening was performed, and to select the best catalytic system, productivity was considered, in line with the future perspective of using the extruder in a potential continuous-flow process. The best catalytic system was found to be **1Pd/CNi**, with a productivity of 8.7 mol/(g_{Pd}h). With this system, temperature and time optimization was carried out, having previously seen that the rotation speed of the twin screw in the extruder did not significantly affect the yield. Finally, the optimal operating conditions were determined as follows: iodobenzene (4 mmol), phenylboronic acid (1.5 eq.), K_2CO_3 (2 eq.), **1Pd/CNi** (40 mg), 50 RPM twin screw velocity, 80°C, 1h.

All the objectives set in this study have been achieved. Due to time constraints, a more in-depth exploration of the activity of the catalytic systems obtained in the extruder in batch reactions was not possible, but it will be conducted in the following months. In these studies, it will be crucial to

verify the actual increased stability of these catalytic systems, attributed to the presence of the Pd-N bond observed in XPS analysis.

Finally, at every stage of this work, the obtained values were compared with results present in recent literature, demonstrating that the performance of the synthesized catalytic systems aligns with existing data. However, these systems offer the advantage of using a renewable source-based support, thus valorizing an important waste product from the seafood industry. Therefore, these catalytic systems can serve as a more sustainable alternative to conventional fossil-based catalysts.

In conclusion, based on the results obtained during the development of a mechanochemical protocol for the Suzuki-Miyaura reaction, an article titled "Mechanochemistry through Extrusion: Opportunities for Nanomaterials Design and Catalysis in the Continuous Mode" has been published, and it is included in the appendices.

BIBLIOGRAFIA

(1)   Xu, C.; Paone, E.; Rodríguez-Padrón, D.; Luque, R.; Mauriello, F. Recent Catalytic Routes for the Preparation and the Upgrading of Biomass Derived Furfural and 5-Hydroxymethylfurfural. *Chem Soc Rev* **2020**, *49* (13), 4273–4306. https://doi.org/10.1039/D0CS00041H.

(2)   United Nations. *World Population Prospects 2022 Summary of Results*; 2022.

(3)   United Nations. *TRANSFORMING OUR WORLD: THE 2030 AGENDA FOR SUSTAINABLE DEVELOPMENT*; 2015. https://www.un.org/en/development/desa/population/migration/generalassembly/docs/globalcompact/A_RES_70_1_E.pdf (accessed 2023-09-01).

(4)   CEFIC. *SUSTAINABILITY PROGRESS UPDATE 2022*; 2022.

(5)   CEFIC. *2019 SUSTAINABILITY PROGRESS REPORT of the European Chemical Industry Council*; 2019.

(6)   Ivanković, A. Review of 12 Principles of Green Chemistry in Practice. *International Journal of Sustainable and Green Energy* **2017**, *6* (3), 39. https://doi.org/10.11648/j.ijrse.20170603.12.

(7)   Warner, J. C.; Cannon, A. S.; Dye, K. M. Green Chemistry. *Environ Impact Assess Rev* **2004**, *24* (7–8), 775–799. https://doi.org/10.1016/j.eiar.2004.06.006.

(8)   Sariatli, F. Linear Economy Versus Circular Economy: A Comparative and Analyzer Study for Optimization of Economy for Sustainability. *Visegrad Journal on Bioeconomy and Sustainable Development* **2017**, *6* (1), 31–34. https://doi.org/10.1515/vjbsd-2017-0005.

(9)   Clark, J. H.; Farmer, T. J.; Herrero-Davila, L.; Sherwood, J. Circular Economy Design Considerations for Research and Process Development in the Chemical Sciences. *Green Chemistry* **2016**, *18* (14), 3914–3934. https://doi.org/10.1039/c6gc00501b.

(10)   Bridgwater, T. Biomass for Energy. *J Sci Food Agric* **2006**, *86* (12), 1755–1768. https://doi.org/10.1002/jsfa.2605.

(11)   Espro, C.; Paone, E.; Mauriello, F.; Gotti, R.; Uliassi, E.; Bolognesi, M. L.; Rodríguez-Padrón, D.; Luque, R. Sustainable Production of Pharmaceutical, Nutraceutical and Bioactive Compounds from Biomass and Waste. *Chem Soc Rev* **2021**, *50* (20), 11191–11207. https://doi.org/10.1039/D1CS00524C.

(12)   Costello, C.; Cao, L.; Gelcich, S.; Cisneros-Mata, M.; Free, C. M.; Froehlich, H. E.; Golden, C. D.; Ishimura, G.; Maier, J.; Macadam-Somer, I.; Mangin, T.; Melnychuk, M. C.; Miyahara, M.; de Moor, C. L.; Naylor, R.; Nøstbakken, L.; Ojea, E.; O'Reilly, E.; Parma, A. M.; Plantinga, A. J.; Thilsted, S. H.; Lubchenco, J. The Future of Food from the Sea. *Nature* **2020**, *588* (7836), 95–100. https://doi.org/10.1038/s41586-020-2616-y.

(13) FAO. *The State of World Fisheries and Aquaculture 2022*; FAO, 2022. https://doi.org/10.4060/cc0461en.

(14) Yan, N.; Chen, X. Sustainability: Don't Waste Seafood Waste. *Nature* **2015**, *524* (7564), 155–157. https://doi.org/10.1038/524155a.

(15) Kandra, P.; Challa, M. M.; Kalangi Padma Jyothi, H. Efficient Use of Shrimp Waste: Present and Future Trends. *Appl Microbiol Biotechnol* **2012**, *93* (1), 17–29. https://doi.org/10.1007/s00253-011-3651-2.

(16) Wani, A. K.; Akhtar, N.; Mir, T. ul G.; Rahayu, F.; Suhara, C.; Anjli, A.; Chopra, C.; Singh, R.; Prakash, A.; El Messaoudi, N.; Fernandes, C. D.; Ferreira, L. F. R.; Rather, R. A.; Américo-Pinheiro, J. H. P. Eco-Friendly and Safe Alternatives for the Valorization of Shrimp Farming Waste. *Environmental Science and Pollution Research* **2023**. https://doi.org/10.1007/s11356-023-27819-z.

(17) Sachindra, N. M.; Bhaskar, N.; Mahendrakar, N. S. Carotenoids in Different Body Components of Indian Shrimps. *J Sci Food Agric* **2005**, *85* (1), 167–172. https://doi.org/10.1002/jsfa.1977.

(18) Mao, X.; Guo, N.; Sun, J.; Xue, C. Comprehensive Utilization of Shrimp Waste Based on Biotechnological Methods: A Review. *Journal of Cleaner Production*. Elsevier Ltd February 1, 2017, pp 814–823. https://doi.org/10.1016/j.jclepro.2016.12.042.

(19) Ray, S.; Mondal, P.; Paul, A. K.; Iqbal, S.; Atique, U.; Islam, M. S.; Mahboob, S.; Al-Ghanim, K. A.; Al-Misned, F.; Begum, S. Role of Shrimp Farming in Socio-Economic Elevation and Professional Satisfaction in Coastal Communities of Southern Bangladesh. *Aquac Rep* **2021**, *20*. https://doi.org/10.1016/j.aqrep.2021.100708.

(20) Guerrero-galva, L. R.; Ruiz-fern, A. C. The Environmental Impact of Shrimp Aquaculture and the Coastal Pollution in Mexico. *Marine Pollution Bulletl* **1998**, *36* (1), 65–75.

(21) Gimeno, M.; Ramírez-Hernández, J. Y.; Mártinez-Ibarra, C.; Pacheco, N.; García-Arrazola, R.; Bárzana, E.; Shirai, K. One-Solvent Extraction of Astaxanthin from Lactic Acid Fermented Shrimp Wastes. *J Agric Food Chem* **2007**, *55* (25), 10345–10350. https://doi.org/10.1021/jf071469h.

(22) Blumenthal, H. J.; Roseman, S. Quantitative Estimation of Chitin in Fungi. *J Bacteriol* **1957**, *74* (2), 222–224. https://doi.org/10.1128/jb.74.2.222-224.1957.

(23) Khoushab, F.; Yamabhai, M. Chitin Research Revisited. *Mar Drugs* **2010**, *8* (7), 1988–2012. https://doi.org/10.3390/md8071988.

(24) Wagner, G. P.; Lo, J.; Laine, R.; Almeder, M. Chitin in the Epidermal Cuticle of a Vertebrate (Paralipophrys Trigloides, Blenniidae, Teleostei). *Experientia* **1993**, *49* (4), 317–319. https://doi.org/10.1007/BF01923410.

(25)   Rinaudo, M. Chitin and Chitosan: Properties and Applications. *Prog Polym Sci* **2006**, *31* (7), 603–632. https://doi.org/10.1016/j.progpolymsci.2006.06.001.

(26)   Rudall, K. M.; Kenchington, W. The Chitin System. *Biological Reviews* **1973**, *48* (4), 597–633. https://doi.org/10.1111/j.1469-185X.1973.tb01570.x.

(27)   Klokkeuold, P. R.; Fukayama, H.; Sung, E. C.; Bertolami, C. N. The Effect of Chitosan (Poly-N-Acetyl Glucosamine) on Lingual Hemostasis in Heparinized Rabbits. *J Oral Maxillofac Surg* **1999**, *57*, 49–52.

(28)   Aam, B. B.; Heggset, E. B.; Norberg, A. L.; Sørlie, M.; Vårum, K. M.; Eijsink, V. G. H. Production of Chitooligosaccharides and Their Potential Applications in Medicine. *Mar Drugs* **2010**, *8* (5), 1482–1517. https://doi.org/10.3390/md8051482.

(29)   Freier, T.; Montenegro, R.; Koh, H. S.; Shoichet, M. S. Chitin-Based Tubes for Tissue Engineering in the Nervous System. *Biomaterials* **2005**, *26* (22), 4624–4632. https://doi.org/10.1016/j.biomaterials.2004.11.040.

(30)   Sakaguchi, T.; Horikoshi, T.; Nakajima, A. Adsorption of Uranium by Chitin Phosphate and Chitosan Phosphate*. *Biol Chem* **1981**, *45* (10), 2191–2195.

(31)   Cheng, J. C.; Pisano, A. P. Photolithographic Process for Integration of the Biopolymer Chitosan into Micro/Nanostructures. *Journal of Microelectromechanical Systems* **2008**, *17* (2), 402–409. https://doi.org/10.1109/JMEMS.2008.916325.

(32)   Franco, L. de O.; Maia, R. de C. C.; Porto, A. L. F.; Messias, A. S.; Fukushima, K.; Campos-Takaki, G. M. de. Heavy Metal Biosorption by Chitin and Chitosan Isolated from Cunninghamella Elegans (IFM 46109). *Brazilian Journal of Microbiology* **2004**, *35* (3), 243–247. https://doi.org/10.1590/S1517-83822004000200013.

(33)   Day, R. B.; Okada, M.; Ito, Y.; Tsukada, K.; Zaghouani, H.; Shibuya, N.; Stacey, G. Binding Site for Chitin Oligosaccharides in the Soybean Plasma Membrane. *Plant Physiol* **2001**, *126* (3), 1162–1173. https://doi.org/10.1104/pp.126.3.1162.

(34)   Zia, K. M.; Zuber, M.; Barikani, M.; Bhatti, I. A.; Khan, M. B. Surface Characteristics of Chitin-Based Shape Memory Polyurethane Elastomers. *Colloids Surf B Biointerfaces* **2009**, *72* (2), 248–252. https://doi.org/10.1016/j.colsurfb.2009.04.011.

(35)   Healy, M. G.; Romo, C. R.; Bustos, R. Bioconversion of Marine Crustacean Shell Waste. *Resour Conserv Recycl* **1994**, *11* (1–4), 139–147. https://doi.org/10.1016/0921-3449(94)90085-X.

(36)   Mahmoud, N. S.; Ghaly, A. E.; Arab, F. Unconventional Approach for Demineralization of Deproteinized Crustacean Shells for Chitin Production. *Am J Biochem Biotechnol* **2007**, *3* (1), 1–9. https://doi.org/10.3844/ajbbsp.2007.1.9.

(37) Mahmoud, N. S.; Ghaly, A. E.; Arab, F. Unconventional Approach for Demineralization of Deproteinized Crustacean Shells for Chitin Production. *Am J Biochem Biotechnol* **2007**, *3* (1), 1–9. https://doi.org/10.3844/ajbbsp.2007.1.9.

(38) Rao, M. S.; Muñoz, J.; Stevens, W. F. Critical Factors in Chitin Production by Fermentation of Shrimp Biowaste. *Appl Microbiol Biotechnol* **2000**, *54* (6), 808–813. https://doi.org/10.1007/s002530000449.

(39) Yang, J.-K.; Shih, I.-L.; Tzeng, Y.-M.; Wang, S.-L. Production and Purification of Protease from a Bacillus Subtilis That Can Deproteinize Crustacean Wastes. *Enzyme Microb Technol* **2000**, *26* (5–6), 406–413. https://doi.org/10.1016/S0141-0229(99)00164-7.

(40) Tolesa, L. D.; Gupta, B. S.; Lee, M. J. Chitin and Chitosan Production from Shrimp Shells Using Ammonium-Based Ionic Liquids. *Int J Biol Macromol* **2019**, *130*, 818–826. https://doi.org/10.1016/j.ijbiomac.2019.03.018.

(41) Rodríguez-Padrón, D.; Puente-Santiago, A. R.; Balu, A. M.; Muñoz-Batista, M. J.; Luque, R. Environmental Catalysis: Present and Future. *ChemCatChem* **2019**, *11* (1), 18–38. https://doi.org/10.1002/cctc.201801248.

(42) Svehla, G. Nomenclature of Kinetic Methods of Analysis (IUPAC Recommendations 1993). *Pure and Applied Chemistry* **1993**, *65* (10), 2291–2298. https://doi.org/10.1351/pac199365102291.

(43) Mao, S.; Wang, C.; Wang, Y. The Chemical Nature of N Doping on N Doped Carbon Supported Noble Metal Catalysts. *J Catal* **2019**, *375*, 456–465. https://doi.org/10.1016/j.jcat.2019.06.039.

(44) Liu, X.; Zhao, R.; Zhao, H.; Wang, Z.; Li, F.; Xue, W.; Wang, Y. Enhanced Stability of Nitrogen-Doped Carbon-Supported Palladium Catalyst for Oxidative Carbonylation of Phenol. *Chin J Chem Eng* **2023**. https://doi.org/10.1016/j.cjche.2023.08.001.

(45) Polidoro, D.; Perosa, A.; Selva, M.; Rodríguez-Padrón, D. Metal-Free Carbonaceous Catalytic Materials: Biomass Feedstocks for a Greener Future. *ChemCatChem* **2023**, *15* (13). https://doi.org/10.1002/cctc.202300415.

(46) Arrigo, R.; Schuster, M. E.; Xie, Z.; Yi, Y.; Wowsnick, G.; Sun, L. L.; Hermann, K. E.; Friedrich, M.; Kast, P.; Hävecker, M.; Knop-Gericke, A.; Schlögl, R. Nature of the N–Pd Interaction in Nitrogen-Doped Carbon Nanotube Catalysts. *ACS Catal* **2015**, *5* (5), 2740–2753. https://doi.org/10.1021/acscatal.5b00094.

(47) Polidoro, D.; Perosa, A.; Rodríguez-Castellón, E.; Canton, P.; Castoldi, L.; Rodríguez-Padrón, D.; Selva, M. Metal-Free N-Doped Carbons for Solvent-Less CO2 Fixation Reactions: A Shrimp Shell Valorization Opportunity. *ACS Sustain Chem Eng* **2022**, *10* (41), 13835–13848. https://doi.org/10.1021/acssuschemeng.2c04443.

(48) Trentin, O.; Polidoro, D.; Perosa, A.; Rodríguez-Castellon, E.; Rodríguez-Padrón, D.; Selva, M. Mechanochemistry through Extrusion: Opportunities for Nanomaterials Design and Catalysis in the Continuous Mode. *Chemistry (Easton)* **2023**, *5* (3), 1760–1769. https://doi.org/10.3390/chemistry5030120.

(49) Polidoro, D.; Ballesteros-Plata, D.; Perosa, A.; Rodríguez-Castellón, E.; Rodríguez-Padrón, D.; Selva, M. Controlled Alcohol Oxidation Reactions by Supported Non-Noble Metal Nanoparticles on Chitin-Derived N-Doped Carbons. *Catal Sci Technol* **2023**, *13* (7), 2223–2238. https://doi.org/10.1039/d3cy00082f.

(50) Polidoro, D.; Rodriguez-Padron, D.; Perosa, A.; Luque, R.; Selva, M. Chitin-Derived Nanocatalysts for Reductive Amination Reactions. *Materials* **2023**, *16* (2). https://doi.org/10.3390/ma16020575.

(51) Farhang, M.; Akbarzadeh, A. R.; Rabbani, M.; Ghadiri, A. M. A Retrospective-Prospective Review of Suzuki–Miyaura Reaction: From Cross-Coupling Reaction to Pharmaceutical Industry Applications. *Polyhedron* **2022**, *227*, 116124. https://doi.org/10.1016/j.poly.2022.116124.

(52) Ashraf, M.; Ahmad, M. S.; Inomata, Y.; Ullah, N.; Tahir, M. N.; Kida, T. Transition Metal Nanoparticles as Nanocatalysts for Suzuki, Heck and Sonogashira Cross-Coupling Reactions. *Coord Chem Rev* **2023**, *476*, 214928. https://doi.org/10.1016/j.ccr.2022.214928.

(53) Knowles, J. P.; Whiting, A. The Heck-Mizoroki Cross-Coupling Reaction: A Mechanistic Perspective. *Org Biomol Chem* **2007**, *5* (1), 31–44. https://doi.org/10.1039/b611547k.

(54) Astruc, D. The 2010 Chemistry Nobel Prize to R.F. Heck, E. Negishi, and A. Suzuki for Palladium-Catalyzed Cross-Coupling Reactions. *Anal Bioanal Chem* **2011**, *399* (5), 1811–1814. https://doi.org/10.1007/s00216-010-4555-1.

(55) Ahmadvand, Z.; Bayat, M.; Zolfigol, M. A. Toward Prediction of the Precatalyst Activation Mechanism through the Cross-Coupling Reactions: Reduction of Pd(II) to Pd(0) in Precatalyst of the Type Pd-PEPPSI. *J Comput Chem* **2020**, *41* (26), 2296–2309. https://doi.org/10.1002/jcc.26393.

(56) Díez-González, S.; Marion, N.; Nolan, S. P. N-Heterocyclic Carbenes in Late Transition Metal Catalysis. *Chem Rev* **2009**, *109* (8), 3612–3676. https://doi.org/10.1021/cr900074m.

(57) Szulmanowicz, M. S.; Gniewek, A.; Gil, W.; Trzeciak, A. M. Palladium(II) Complexes with Small N-Heterocyclic Carbene Ligands as Highly Active Catalysts for the Suzuki-Miyaura Cross-Coupling Reaction. *ChemCatChem* **2013**, *5* (5), 1152–1160. https://doi.org/10.1002/cctc.201200428.

(58) Ashraf, M.; Ahmad, M. S.; Inomata, Y.; Ullah, N.; Tahir, M. N.; Kida, T. Transition Metal Nanoparticles as Nanocatalysts for Suzuki, Heck and Sonogashira Cross-Coupling Reactions. *Coord Chem Rev* **2023**, *476*, 214928. https://doi.org/10.1016/j.ccr.2022.214928.

(59)   Díaz-Sánchez, M.; Díaz-García, D.; Prashar, S.; Gómez-Ruiz, S. Palladium Nanoparticles Supported on Silica, Alumina or Titania: Greener Alternatives for Suzuki–Miyaura and Other C–C Coupling Reactions. *Environ Chem Lett* **2019**, *17* (4), 1585–1602. https://doi.org/10.1007/s10311-019-00899-5.

(60)   Huang, L.; Wang, Z.; Ang, T. P.; Tan, J.; Wong, P. K. A Novel SiO2 Supported Pd Metal Catalyst for the Heck Reaction. *Catal Letters* **2006**, *112* (3–4), 219–225. https://doi.org/10.1007/s10562-006-0206-8.

(61)   Climent, M. J.; Corma, A.; Iborra, S.; Mifsud, M. Heterogeneous Palladium Catalysts for a New One-Pot Chemical Route in the Synthesis of Fragrances Based on the Heck Reaction. *Adv Synth Catal* **2007**, *349* (11–12), 1949–1954. https://doi.org/10.1002/adsc.200700026.

(62)   Hossain, A. M. S.; Balbín, A.; Erami, R. S.; Prashar, S.; Fajardo, M.; Gómez-Ruiz, S. Synthesis and Study of the Catalytic Applications in C–C Coupling Reactions of Hybrid Nanosystems Based on Alumina and Palladium Nanoparticles. *Inorganica Chim Acta* **2017**, *455*, 645–652. https://doi.org/10.1016/j.ica.2016.04.045.

(63)   Ncube, P.; Hlabathe, T.; Meijboom, R. Palladium Nanoparticles Supported on Mesoporous Silica as Efficient and Recyclable Heterogenous Nanocatalysts for the Suzuki C–C Coupling Reaction. *J Clust Sci* **2015**, *26* (5), 1873–1888. https://doi.org/10.1007/s10876-015-0885-7.

(64)   Liu, Y.; Bai, X. Argon Glow Discharge Plasma-Reduced Palladium Nanoparticles Supported on Activated Carbon for Suzuki and Heck Coupling Reactions. *Appl Organomet Chem* **2017**, *31* (2), e3561. https://doi.org/10.1002/aoc.3561.

(65)   Ghorbani-Choghamarani, A.; Tahmasbi, B.; Noori, N.; Faryadi, S. Pd–S-Methylisothiourea Supported on Magnetic Nanoparticles as an Efficient and Reusable Nanocatalyst for Heck and Suzuki Reactions. *Comptes Rendus Chimie* **2017**, *20* (2), 132–139. https://doi.org/10.1016/j.crci.2016.06.010.

(66)   Hosseini-Sarvari, M.; Dehghani, A. Nickel/TiO2-Catalyzed Suzuki–Miyaura Cross-Coupling of Arylboronic Acids with Aryl Halides in MeOH/H2O. *Monatshefte für Chemie - Chemical Monthly* **2023**, *154* (3–4), 397–405. https://doi.org/10.1007/s00706-023-03052-9.

(67)   Colacot, T. J. The 2010 Nobel Prize in Chemistry: Palladium-Catalysed Cross-Coupling&lt. *Platin Met Rev* **2011**, *55* (2), 84–90. https://doi.org/10.1595/147106711X558301.

(68)   Heck, R. F. Palladium-Catalyzed Reactions of Organic Halides with Olefins. *Acc Chem Res* **1979**, *12* (4), 146–151. https://doi.org/10.1021/ar50136a006.

(69)   Jutand, A.; Mosleh, A. Rate and Mechanism of Oxidative Addition of Aryl Triflates to Zerovalent Palladium Complexes. Evidence for the Formation of Cationic (σ-Aryl)Palladium Complexes. *Organometallics* **1995**, *14* (4), 1810–1817. https://doi.org/10.1021/om00004a038.

(70) Fauvarque, J.-F.; Pflüger, F.; Troupel, M. Kinetics of Oxidative Addition of Zerovalent Palladium to Aromatic Iodides. *J Organomet Chem* **1981**, *208* (3), 419–427. https://doi.org/10.1016/S0022-328X(00)86726-1.

(71) Miyaura, N.; Yamada, K.; Suginome, H.; Suzuki, A. Novel and Convenient Method for the Stereo- and Regiospecific Synthesis of Conjugated Alkadienes and Alkenynes via the Palladium-Catalyzed Cross-Coupling Reaction of 1-Alkenylboranes with Bromoalkenes and Bromoalkynes. *J Am Chem Soc* **1985**, *107* (4), 972–980. https://doi.org/10.1021/ja00290a037.

(72) Sherwood, J.; Clark, J. H.; Fairlamb, I. J. S.; Slattery, J. M. Solvent Effects in Palladium Catalysed Cross-Coupling Reactions. *Green Chemistry* **2019**, *21* (9), 2164–2213. https://doi.org/10.1039/C9GC00617F.

(73) Amatore, C.; Le Duc, G.; Jutand, A. Mechanism of Palladium-Catalyzed Suzuki-Miyaura Reactions: Multiple and Antagonistic Roles of Anionic "Bases" and Their Countercations. *Chemistry - A European Journal* **2013**, *19* (31), 10082–10093. https://doi.org/10.1002/chem.201300177.

(74) Durap, F.; Rakap, M.; Aydemir, M.; Özkar, S. Room Temperature Aerobic Suzuki Cross-Coupling Reactions in DMF/Water Mixture Using Zeolite Confined Palladium(0) Nanoclusters as Efficient and Recyclable Catalyst. *Appl Catal A Gen* **2010**, *382* (2), 339–344. https://doi.org/10.1016/j.apcata.2010.05.021.

(75) Akkoç, S. Importance of Some Factors on the Suzuki-Miyaura Cross-coupling Reaction. *Journal of the Chinese Chemical Society* **2021**, *68* (6), 942–951. https://doi.org/10.1002/jccs.202000351.

(76) Liu, C.; Ni, Q.; Bao, F.; Qiu, J. A Simple and Efficient Protocol for a Palladium-Catalyzed Ligand-Free Suzuki Reaction at Room Temperature in Aqueous DMF. *Green Chemistry* **2011**, *13* (5), 1260. https://doi.org/10.1039/c0gc00176g.

(77) Braga, A. A. C.; Morgon, N. H.; Ujaque, G.; Maseras, F. Computational Characterization of the Role of the Base in the Suzuki–Miyaura Cross-Coupling Reaction. *J Am Chem Soc* **2005**, *127* (25), 9298–9307. https://doi.org/10.1021/ja050583i.

(78) Amatore, C.; Le Duc, G.; Jutand, A. Mechanism of Palladium-Catalyzed Suzuki-Miyaura Reactions: Multiple and Antagonistic Roles of Anionic "Bases" and Their Countercations. *Chemistry - A European Journal* **2013**, *19* (31), 10082–10093. https://doi.org/10.1002/chem.201300177.

(79) Lennox, A. J. J.; Lloyd-Jones, G. C. Transmetalation in the Suzuki-Miyaura Coupling: The Fork in the Trail. *Angewandte Chemie International Edition* **2013**, *52* (29), 7362–7370. https://doi.org/10.1002/anie.201301737.

(80) Lennox, A. J. J.; Lloyd-Jones, G. C. The Slow-Release Strategy in Suzuki-Miyaura Coupling. *Isr J Chem* **2010**, *50* (5–6), 664–674. https://doi.org/10.1002/ijch.201000074.

(81) Adamo, C.; Amatore, C.; Ciofini, I.; Jutand, A.; Lakmini, H. Mechanism of the Palladium-Catalyzed Homocoupling of Arylboronic Acids: Key Involvement of a Palladium Peroxo Complex. *J Am Chem Soc* **2006**, *128* (21), 6829–6836. https://doi.org/10.1021/ja0569959.

(82) Nahabedian, K. V.; Kuivila, H. G. Electrophilic Displacement Reactions. XII. Substituent Effects in the Protodeboronation of Areneboronic Acids. *J Am Chem Soc* **1961**, *83* (9), 2167–2174. https://doi.org/10.1021/ja01470a030.

(83) Ahmadi, Z.; McIndoe, J. S. A Mechanistic Investigation of Hydrodehalogenation Using ESI-MS. *Chemical Communications* **2013**, *49* (98), 11488–11490. https://doi.org/10.1039/c3cc46271d.

(84) Navarro, O.; Kaur, H.; Mahjoor, P.; Nolan, S. P. Cross-Coupling and Dehalogenation Reactions Catalyzed by (N-Heterocyclic Carbene)Pd(Allyl)Cl Complexes. *Journal of Organic Chemistry* **2004**, *69* (9), 3173–3180. https://doi.org/10.1021/jo035834p.

(85) Sheldon, R. A. The E Factor 25 Years on: The Rise of Green Chemistry and Sustainability. *Green Chemistry* **2017**, *19* (1), 18–43. https://doi.org/10.1039/C6GC02157C.

(86) Constable, D. J. C.; Jimenez-Gonzalez, C.; Henderson, R. K. Perspective on Solvent Use in the Pharmaceutical Industry. *Org Process Res Dev* **2007**, *11* (1), 133–137. https://doi.org/10.1021/op060170h.

(87) Jiménez-González, C.; Curzons, A. D.; Constable, D. J. C.; Cunningham, V. L. Expanding GSK's Solvent Selection Guide-Application of Life Cycle Assessment to Enhance Solvent Selections. *Clean Technol Environ Policy* **2004**, *7* (1), 42–50. https://doi.org/10.1007/s10098-004-0245-z.

(88) Gkika, D. A.; Mitropoulos, A. C.; Lambropoulou, D. A.; Kalavrouziotis, I. K.; Kyzas, G. Z. Cosmetic Wastewater Treatment Technologies: A Review. *Environmental Science and Pollution Research* **2022**, *29* (50), 75223–75247. https://doi.org/10.1007/s11356-022-23045-1.

(89) Shrivastava, V.; Ali, I.; Marjub, M. M.; Rene, E. R.; Soto, A. M. F. Wastewater in the Food Industry: Treatment Technologies and Reuse Potential. *Chemosphere* **2022**, *293*, 133553. https://doi.org/10.1016/j.chemosphere.2022.133553.

(90) Alder, C. M.; Hayler, J. D.; Henderson, R. K.; Redman, A. M.; Shukla, L.; Shuster, L. E.; Sneddon, H. F. Updating and Further Expanding GSK's Solvent Sustainability Guide. *Green Chemistry* **2016**, *18* (13), 3879–3890. https://doi.org/10.1039/C6GC00611F.

(91) Horie, K.; Barón, M.; Fox, R. B.; He, J.; Hess, M.; Kahovec, J.; Kitayama, T.; Kubisa, P.; Maréchal, E.; Mormann, W.; Stepto, R. F. T.; Tabak, D.; Vohlídal, J.; Wilks, E. S.; Work, W. J. Definitions of Terms Relating to Reactions of Polymers and to Functional Polymeric Materials (IUPAC Recommendations 2003). *Pure and Applied Chemistry* **2004**, *76* (4), 889–906. https://doi.org/10.1351/pac200476040889.

(92) Espro, C.; Rodríguez-Padrón, D. Re-Thinking Organic Synthesis: Mechanochemistry as a Greener Approach. *Curr Opin Green Sustain Chem* **2021**, *30*, 100478. https://doi.org/10.1016/j.cogsc.2021.100478.

(93) Wang, S.; Zhang, R.; Song, X.; Wei, M.; Xie, T.; Cao, J. Mechanochemical-Assisted Extraction of Active Alkaloids from Plant with Solid Acids. *ACS Sustain Chem Eng* **2019**, *7* (1), 197–207. https://doi.org/10.1021/acssuschemeng.8b02902.

(94) Friščić, T.; Mottillo, C.; Titi, H. M. Mechanochemistry for Synthesis. *Angewandte Chemie* **2020**, *132* (3), 1030–1041. https://doi.org/10.1002/ange.201906755.

(95) Muñoz-Batista, M. J.; Rodriguez-Padron, D.; Puente-Santiago, A. R.; Luque, R. Mechanochemistry: Toward Sustainable Design of Advanced Nanomaterials for Electrochemical Energy Storage and Catalytic Applications. *ACS Sustain Chem Eng* **2018**, *6* (8), 9530–9544. https://doi.org/10.1021/acssuschemeng.8b01716.

(96) Bolt, R. R. A.; Leitch, J. A.; Jones, A. C.; Nicholson, W. I.; Browne, D. L. Continuous Flow Mechanochemistry: Reactive Extrusion as an Enabling Technology in Organic Synthesis. *Chem Soc Rev* **2022**, *51* (11), 4243–4260. https://doi.org/10.1039/D1CS00657F.

(97) Galant, O.; Cerfeda, G.; McCalmont, A. S.; James, S. L.; Porcheddu, A.; Delogu, F.; Crawford, D. E.; Colacino, E.; Spatari, S. Mechanochemistry Can Reduce Life Cycle Environmental Impacts of Manufacturing Active Pharmaceutical Ingredients. *ACS Sustain Chem Eng* **2022**, *10* (4), 1430–1439. https://doi.org/10.1021/acssuschemeng.1c06434.

(98) Huang, Y.; Yan, H.; Zhang, C.; Wang, Y.; Wei, Q.; Zhang, R. Interfacial Electronic Effects in Co@N-Doped Carbon Shells Heterojunction Catalyst for Semi-Hydrogenation of Phenylacetylene. *Nanomaterials* **2021**, *11* (11), 2776. https://doi.org/10.3390/nano11112776.

(99) Wu, Q.; Wang, L.; Zhao, B.; Huang, L.; Yu, S.; Ragauskas, A. J. Highly Selective Hydrogenation of Phenol to Cyclohexanone over a Pd-Loaded N-Doped Carbon Catalyst Derived from Chitosan. *J Colloid Interface Sci* **2022**, *605*, 82–90. https://doi.org/10.1016/j.jcis.2021.07.077.

(100) Xu, C.; Puente-Santiago, A. R.; Rodríguez-Padrón, D.; Caballero, A.; Balu, A. M.; Romero, A. A.; Muñoz-Batista, M. J.; Luque, R. Controllable Design of Polypyrrole-Iron Oxide Nanocoral Architectures for Supercapacitors with Ultrahigh Cycling Stability. *ACS Appl Energy Mater* **2019**, *2* (3), 2161–2168. https://doi.org/10.1021/acsaem.8b02167.

(101) Kumar, R.; Oh, J. H.; Kim, H. J.; Jung, J. H.; Jung, C. H.; Hong, W. G.; Kim, H. J.; Park, J. Y.; Oh, I. K. Nanohole-Structured and Palladium-Embedded 3D Porous Graphene for Ultrahigh Hydrogen Storage and CO Oxidation Multifunctionalities. *ACS Nano* **2015**, *9* (7), 7343–7351. https://doi.org/10.1021/acsnano.5b02337.

(102) Strappaveccia, G.; Ismalaj, E.; Petrucci, C.; Lanari, D.; Marrocchi, A.; Drees, M.; Facchetti, A.; Vaccaro, L. A Biomass-Derived Safe Medium to Replace Toxic Dipolar Solvents and Access

Cleaner Heck Coupling Reactions. *Green Chemistry* **2015**, *17* (1), 365–372. https://doi.org/10.1039/c4gc01677g.

(103) Perosa, A.; Tundo, P.; Selva, M.; Zinovyev, S.; Testa, A. Heck Reaction Catalyzed by Pd/C, in a Triphasic - Organic/Aliquat 336/Aqueous - Solvent System. *Org Biomol Chem* **2004**, *2* (15), 2249–2252. https://doi.org/10.1039/b406822j.

(104) Melchiorre, M.; Budzelaar, P. H. M.; Cucciolito, M. E.; Esposito, R.; Santagata, E.; Ruffo, F. 1,3-Dioxolane Compounds (DOXs) as Biobased Reaction Media. *Green Chemistry* **2023**. https://doi.org/10.1039/d3gc00227f.

(105) Rigo, D.; Polidoro, D.; Marcuzzo, L.; Perosa, A.; Selva, M. Isopropenyl Acetate for the Continuous-Flow Synthesis of Triacetin, Solketal Acetate, and Allyl Acetate from Pure or Crude Glycerol. *ACS Sustain Chem Eng* **2023**, *11* (34), 12602–12613. https://doi.org/10.1021/acssuschemeng.3c02197.

(106) Du, Y.; Wei, S.; Tang, M.; Ye, M.; Tao, H.; Qi, C.; Shao, L. Palladium Nanoparticles Stabilized by Chitosan/PAAS Nanofibers: A Highly Stable Catalyst for Heck Reaction. *Appl Organomet Chem* **2020**, *34* (5). https://doi.org/10.1002/aoc.5619.

(107) Ye, Z.; Zhang, B.; Shao, L.; Xing, G.; Qi, C.; Tao, H. Palladium Nanoparticles Embedded Chitosan/Poly(Vinyl Alcohol) Composite Nanofibers as an Efficient and Stable Heterogeneous Catalyst for Heck Reaction. *J Appl Polym Sci* **2019**, *136* (41). https://doi.org/10.1002/app.48026.

(108) Pei, X.; Li, Y.; Deng, Y.; Lu, L.; Li, W.; Shi, R.; Lei, A.; Zhang, L. Chitin Microsphere Supported Pd Nanoparticles as an Efficient and Recoverable Catalyst for CO Oxidation and Heck Coupling Reaction. *Carbohydr Polym* **2021**, *251*, 117020. https://doi.org/10.1016/j.carbpol.2020.117020.

(109) Jin, T.; Hicks, M.; Kurdyla, D.; Hrapovic, S.; Lam, E.; Moores, A. Palladium Nanoparticles Supported on Chitin-Based Nanomaterials as Heterogeneous Catalysts for the Heck Coupling Reaction. *Beilstein Journal of Organic Chemistry* **2020**, *16*, 2477–2483. https://doi.org/10.3762/bjoc.16.201.

(110) Prat, D.; Wells, A.; Hayler, J.; Sneddon, H.; McElroy, C. R.; Abou-Shehada, S.; Dunn, P. J. CHEM21 Selection Guide of Classical- and Less Classical-Solvents. *Green Chemistry* **2015**, *18* (1), 288–296. https://doi.org/10.1039/c5gc01008j.

(111) McElroy, C. R.; Constantinou, A.; Jones, L. C.; Summerton, L.; Clark, J. H. Towards a Holistic Approach to Metrics for the 21st Century Pharmaceutical Industry. *Green Chemistry* **2015**, *17* (5), 3111–3121. https://doi.org/10.1039/c5gc00340g.

(112) Khosravi, F.; Centeno-Pedrazo, A.; Rajabi, F.; Len, T.; Voskressensky, L. G.; Luque, R.; Garcia-Suarez, E. J. Efficient Ullmann and Suzuki-Miyaura Cross-Coupling Reactions Catalyzed by

Heterogeneous Pd-Porous Carbon Beads Catalysts in Aqueous Media. *Sustain Chem Pharm* **2022**, *30*, 100869. https://doi.org/10.1016/j.scp.2022.100869.

(113) Mhaldar, P.; Vibhute, S.; Rashinkar, G.; Pore, D. Highly Effective Cellulose Supported 2-Aminopyridine Palladium Complex (Pd(II)-AMP-Cell@Al2O3) for Suzuki-Miyaura and Mizoroki–Heck Cross-Coupling. *React Funct Polym* **2020**, *152*, 104586. https://doi.org/10.1016/j.reactfunctpolym.2020.104586.

(114) Jiang, Y.; Xie, B.; Zhang, J. Highly Reactive and Reusable Heterogeneous Activated Carbons-Based Palladium Catalysts for Suzuki–Miyaura Reaction. *Chin J Chem Eng* **2023**, *60*, 165–172. https://doi.org/10.1016/j.cjche.2023.02.013.

(115) Li, X.; Yu, X.; Zhang, W.; Pan, C.; Tang, J.; Yu, G. Effective Suzuki Coupling Reaction Enabled by Palladium–Polycarbene Catalyst Derived from Porous Polyimidazolium. *Journal of Porous Materials* **2022**, *29* (2), 601–608. https://doi.org/10.1007/s10934-021-01193-y.

(116) Martín-Perales, A. I.; Rodríguez-Padrón, D.; García Coleto, A.; Len, C.; de Miguel, G.; Muñoz-Batista, M. J.; Luque, R. Photocatalytic Production of Vanillin over CeO $_x$ and ZrO $_2$ Modified Biomass-Templated Titania. *Ind Eng Chem Res* **2020**, *59* (39), 17085–17093. https://doi.org/10.1021/acs.iecr.0c01846.

(117) Rodríguez-Padrón, D.; Zhao, D.; Carrillo-Carrion, C.; Morales-Torres, C.; Elsharif, A. M.; Balu, A. M.; Luque, R.; Len, C. Exploring the Potential of Biomass-Templated Nb/ZnO Nanocatalysts for the Sustainable Synthesis of N-Heterocycles. *Catal Today* **2021**, *368*, 243–249. https://doi.org/10.1016/j.cattod.2020.06.076.

(118) Zuliani, A.; Balu, A. M.; Luque, R. Efficient and Environmentally Friendly Microwave-Assisted Synthesis of Catalytically Active Magnetic Metallic Ni Nanoparticles. *ACS Sustain Chem Eng* **2017**, *5* (12), 11584–11587. https://doi.org/10.1021/acssuschemeng.7b02945.

(119) Cui, D.; Yang, J.; Lu, B.; Deng, L.; Shen, H. Extraction and Characterization of Chitin from Oratosquilla Oratoria Shell Waste and Its Application in Brassica Campestris L.Ssp. *Int J Biol Macromol* **2022**, *198*, 204–213. https://doi.org/10.1016/j.ijbiomac.2021.12.173.

(120) Cárdenas, G.; Cabrera, G.; Taboada, E.; Miranda, S. P. Chitin Characterization by SEM, FTIR, XRD, and [13] C Cross Polarization/Mass Angle Spinning NMR. *J Appl Polym Sci* **2004**, *93* (4), 1876–1885. https://doi.org/10.1002/app.20647.

(121) Tamoradi, T.; Ghorbani-Choghamarani, A.; Ghadermazi, M. Synthesis of a New Pd(0)-Complex Supported on Magnetic Nanoparticles and Study of Its Catalytic Activity for Suzuki and Stille Reactions and Synthesis of 2,3-Dihydroquinazolin-4(1H)-One Derivatives. *Polyhedron* **2018**, *145*, 120–130. https://doi.org/10.1016/j.poly.2018.01.016.

(122) Baruah, D.; Das, R. N.; Hazarika, S.; Konwar, D. Biogenic Synthesis of Cellulose Supported Pd(0) Nanoparticles Using Hearth Wood Extract of Artocarpus Lakoocha Roxb — A Green, Efficient

and Versatile Catalyst for Suzuki and Heck Coupling in Water under Microwave Heating. *Catal Commun* **2015**, *72*, 73–80. https://doi.org/10.1016/j.catcom.2015.09.011.

(123) Kibasomba, P. M.; Dhlamini, S.; Maaza, M.; Liu, C.-P.; Rashad, M. M.; Rayan, D. A.; Mwakikunga, B. W. Strain and Grain Size of TiO2 Nanoparticles from TEM, Raman Spectroscopy and XRD: The Revisiting of the Williamson-Hall Plot Method. *Results Phys* **2018**, *9*, 628–635. https://doi.org/10.1016/j.rinp.2018.03.008.

(124) Holzwarth, U.; Gibson, N. The Scherrer Equation versus the "Debye-Scherrer Equation." *Nat Nanotechnol* **2011**, *6* (9), 534–534. https://doi.org/10.1038/nnano.2011.145.

(125) He, Z.; Dong, B.; Wang, W.; Yang, G.; Cao, Y.; Wang, H.; Yang, Y.; Wang, Q.; Peng, F.; Yu, H. Elucidating Interaction between Palladium and N-Doped Carbon Nanotubes: Effect of Electronic Property on Activity for Nitrobenzene Hydrogenation. *ACS Catal* **2019**, *9* (4), 2893–2901. https://doi.org/10.1021/acscatal.8b03965.

(126) Pentsak, E. O.; Ananikov, V. P. Pseudo-Solid-State Suzuki–Miyaura Reaction and the Role of Water Formed by Dehydration of Arylboronic Acids. *European J Org Chem* **2019**, *2019* (26), 4239–4247. https://doi.org/10.1002/ejoc.201900410.

(127) Pickhardt, W.; Beaković, C.; Mayer, M.; Wohlgemuth, M.; Kraus, F. J. L.; Etter, M.; Grätz, S.; Borchardt, L. The Direct Mechanocatalytic Suzuki–Miyaura Reaction of Small Organic Molecules. *Angewandte Chemie International Edition* **2022**, *61* (34). https://doi.org/10.1002/anie.202205003.

(128) Wohlgemuth, M.; Schmidt, S.; Mayer, M.; Pickhardt, W.; Grätz, S.; Borchardt, L. Milling Media-Free Suzuki Coupling by Direct Mechanocatalysis- From Mixer Mills to Resonant Acoustic Mixers. *Chemistry – A European Journal* **2023**. https://doi.org/10.1002/chem.202301714.

(129) Seo, T.; Kubota, K.; Ito, H. Mechanochemistry-Directed Ligand Design: Development of a High-Performance Phosphine Ligand for Palladium-Catalyzed Mechanochemical Organoboron Cross-Coupling. *J Am Chem Soc* **2023**, *145* (12), 6823–6837. https://doi.org/10.1021/jacs.2c13543.

APPENDICE

Below, we present the XPS analysis for the catalysts **P-5Pd/CN-ex** and **P-5Pd/CN-ex-Na₂CO₃**, followed by the published article titled "Mechanochemistry through Extrusion: Opportunities for Nanomaterials Design and Catalysis in the Continuous Mode."
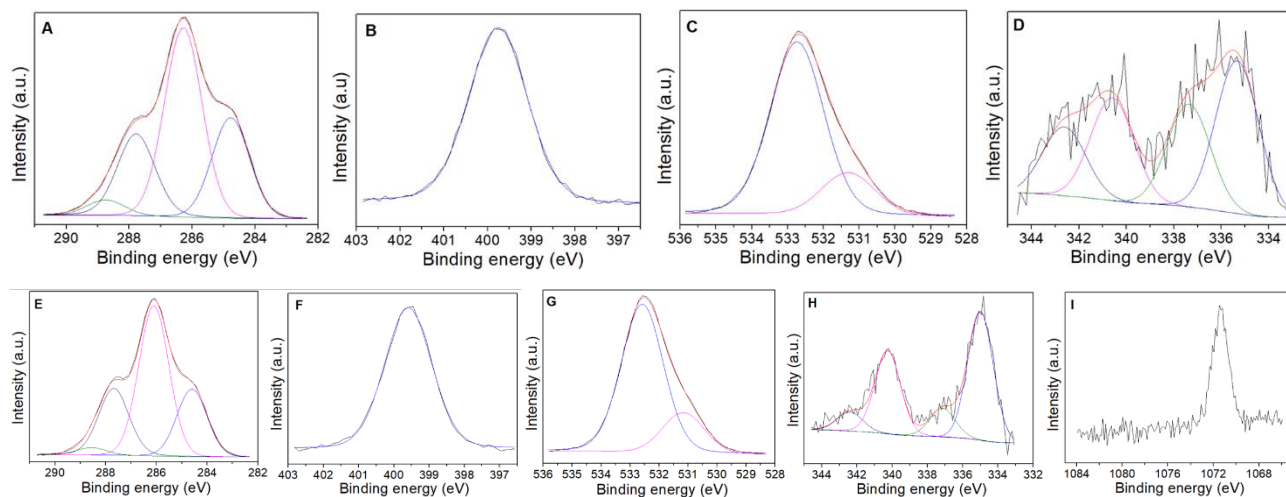
Figure 42: XPS spectra of **P-5Pd/CN-ex** (A-D) and **P-5Pd/CN-ex-Na₂CO₃** (E-I). For each catalytic system, it's represented in this order the C1s, N1s, O1s and Pd3d XPS regions. For **P-5Pd/CN-ex-Na₂CO₃** it's also available the Na1s region.

Mechanochemistry through Extrusion: Opportunities for Nanomaterials Design and Catalysis in the Continuous Mode

Oscar Trentin [1], Daniele Polidoro [1], Alvise Perosa [1], Enrique Rodríguez-Castellon [2], Daily Rodríguez-Padrón [1,*] and Maurizio Selva [1,*]

1 Department of Molecular Science and Nanosystems, Ca' Foscari University of Venice, Via Torino 155, 30175 Venezia, Italy; 876032@stud.unive.it (O.T.); daniele.polidoro@unive.it (D.P.); alvise@unive.it (A.P.)
2 Department of Inorganic Chemistry, Facultad de Ciencias, Universidad de Malaga, Campus de Teatinos s/n, 29071 Málaga, Spain; castellon@uma.es
* Correspondence: daily.rodriguez@unive.it (D.R.-P.); selva@unive.it (M.S.)

Abstract: The potentialities of mechanochemistry trough extrusion have been investigated for the design of nanosized catalysts and their use in C-C bond-forming reactions. The mechanochemical approach proved successful for the synthesis of supported palladium nanoparticles with mean diameter within 6–10 nm, achieved by the reduction of Pd(II) acetate with ethylene glycol, in the absence of any solvent. A mesoporous N-doped carbon derived from chitin as a renewable biopolymer, was used as a support. Thereafter, the resulting nanomaterials were tested as catalysts to implement a second extrusion based-protocol for the Suzuki-Miyaura cross-coupling reaction of iodobenzene and phenylboronic acid. The conversion and the selectivity of the reaction were 81% and >99%, respectively, with a productivity of the desired derivative, biphenyl, of 41 mmol g_{cat}^{-1} h^{-1}.

Keywords: mechanochemistry; extrusion; catalytic nanomaterials; Suzuki-Miyaura cross-coupling reaction

1. Introduction

In recent years, mechanochemistry has emerged as a promising avenue for the synthesis and design of nanomaterials with an environmentally friendly perspective [1]. Due to their simplicity and cost-efficiency, mechanochemical strategies have been implemented to prepare a variety of nanomaterials including supported metal nanoparticles or biomass-templated metal oxides to perovskites and bioconjugates [2–11]. Thrilling opportunities for mechanochemistry are also found in the field of organic synthesis, to obtain peptides, DNA fragments or even active pharmaceutical ingredients [12–18]. This scenario testifies to the tremendous versatility and potential of this branch of chemistry, which aims at improving the sustainability of chemical processes by exploiting the mechanical energy typically generated from grinding, milling, and extrusion, to promote reactions. The most common techniques make use of planetary ball mills, mixer mills, drum mills, or cryomills that are limited to batch conditions. Although these procedures are efficient in conducting mechanochemically assisted transformations, ref. [1] and in some cases, accurate on the temperature control, ref. [19–21], the combined contributions of mechanical and thermal energy inputs are often hardly differentiated.

Far more promising in this respect are continuous flow (CF) mechanochemical reactors which not only allow a better control of the reaction parameters compared to conventional batch systems but are excellent in designing scalable applications. Extrusion is particularly suitable to this scope since, in a typical process, solid reactants, fed and confined under high pressure, are constantly subjected to shear forces originated by one or more screws, which induce the deformation, comminution, and activation of surface species throughout the passage in the CF-reactor [22]. Under such conditions, the mixing of different components, the temperature of the mixture, the solid-state diffusion, and, finally, the physical and

---

chemical changes in reagents, are tuned by the screw speed and the residence time, so that both the product's distribution and the corresponding yields can be optimized [23,24].

Extrusion also provides a platform for the synthesis of heterogeneous catalysts with tailored functionalities, where different precursors or additives are incorporated into each other during the (extrusion) process, to achieve nanocomposites and hybrid materials with improved mechanical strength and enhanced surface reactivity. Excellent examples have been described in the preparation of the supported metal nanoparticles used to catalyzed C-C bond forming and cross-coupling reactions via extrusion [25]. Among the most renowned strategies for C-C bond formation, the Suzuki-Miyaura cross-coupling reaction has gained significant attention in recent years for its environmentally friendly nature. The sustainability of the reaction can indeed be optimized through several key considerations. One approach is based on the use of green and renewable solvents such as water, ethanol, and bio-based derivatives or, alternatively, on solvent-less procedures. The latter, for instance, can be achieved through mechanochemical methods such as extrusion. Additionally, the design of recyclable and reusable heterogeneous catalysts can greatly reduce the carbon footprint of the reaction and improve the cost efficiency. Promising results have already been reported with cheap and non-toxic catalysts based on non-endangered metals such as nickel and copper [26–30]. However, Pd-based catalysts continue to be recognized as some of the most popular systems for the Suzuki-Miyaura cross-coupling [31–34]. Herein, a mechanochemical approach through extrusion was designed through the preparation of such catalytic materials by using palladium acetate as a metal precursor, ethylene glycol as a green reducing agent, and chitin for the synthesis of the catalyst support [35]. Chitin was selected not only for its natural abundance, but also for its high content of nitrogen, which made it an excellent candidate to produce N-doped carbons [36–38]. Notably, such (N-doped) carbons can serve as catalysts by themselves, for base-catalyzed reactions and/or facilitate the incorporation and dispersion of metal entities, mostly thanks to the presence of pyridinic surface groups.

2. Materials and Methods

Materials and equipment. Iodobenzene, phenylboronic acid, K_2CO_3, Na_2CO_3, ethylene glycol, ethanol, 2-propanol, chitin, and $Pd(Ac)_2$ were commercially available compounds sourced from Sigma-Aldrich. If not otherwise specified, reagents and solvents were employed without further purification. Gas Chromatography-Mass Spectrometry (GC-MS) (Electron Ionization (EI), 70 eV) analyses were performed on a HP5-MS capillary column (L = 30 m, Ø = 0.32 mm, film = 0.25 mm). GC (flame ionization detector; FID) analyses were performed with an Elite-624 capillary column (L = 30 m, Ø = 0.32 mm, film = 1.8 mm). All reactions were performed in duplicate to verify reproducibility.

Synthesis of supported palladium nanoparticles on chitin-derived N-doped carbonaceous materials. The materials were prepared following a mechanochemical trough extrusion approach employing chitin (5 g) with a $Pd(Ac)_2$ (0.5 mmol) and ethylene glycol (15 mL). The mixture was extruded at 200 °C and at 50 rpm. The resulting material was oven dried at 100 °C under vacuum overnight and further employed in the catalytic tests. In addition, a thermal treatment at 500 °C (heating rate was 5 °C/min) for 1 h under N_2 flow (10 mL·min^{-1}) for 1 h was carried out and the resulting material was also tested for comparison. The syntheses were performed, also adding Na_2CO_3 (0.5 mmol) under the conditions previously described.

Material Characterization. The crystalline structure of the samples was investigated by X-ray Diffraction (XRD) in the D8 Advance diffractometer of Bruker® AXS (Berlin, Germany), using the X-ray source of the Cu Kα radiation, coupled to a Lynxeye detector, and monitoring the 2θ within 8–80° at a rate of 0.08° min^{-1}. The textural properties, i.e., surface area, the volume of the pore, and pore size were determined from N_2 physisorption at 77 K, performed in ASAP 2000 equipment from Micromeritics® (Norcross, GA, USA). The samples were outgassed at 120 °C for 2 h. Then, adsorption–desorption isotherms were recorded at −196 °C. The specific surface areas were calculated by the BET method; the

pore volumes were calculated from adsorption isotherms and the pore size distributions were estimated using the Barrett, Joyner, and Halenda (BJH) algorithm available as a built-in software from Micromeritics. ICP-OES analysis was carried out in the Avio 550 Max ICP-OES Optical Emission Spectrometer.

Typical CF-Mechanochemical Suzuki-Miyaura cross-coupling reaction. The performance of the catalysts was evaluated under mechanochemical continuous flow conditions in the ZE 12 HMI extruder from Three Tec. In a typical reaction, iodobenzene (2 mmol); PhB(OH)$_2$ (3 mmol); K$_2$CO$_3$ (4 mmol), and the selected catalysts (40 mg) were extruded at 80 °C, 50 rpm, with a residence time of 1 h. Conversion and selectivity were determined by GC-FID and the product structures were assigned by GC-MS. Characterization data are available in the SI Section, Figures S1–S4.

3. Results and Discussion

The preparation of the catalysts through extrusion was carried out according to the procedure schematized in Figure 1. The experimental parameters were chosen based on the previous experience of our research group on the mechanochemical synthesis of nanomaterials [1,39,40]. A suspension of palladium acetate (0.50 mmol, 112 mg), ethylene glycol (15 mL, 0.26 mol), and chitin (5 g) was fed to a mini-extruder (ZE 12 HMI extruder from Three Tec., Seon, Switzerland) heated to 200 °C, whose conveying screws were set to 50 rpm at a torque of 2 Nm. At the end of the extrusion segment, a material in the form of small cylindrical pieces (ca 1 mm diameter) was recovered and used either as such or after a thermal treatment at 500 °C under N$_2$ atmosphere, to catalyze C-C bond forming reactions as Suzuki-Miyaura cross-couplings (see below). A variation of this procedure was designed by adding Na$_2$CO$_3$ (53 mg, 0.5 mmol) to the reacting mixture in order to enhance the basic properties of the sample. Overall, the four prepared materials were labelled as: Pd-chitin and Pd-chitin-500, in order to describe the catalysts achieved without and with calcination in the absence of a base, respectively, and Pd-chitin-Na$_2$CO$_3$ and Pd-chitin-Na$_2$CO$_3$-500, in order to describe the catalysts obtained without and with calcination in the presence of Na$_2$CO$_3$, respectively.
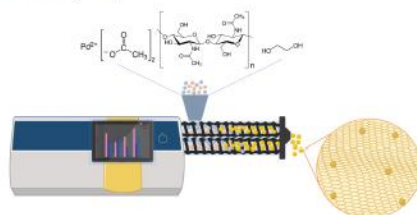

Figure 1. Schematic representation of the mechanochemically assisted synthesis of catalytic materials.

The crystal structure and arrangement of the samples were evaluated by XRD analysis. Figure 2A depicts the XRD patterns of the samples before the thermal treatment, while Figure 2B shows the results for the calcined samples. The Pd-chitin and Pd-chitin-Na$_2$CO$_3$ materials displayed the typical diffraction peaks of chitin at ca. 10, 20, 21, 23, and 26°, related to the (020), (110), (120), (101), and (130) crystallographic planes, respectively [41,42]. The overlapping of a wide peak observed in the region between 20 and 30° was most likely due to the presence of amorphous carbon formed during the mechanochemical synthesis of 200 °C. In addition, the presence of a signal at 39° indicated the (successful) reduction of palladium (II) and the formation Pd(0) nanoparticles. In Figure 2B, instead, the complete

disappearance of the typical chitin peaks, and the simultaneous presence of a wide signal at ca. 24°, were consistent with the decomposition of chitin into amorphous carbon due to the thermal treatment at 500 °C. The sharp and well-defined crystallographic peaks at 39, 47, and 68° were attributed to the (111), (200), and (220) crystallographic planes of Pd(0), respectively [43–45].
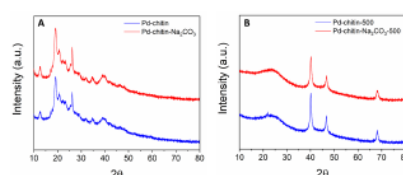

Figure 2. XRD pattern of the catalytic materials (**A**): before and (**B**): after calcination.

For comparison, the SI section reports the XRD data for commercial chitin, while the XRD diffraction patterns of palladium acetate and Na$_2$CO$_3$ are available in the literature [46,47].

The two calcined samples with and without the base, which presented consistent and clearer Pd diffraction signals, were further characterized. The results are reported in Table 1. From the XRD diffraction patterns, metal particle sizes of (6.7 ± 0.5) and (9.7 ± 0.5) nm for Pd-chitin-500 and Pd-chitin-Na$_2$CO$_3$-500, respectively, were calculated using the Scherrer equation [48,49]. The palladium loading, determined by ICP-MS, was around 4 mg g$_{catalyst}$$^{-1}$ for both samples. The textural properties including surface area, pore volume, and pore size were investigated by N$_2$-physisorption. Figure 3 displays the result for Pd-chitin-500. A type IV isotherm and type II adsorption hysteresis were representative of the formation of a mesoporous material. The same held true for Pd-chitin-Na$_2$CO$_3$-500. Both samples exhibited a remarkably high surface area of 452–498 m^{2}g^{-1}, while the range of pore diameter (4.9–5.3 nm) further proved the occurrence of mesoporous solids.

Table 1. Textural properties, particle size, and palladium content of the catalytic materials.

Material	S_{BET} [m^{2}g^{-1}] [a]	D_{BJH} (nm) [b]	V_{BJH} [cm^3/g] [c]	Pd conc./mg g^{-1} [d]	Pd Particle Size (nm) [e]
Pd-chitin-500	498	4.9	0.61	4.3	9.7
Pd-chitin-Na$_2$CO$_3$-500	452	5.3	0.53	3.9	6.7

[a] S_{BET}: specific surface area was calculated using the Brunauer-Emmett-Teller (BET) equation. [b] D_{BJH}: mean pore size diameter was calculated using the Barret-Joyner-Halenda (BJH) equation. [c] V_{BJH}: pore volumes were calculated using the Barret-Joyner-Halenda (BJH) equation. Pd concentrations were determined by [d] ICP-OES and [e] Pd particle size was calculated using XRD analyses employing the Scherrer Equation.

The smaller size of palladium particles in Pd-chitin-Na$_2$CO$_3$-500 was correlated to an occlusion phenomenon in the carbonaceous matrix, which plausibly led to a higher mean pore diameter and a slightly lower surface area, in comparison with the Pd-chitin analogue.

Overall, the characterization studies confirmed the suitability of the mechanochemically assisted protocol for the preparation of supported metal nanoparticles on a mesoporous N-doped carbon-base matrix [50,51].

A well-known C-C bond-forming reaction, such as Suzuki-Miyaura cross-coupling, was selected as a model to test the activity of the Pd-based materials. The same approach used for the synthesis of the catalysts, i.e., mechanochemistry based on extrusion, was considered to carry out the reactions. Figure 4 summarizes the design of the experiments. A mixture of phenyl boronic acid (366 mg, 3 mmol), iodobenzene (408 mg, 2 mmol), and the Pd-based catalyst (40 mg) was fed to a mini-extruder heated to 80 °C, the conveying screws

of which were set to 50 rpm at a torque of 2 Nm. The residence time was 1 h. Other tests were performed by adding K_2CO_3 (53 mg, 0.5 mmol). The use of an extra base reactant is reported by most, if not all, protocols for the Suzuki-Miyaura process. The extrudate was collected in the form of a solid. A portion of this material (100 mg) was rinsed with ethanol as a solvent (5 mL). The resulting solution was analyzed by GC-FID and GC-MS to evaluate the conversion and the selectivity, and to assign the structure of the products. The most representative results are reported in Table 2.
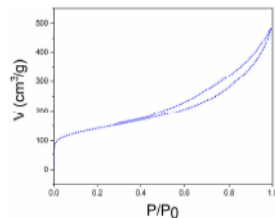
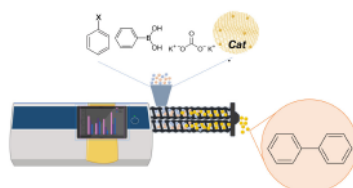**Figure 3.** N_2 physisorption isotherm of Pd-chitin-500 sample.

Figure 4. The design of the mechanochemically assisted catalytic Suzuki-Miyaura cross-coupling reaction.

Table 2. The Suzuki-Miyaura cross-coupling under mechanochemistry conditions based on extrusion.

Entry	Catalyst	Base	Conversion (%) [a]	Selectivity (%) [b]
1	Pd-chitin-500	/	<10	>99
2	Pd-chitin-Na$_2$CO$_3$	/	<10	>99
3	Pd-chitin-Na$_2$CO$_3$-500	/	<10	>99
4	Pd-chitin	K$_2$CO$_3$	73	>99
5	**Pd-chitin-500**	**K$_2$CO$_3$**	**81**	**>99**
6	Pd-chitin-Na$_2$CO$_3$-500	K$_2$CO$_3$	78	>99

Reaction conditions: Iodobenzene (2 mmol); PhB(OH)$_2$ (3 mmol); K$_2$CO$_3$ (4 mmol); Catalysts amount: 40 mg, 80 °C, 50 rpm, residence time 1 h. [a,b] Conversion of iodobenzene and selectivity to biphenyl were determined by GC. The best catalytic result is highlighted in bold.

All reactions provided the expected product, biphenyl, with >99% selectivity (details on the characterization of the product are in the SI section), though the conversion was largely affected by the experimental conditions. The reaction outcome was not satisfactory without an added base (entries 1–3); regardless of the use of calcined or not calcined catalysts and the presence/absence of Na$_2$CO$_3$ incorporated in the samples, the cross-coupling proceeded to a very limited extent, with a conversion not exceeding 10%. The catalyst preparation was modified using K$_2$CO$_3$ in place of Na$_2$CO$_3$. This change, however, did not impact on the reaction outcome; the activity of the newly prepared sample was as low as that of Pd-chitin-Na$_2$CO$_3$-500. In the presence of K$_2$CO$_3$ as an extra base, however, the conversion of iodobenzene was remarkably improved to 73 and 81% using Pd-chitin and Pd-chitin-500, respectively, with an overall biphenyl productivity of up to 41 mmol g_{cat}^{-1} h^{-1} (entries 4 and 5). This clearly confirmed the role of excess (free) base for the cross-coupling process. According to the most accepted mechanistic hypothesis, the base assists the activation of boronic acid, enabling a Pd-B transmetallation step which is critical for the C-C bond formation. Although there are still uncertainties about the occurrence of such a step, a plausible pathway has been proposed whereby the reaction of the base with the organoboron compound produces an anionic organoboronate species which, in turn, performs a nucleophilic attack on a Pd-halide intermediate [52,53].

Overall, our findings not only proved the suitability of the extrusion-assisted protocol to perform the reaction, but it demonstrated that: (i) the base fundamental for the reaction was effective only when added as such and could in no way be made available by incorporating it in the solid catalyst; (ii) the basic sites on the N-doped carbon used as a support were moderately, if at all, involved in the investigated cross-coupling process; and (iii) the calcined catalysts performed slightly better than non-calcined ones. This was highlighted once the reaction took place at a substantial conversion (≥70%) and was even corroborated by the behavior of Pd-chitin-Na$_2$CO$_3$-500 (calcined) sample, of which a 78% conversion was reached (entry 6), thereby suggesting that the thermal activation used to prepare the former (calcined) samples made the metal nanoparticles dispersed on them more accessible and active for catalysis. An additional test was carried out by employing Pd(OAc)$_2$ (4 mg) as a catalyst in place of Pd-chitin-500, though the iodobenzene:Pd molar ratio was kept unaltered. Other conditions can be seen in Table 2 (80 °C, 50 rpm, residence time 1 h). The reaction proceeded with both quantitative conversion and selectivity, thereby indicating (as expected) that the availability of the active sites on the acetate complex was superior to that of the heterogenous system. The use of Pd(OAc)$_2$, however, suffered from the well-known disadvantages associated to homogeneous catalysts including the very difficult separation from the product and the virtually impossible reuse for subsequent reactions. For comparison, this last aspect (catalyst recycle) was explored with the heterogenous Pd-chitin-500 system. Under the conditions of entry 5 in Table 2, once the reaction was complete, the catalyst was washed, dried, and reused without any further treatment, and a second reaction was run in exactly the same way as the first one (entry 5). The recycle test confirmed that Pd-chitin-500 preserved its original activity yielding an iodobenzene conversion and a biphenyl selectivity of 79% and >99%, respectively. Moreover, the stability of the used catalyst was examined by comparing its Pd content to that of the fresh catalyst: ICP-OES analyses proved that a negligible metal leaching (<5%) occurred (4.1 and 4.3 mg$_{Pd}$ g^{-1}, for the used and the fresh catalyst, respectively).

Pd-chitin-500 was also tested using bromobenzene and chlorobenzene in place of iodobenzene as a reactant. Under the conditions of entry 5, however, the reactions showed a negligible conversion (ca. 5%) consistent with the general effect of the halide as a leaving group in the Suzuki-Miyaura cross-coupling reactions [52]. Thereafter, to gather further information on the general applicability of the protocol, the organoborane reaction partner was changed. An additional experiment was run by coupling iodobenzene with *m*-tolylboronic acid in place of phenylboronic acid. The test was successful; the conversion was 75% and the selectivity towards the desired product, 3-methyl-1,1'-biphenyl, was 95% (details on the characterization of the product are in the SI section). This proved

that, under the reactive extrusion conditions, the onset of secondary reactions, such as the homocoupling of aryl boronic acids, was not significant.

An additional experiment was designed to test the activity of Pd-chitin-500 also under conventional batch conditions. Accordingly, the same reactants mixture used in Table 2 [phenyl boronic acid (43 mg, 0.35 mmol), iodobenzene (51 mg, 0.25 mmol), K_2CO_3 (70 mg, 0.50 mmol), and the catalyst (10 mg)] was set to react in a 10 mL glass flask, at 80 °C for 1 h, using ethanol (3 mL) as the solvent. The reaction proceeded with complete selectivity to biphenyl, but the reaction conversion was only 58%, ca. 25% lower than that achieved under the reactive extrusion conditions of entry 5 in Table 2. This result, plausibly due to a solvation/dilution effect, highlighted the higher efficiency of the mechanochemical approach compared to traditional procedures in a solution.

4. Conclusions

Mechanochemistry is among the strategies working towards the innovative design of sustainable and cost-efficient synthetic processes. This contribution provides a proof of concept aimed at expanding the applications in this field, using the reactive extrusion that combines the potential of mechanochemistry with the benefits of continuous-flow processes. Albeit at an early stage, the research communication proposed here offers the reliability and reproducibility that demonstrate the suitability of extrusion methods for both the preparation of nanostructured catalysts and the implementation of remarkable catalytic processes for the C-C bond-forming reactions. Supported Pd-based nanoparticles with excellent textural properties (surface area up to 498 m^2 g^{-1}) were prepared via mechanochemistry, in the absence of solvents. Such materials have proven active for the Suzuki-Miyaura cross-coupling of aryl boronic acid with iodobenzene, achieving conversion and selectivity values of up to 81% and 99%, respectively, and a productivity on the desired coupling products of up to 41 mmol g^{-1} h^{-1}, making them amenable for further scaled up studies of the process.

References

1. Muñoz-Batista, M.J.; Rodriguez-Padron, D.; Puente-Santiago, A.R.; Luque, R. Mechanochemistry: Toward Sustainable Design of Advanced Nanomaterials for Electrochemical Energy Storage and Catalytic Applications. *ACS Sustain. Chem. Eng.* **2018**, *6*, 9530–9544. [CrossRef]
2. Rodriguez-Padrón, D.; Puente-Santiago, A.R.; Caballero, A.; Balu, A.M.; Romero, A.A.; Luque, R. Highly Efficient Direct Oxygen Electro-Reduction by Partially Unfolded Laccases Immobilized on Waste-Derived Magnetically Separable Nanoparticles. *Nanoscale* **2018**, *10*, 3961–3968. [CrossRef] [PubMed]
3. Garcia-Espejo, G.; Rodriguez-Padrón, D.; Luque, R.; Camacho, L.; De Miguel, G. Mechanochemical Synthesis of Three Double Perovskites: $Cs_2AgBiBr_6$, $(CH_3NH_3)_2TlBiBr_6$ and $Cs_2AgSbBr_6$. *Nanoscale* **2019**, *11*, 16650–16657. [CrossRef] [PubMed]
4. Rodriguez-Padrón, D.; Jodlowski, A.D.; De Miguel, G.; Puente-Santiago, A.R.; Balu, A.M.; Luque, R. Synthesis of Carbon-Based Fluorescent Polymers Driven by Catalytically Active Magnetic Bioconjugates. *Green Chem.* **2018**, *20*, 225–229. [CrossRef]
5. Rodriguez-Padrón, D.; Puente-Santiago, A.R.; Balu, A.M.; Romero, A.A.; Muñoz-Batista, M.J.; Luque, R. Benign-by-Design Orange Peellated Nanocatalysts for Continuous Flow Conversion of Levulinic Acid to N-Heterocycles. *ACS Sustain. Chem. Eng.* **2018**, *6*, 16637–16644. [CrossRef]
6. Rodriguez-Padrón, D.; Puente-Santiago, A.R.; Balu, A.M.; Romero, A.A.; Luque, R. Solventless Mechanochemical Preparation of Novel Magnetic Bioconjugates. *Chem. Commun.* **2017**, *53*, 7635–7637. [CrossRef]
7. Caudillo-Flores, U.; Rodriguez-Padrón, D.; Muñoz-Batista, M.J.; Kubacka, A.; Luque, R.; Fernández-Garcia, M. Facile Synthesis of $B/g-C_3N_4$composite Materials for the Continuous-Flow Selective Photo-Production of Acetone. *Green Chem.* **2020**, *22*, 4975–4984. [CrossRef]
8. Rodriguez-Padrón, D.; Puente-Santiago, A.R.; Caballero, A.; Benítez, A.; Balu, A.M.; Romero, A.A.; Luque, R. Mechanochemical Design of Hemoglobin-Functionalised Magnetic Nanomaterials for Energy Storage Devices. *J. Mater. Chem. A* **2017**, *5*, 16404–16411. [CrossRef]
9. Garcia-Espejo, G.; Rodriguez-Padrón, D.; Pérez-Morales, M.; Luque, R.; De Miguel, G.; Camacho, L. Mechanochemical Synthesis of One-Dimensional (1D) Hybrid Perovskites Incorporating Polycyclic Aromatic Spacers: Highly Fluorescent Cation-Based Materials. *J. Mater. Chem. C* **2018**, *6*, 7677–7682. [CrossRef]
10. Liu, X.; Li, Y.; Zeng, L.; Li, X.; Chen, N.; Bai, S.; He, H.; Wang, Q.; Zhang, C. A Review on Mechanochemistry: Approaching Advanced Energy Materials with Greener Force. *Adv. Mater.* **2022**, *34*, 2108327. [CrossRef]
11. Jiao, Y.; Nan, Y.; Wu, Z.; Wang, X.; Zhang, J.; Zhang, B.; Huang, S.; Shi, J. Mechanochemical Synthesis of Enzyme@covalent Organic Network Nanobiohybrids. *Appl. Mater. Today* **2022**, *26*, 101381. [CrossRef]
12. Espro, C.; Rodriguez-Padrón, D. Re-Thinking Organic Synthesis: Mechanochemistry as a Greener Approach. *Curr. Opin. Green Sustain. Chem.* **2021**, *30*, 100478. [CrossRef]
13. Martin-Perales, A.I.; Balu, A.M.; Malpartida, I.; Luque, R. Prospects for the Combination of Mechanochemistry and Flow Applied to Catalytic Transformations. *Curr. Opin. Green Sustain. Chem.* **2022**, *38*, 100714. [CrossRef]
14. Wang, G.W. Mechanochemical Organic Synthesis. *Chem. Soc. Rev.* **2013**, *42*, 7668–7700. [CrossRef]
15. Andersen, J.; Mack, J. Mechanochemistry and Organic Synthesis: From Mystical to Practical. *Green Chem.* **2018**, *20*, 1435–1443. [CrossRef]
16. James, S.L.; Friščic, T. Mechanochemistry. *Chem. Soc. Rev.* **2013**, *42*, 7494–7496. [CrossRef]
17. Friščic, T.; Mottillo, C.; Titi, H.M. Mechanochemistry for Synthesis. *Angew. Chem.* **2020**, *132*, 1030–1041. [CrossRef]
18. Do, J.; Titi, H.M.; Auvray, T.; Lennox, C.B.; Cuccia, L.A. Rapid, room-temperature, solvent-free mechanochemical oxidation of elemental gold into organosoluble gold salts †. *Green Chem.* **2023**, *25*, 5774. [CrossRef]
19. Brekalo, I.; Martinez, V.; Karadeniz, B.; Orešković, P.; Drapanauskaite, D.; Vriesema, R.; Etter, M.; Dejanović, I.; Baltrusaitis, J.; et al. Scale-Up of Agrochemical Urea-Gypsum Cocrystal Synthesis Using Thermally Controlled Mechanochemistry. *ACS Sustain. Chem. Eng.* **2022**, *10*, 6743–6754. [CrossRef]
20. Bolt, R.R.A.; Raby-Buck, S.E.; Ingram, K.; Leitch, J.A.; Browne, D.L. Temperature-Controlled Mechanochemistry for the Nickel-Catalyzed Suzuki-Miyaura-Type Coupling of Aryl Sulfamates via Ball Milling and Twin-Screw Extrusion. *Angew. Chem. Int. Ed.* **2022**, *61*, e202210508. [CrossRef]
21. Andersen, J.; Brunemann, J.; Mack, J. Exploring Stable, Sub-Ambient Temperatures in Mechanochemistry: Via a Diverse Set of Enantioselective Reactions. *React. Chem. Eng.* **2019**, *4*, 1229–1236. [CrossRef]
22. Bolt, R.R.A.; Leitch, J.A.; Jones, A.C.; Nicholson, W.L.; Browne, D.L. Continuous Flow Mechanochemistry: Reactive Extrusion as an Enabling Technology in Organic Synthesis. *Chem. Soc. Rev.* **2022**, *51*, 4243–4260. [CrossRef] [PubMed]
23. Vidakis, N.; Petousis, M.; Mountakis, N.; Grammatikos, S.; Papadakis, V.; Kechagias, J.D.; Das, S.C. On the Thermal and Mechanical Performance of Polycarbonate/Titanium Nitride Nanocomposites in Material Extrusion Additive Manufacturing. *Compos. Part C Open Access* **2022**, *8*, 100291. [CrossRef]
24. Galant, O.; Cerfeda, G.; McCalmont, A.S.; James, S.L.; Porcheddu, A.; Delogu, F.; Crawford, D.E.; Colacino, E.; Spatari, S. Mechanochemistry Can Reduce Life Cycle Environmental Impacts of Manufacturing Active Pharmaceutical Ingredients. *ACS Sustain. Chem. Eng.* **2022**, *10*, 1430–1439. [CrossRef]
25. Xu, J.; Hou, S.; Niu, Q.; Zhang, P.; Luo, Z.H. Cyclic Extrusion Synthesis of Mesoporous Carbon-Supported Metal Catalysts for Selective Hydrogenation. *AIChE J.* **2023**, *69*, e18073. [CrossRef]

93

26. Sonei, S.; Taghavi, F.; Khojastehnezhad, A.; Gholizadeh, M. Copper-Functionalized Silica-Coated Magnetic Nanoparticles for an Efficient Suzuki Cross-Coupling Reaction. *ChemistrySelect* 2021, 6, 359–368. [CrossRef]
27. Muszka, K.; Szabados, M.; Ádám, A.A.; Kónya, Z.; Kukovecz, Á.; Sipos, P.; Pálinkó, I. Mechanochemically Modified Hydrazine Reduction Method for the Synthesis of Nickel Nanoparticles and Their Catalytic Activities in the Suzuki-Miyaura Cross-Coupling Reaction. *React. Kinet. Mech. Catal.* 2019, 126, 857–868. [CrossRef]
28. Beromi, M.M.; Nova, A.; Balcells, D.; Brasacchio, A.M.; Brudvig, G.W.; Guard, L.M.; Hazari, N.; Vinyard, D.J. Mechanistic Study of an Improved Ni Precatalyst for Suzuki-Miyaura Reactions of Aryl Sulfamates: Understanding the Role of Ni(I) Species. *J. Am. Chem. Soc.* 2017, 139, 922–936. [CrossRef]
29. Hergert, T.; Varga, B.; Thurner, A.; Faigl, F.; Mátravölgyi, B. Copper-Facilitated Suzuki-Miyaura Coupling for the Preparation of 1,3-Dioxolane-Protected 5-Arylthiophene-2-Carboxaldehydes. *Tetrahedron* 2018, 74, 2002–2008. [CrossRef]
30. Liu, F.; Liu, X.; Chen, F.; Fu, Q. Tannic Acid: A Green and Efficient Stabilizer of Au, Ag, Cu and Pd Nanoparticles for the 4-Nitrophenol Reduction, Suzuki-Miyaura Coupling Reactions and Click Reactions in Aqueous Solution. *J. Colloid Interface Sci.* 2021, 604, 281–291. [CrossRef]
31. Seo, T.; Ishiyama, T.; Kubota, K.; Ito, H. Solid-State Suzuki-Miyaura Cross-Coupling Reactions: Olefin-Accelerated C–C Coupling Using Mechanochemistry. *Chem. Sci.* 2019, 10, 8202–8210. [CrossRef]
32. Seo, T.; Kubota, K.; Ito, H. Mechanochemistry-Directed Ligand Design: Development of a High-Performance Phosphine Ligand for Palladium-Catalyzed Mechanochemical Organoboron Cross-Coupling. *J. Am. Chem. Soc.* 2023, 145, 6823–6837. [CrossRef]
33. Zhang, J.; Zhang, P.; Ma, Y.; Szostak, M. Mechanochemical Synthesis of Ketones via Chemoselective Suzuki-Miyaura Cross-Coupling of Acyl Chlorides. *Org. Lett.* 2022, 24, 2338–2343. [CrossRef]
34. Zhang, J.; Zhang, P.; Shao, L.; Wang, R.; Ma, Y.; Szostak, M. Mechanochemical Solvent-Free Suzuki-Miyaura Cross-Coupling of Amides via Highly Chemoselective N–C Cleavage. *Angew. Chem. Int. Ed.* 2022, 61, e202114146. [CrossRef]
35. Zuliani, A.; Balu, A.M.; Luque, R. Efficient and Environmentally Friendly Microwave-Assisted Synthesis of Catalytically Active Magnetic Metallic Ni Nanoparticles. *ACS Sustain. Chem. Eng.* 2017, 5, 11584–11587. [CrossRef]
36. Maschmeyer, T.; Luque, R.; Selva, M. Upgrading of Marine (Fish and Crustaceans) Biowaste for High Added-Value Molecules and Bio(Nano)-Materials. *Chem. Soc. Rev.* 2020, 49, 4527–4563. [CrossRef]
37. Polidoro, D.; Perosa, A.; Rodríguez-Castellón, E.; Canton, P.; Castoldi, L.; Rodríguez-Padrón, D.; Selva, M. Metal-Free N-Doped Carbons for Solvent-Less CO2Fixation Reactions: A Shrimp Shell Valorization Opportunity. *ACS Sustain. Chem. Eng.* 2022, 10, 13835–13848. [CrossRef]
38. Xu, C.; Nasrollahzadeh, M.; Selva, M.; Issaabadi, Z.; Luque, R. Waste-to-Wealth: Biowaste Valorization into Valuable Bio(Nano)Materials. *Chem. Soc. Rev.* 2019, 48, 4791–4822. [CrossRef]
39. Rodríguez-Padrón, D.; Zhao, D.; Carrillo-Carrion, C.; Morales-Torres, C.; Elsharif, A.M.; Balu, A.M.; Luque, R.; Len, C. Exploring the Potential of Biomass-Templated Nb/ZnO Nanocatalysts for the Sustainable Synthesis of N-Heterocycles. *Catal. Today* 2021, 368, 243–249. [CrossRef]
40. Martin-Perales, A.I.; Rodríguez-Padrón, D.; Garcia Coleto, A.; Len, C.; De Miguel, G.; Muñoz-Batista, M.J.; Luque, R. Photocatalytic Production of Vanillin over CeOxand ZrO2 Modified Biomass-Templated Titania. *Ind. Eng. Chem. Res.* 2020, 59, 17085–17093. [CrossRef]
41. Cárdenas, G.; Cabrera, G.; Taboada, E.; Miranda, S.P. Chitin Characterization by SEM, FTIR, XRD, And13C Cross Polarization/Mass Angle Spinning NMR. *J. Appl. Polym. Sci.* 2004, 93, 1876–1885. [CrossRef]
42. Cui, D.; Yang, J.; Lu, B.; Deng, L.; Shen, H. Extraction and Characterization of Chitin from Oratosquilla Oratoria Shell Waste and Its Application in *Brassica campestris* L.ssp. *Int. J. Biol. Macromol.* 2022, 198, 204–213. [CrossRef] [PubMed]
43. Tamoradi, T.; Ghorbani-Choghamarani, A.; Ghadermazi, M. Synthesis of a New Pd(0)-Complex Supported on Magnetic Nanoparticles and Study of Its Catalytic Activity for Suzuki and Stille Reactions and Synthesis of 2,3-Dihydroquinazolin-4(1H)-One Derivatives. *Polyhedron* 2018, 145, 120–130. [CrossRef]
44. Baruah, D.; Das, R.N.; Hazarika, S.; Konwar, D. Biogenic Synthesis of Cellulose Supported Pd(0) Nanoparticles Using Hearth Wood Extract of Artocarpus Lakoocha Roxb—A Green, Efficient and Versatile Catalyst for Suzuki and Heck Coupling in Water under Microwave Heating. *Catal. Commun.* 2015, 72, 73–80. [CrossRef]
45. Polidoro, D.; Rodriguez-Padron, D.; Perosa, A.; Luque, R.; Selva, M. Chitin-Derived Nanocatalysts for Reductive Amination Reactions. *Materials* 2023, 16, 575. [CrossRef]
46. Masood, M.H.; Haleem, N.; Shakeel, I.; Jamal, Y. Carbon Dioxide Conversion into the Reaction Intermediate Sodium Formate for the Synthesis of Formic Acid. *Res. Chem. Intermed.* 2020, 46, 5165–5180. [CrossRef]
47. Kirik, S.D.; Mulagaleev, R.F.; Blokhin, A.I. [Pd(CH3COO)2]n from X-Ray Powder Diffraction Data. *Acta Crystallogr. Sect. C Cryst. Struct. Commun.* 2004, 60, 449–450. [CrossRef]
48. Kibasomba, P.M.; Dhlamini, S.; Maaza, M.; Liu, C.P.; Rashad, M.M.; Rayan, D.A.; Mwakikunga, B.W. Strain and Grain Size of TiO2 Nanoparticles from TEM, Raman Spectroscopy and XRD: The Revisiting of the Williamson-Hall Plot Method. *Results Phys.* 2018, 9, 628–635. [CrossRef]
49. Holzwarth, U.; Gibson, N. The Scherrer Equation versus the "Debye-Scherrer Equation." *Nat. Nanotechnol.* 2011, 6, 534. [CrossRef]
50. Karandikar, P.; Patil, K.R.; Mitra, A.; Kakade, B.; Chandwadkar, A.J. Synthesis and Characterization of Mesoporous Carbon through Inexpensive Mesoporous Silica as Template. *Microporous Mesoporous Mater.* 2007, 98, 189–199. [CrossRef]

51. Polidoro, D.; Ballesteros-Plata, D.; Perosa, A.; Rodríguez-Castellón, E.; Rodríguez-Padrón, D.; Selva, M. Controlled Alcohol Oxidation Reactions by Supported Non-Noble Metal Nanoparticles on Chitin-Derived N-doped Carbons. *Catal. Sci. Technol.* 2023, 13, 2223–2238. [CrossRef]
52. Bao, G.; Bai, J.; Li, C. Synergistic Effect of the Pd-Ni Bimetal/Carbon Nanofiber Composite Catalyst in Suzuki Coupling Reaction. *Org. Chem. Front.* 2019, 6, 352–361. [CrossRef]
53. D'Alterio, M.C.; Casals-Cruañas, È.; Tzouras, N.V.; Talarico, G.; Nolan, S.P.; Poater, A. Mechanistic Aspects of the Palladium-Catalyzed Suzuki-Miyaura Cross-Coupling Reaction. *Chem. A Eur. J.* 2021, 27, 13481–13493. [CrossRef]